NOAA Technical Memorandum NESDIS AISC 5

INTERDISCIPLINARY SYNOPTIC ASSESSMENT OF CHESAPEAKE BAY AND THE ADJACENT SHELF

Edited by
David F. Johnson,
Kurt W. Hess, and
Peter J. Pytlowany

Washington, D.C.
August 1986

U.S. DEPARTMENT OF COMMERCE / National Oceanic and Atmospheric Administration / National Environmental Satellite, Data, and Information Service

NOAA TECHNICAL MEMORANDUMS

National Environmental Satellite Data and Information Services,
Assessment and Information Services Center Subseries

The Assessment and Information Services Center provides value - added environmental information to support national needs and goals. The products and services of AISC's staff of environmnental scientists, economists, librarians and information specialists, and computer specialists provide decision assistance to the nation's resource managers. AISC's programs in environmental assessments and environmental information management complement the data collection and archival program of other National Environmental Satellite Data and Information Services (NESDIS) components.

The Technical Memorandum series provides an informal medium for the documentation and quick dissemination of results not appropriate, or not yet ready, for formal publication in the standard journals. The series is used to report on work in progress, to describe technical procedures and practices, or to report to a limited audience.

These papers are available from the originating office and also from the National Technical Information Service (NTIS), U.S. Department of Commerce, 5285 Port Royal Road, Springfield, VA 22151. Prices vary for paper copy and microfiche.

NESDIS Technical Memorandum

AISC 1 Assessment Models for Surface Dispersion of Marine Pollutants. Kurt W. Hess, Fred G. Everdale, and Peter L. Grose, May 1985.

AISC 2 Comparison of Boundary Layer Winds from NWS LFM Output and Instrumented Buoys. Robert W. Reeves and Peter J. Pytlowany, May 1985.

AISC 3 Assessment Model for Estuarine Circulation and Salinity. Kurt W. Hess, June 1985.

AISC 4 Development of a Tropical Cyclone Damage Assessment Methodology. Isobel C. Sheifer and John O. Ellis, January 1986.

NOAA Technical Memorandum NESDIS AISC 5

INTERDISCIPLINARY SYNOPTIC ASSESSMENT OF CHESAPEAKE BAY AND THE ADJACENT SHELF

Edited by
David F. Johnson, Kurt W. Hess,
and Peter J. Pytlowany

Marine Environmental Assessment Division
Assessment and Information Services Center

Washington, D.C.
August 1986

UNITED STATES
DEPARTMENT OF COMMERCE
Malcolm Baldrige,
Secretary

National Oceanic and
Atmospheric Administration
Anthony J. Calio,
Administrator

National Environmental Satellite,
Data, and Information Service
Thomas N. Pyke, Jr.
Assistant Administrator

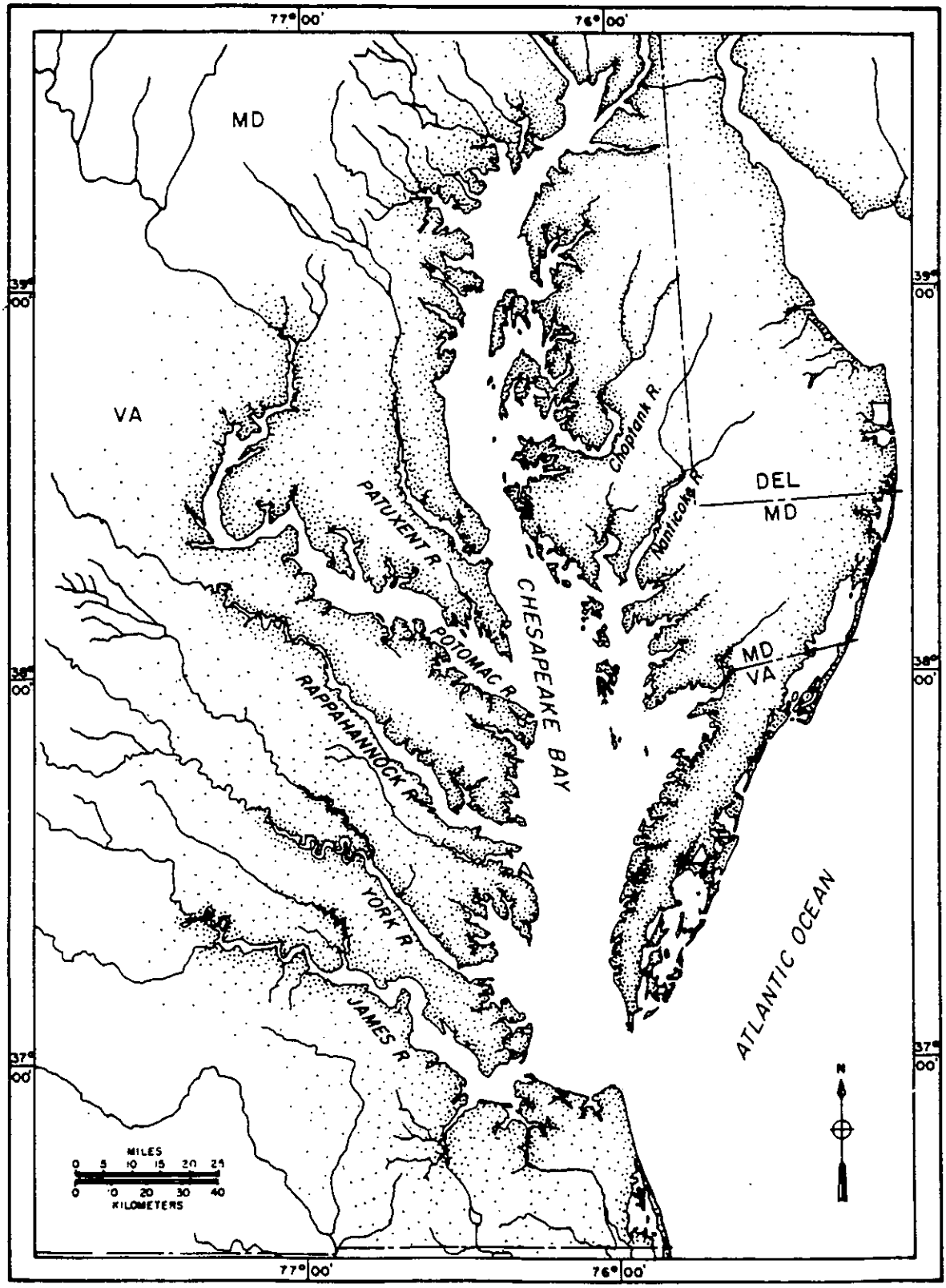
77°00'
76°00'
MD
VA
DEL
MD
39°00'
38°00'
37°00'
Choptank R.
Nanticoke R.
PATUXENT R.
POTOMAC R.
RAPPAHANNOCK R.
YORK R.
JAMES R.
CHESAPEAKE BAY
MD
VA
ATLANTIC OCEAN
N
MILES
0 5 10 15 20 25
0 10 20 30 40
KILOMETERS

TABLE OF CONTENTS

		Page
	LIST OF ABBREVIATIONS AND ACRONYMS	v
	ACKNOWLEDGMENTS	vi
	EXECUTIVE SUMMARY	vii
1.	INTRODUCTION	1
2.	WEATHER AND OCEAN CONDITIONS, Peter J. Pytlowany and Martin C Proedehl	3
3.	SATELLITE METHODS AND APPLICATIONS, Fred G. Everdale and Richard P. Stumpf	11
	3.1 Introduction	11
	3.2 Satellite Techniques	13
	3.2.1 Temperature	13
	3.2.2 Turbidity	15
	3.2.3 Pigments	16
	3.2.4 Image Preparation	20
	3.3 Satellite Imagery Analysis and Interpretation	20
	3.3.1 Chesapeake Bay	22
	3.3.2 Offshore Waters	29
	3.3.3 Summary	30
	3.4 Conclusions	31
	3.5 References	31
4.	SATELLITE IMAGERY AS AN INPUT TO A CIRCULATION MODEL, Marlene K. Stern	33
	4.1 Introduction	33
	4.2 Methods	33
	4.3 Results and Discussion	35
	4.4 Conclusions	42
	4.5 References	42
5.	LFM WINDS AND MASS TRANSPORT, Peter J. Pytlowany	43
	5.1 Introduction	43
	5.2 Analysis and Results	44
	5.2.1 Calibration of LFM Forecasts	44
	5.2.2 Wind-Induced Mass Transport	46
	5.3 Summary and Conclusions	46
	5.4 References	57
6.	NUMERICAL MODELING OF CIRCULATION AND TEMPERATURE, Kurt W. Hess	59
	6.1 Introduction	59
	6.2 The Numerical Model	59
	6.3 Temperature Calculations	59
	6.4 Model Application to the Bay-Shelf Region	61
	6.5 Model Inputs and Initialization	61
	6.5.1 Oceanic Boundaries	61
	6.5.2 Riverine Boundaries	65

TABLE OF CONTENTS (continued)

		Page
	6.5.3 Air-Water Interfacial Boundary	65
	6.5.4 Initialization Procedures	68
6.6	Model Results	68
	6.6.1 Spin-Up Experiments	68
	6.6.2 Verification of Water Levels and Currents	68
	6.6.3 Water Temperatures	72
6.7	Summary and Conclusions	72
6.8	Future Plans	74
6.9	References	74
7.	LARVAL DRIFT MODEL, David F. Johnson and Kurt W. Hess	77
7.1	Introduction	77
7.2	Objectives	79
7.3	Model Formulation	79
7.4	Model Testing	80
7.5	Simulation of Surface Drift: 10-24 April 1982	83
7.6	Future Applications	83
7.7	References	87
8.	CONCLUSIONS AND RECOMMENDATIONS	89

LIST OF ABBREVIATIONS AND ACRONYMS

AISC	Assessment and Information Services Center
AVHRR	Advanced Very High Resolution Radiometer
°C	degrees Celsius
cm	centimeter(s)
CZCS	Coastal Zone Color Scanner
EST	Eastern Standard Time
GMT	Greenwich Mean Time
IR	infrared
°K	degrees Kelvin
km	kilometer(s)
kn	knot(s)
LARTREK	Model for computing larval drift trajectories
LFM	Limited-area, Fine-mesh Model
m	meter(s)
mb	millibar(s)
mm	millimeter(s)
MCSST	Multichannel Sea Surface Temperature
MEAD	Marine Environmental Assessment Division
MECCA	Model for Estuarine and Coastal Circulation Assessment
MSS	Multispectral Scanner
NDBC	NOAA Data Buoy Center
nm	nanometers
NM	nautical miles
NEMP	Northeast Monitoring Program
NESDIS	National Environmental Satellite, Data, and Information Service
NOAA	National Oceanic and Atmospheric Administration
NOS	National Ocean Service
NWS	National Weather Service
pixel	picture element
ppt	parts per thousand
s or sec	second(s)
SST	Sea Surface Temperature
TM	Thematic Mapper
μm	micrometer(s)
USGS	United States Geological Survey

ACKNOWLEDGMENTS

Thanks are given to Dr. Celso Barrientos, Robert Dennis, Jack Ellis, Karl Pechmann, Dr. Isobel Sheifer and Dr. Kenneth Turgeon for review of the manuscript, and Leslie Gruis for review of Chapter 3. Thanks are also given to Pollie Jackson for editorial review and preparation of the final document.

INTERDISCIPLINARY SYNOPTIC ASSESSMENT OF CHESAPEAKE BAY

EXECUTIVE SUMMARY

The Chesapeake Bay, an important national resource, is both complex and dynamic; however, no existing technique provides scientists and managers with a synoptic perspective of environmental or ecological changes within the Bay for specific events. Yet, such a view is vital to an understanding of variations in the Bay system, such as fluctuations in fishery resources and the transport of pollutants. Existing shipboard and moored sampling methods cannot provide the Bay-wide, three-dimensional oceanographic information necessary for an understanding of the synoptic conditions, but an integrated approach to data analysis can.

This report presents work to date on development and testing of the integration of field observations, satellite data, and simulations from wind and circulation models into a synoptic assessment of Chesapeake Bay. For the simulations, the National Weather Service's Limited-area, Fine-mesh Model (LFM) winds are adjusted using observed winds at stations nearest to model grid points to provide a corrected-wind forcing function for the circulation model. Using temperature and salinity observations, river flow data and satellite imagery for boundary conditions, the circulation model, MECCA, calculates current vectors throughout the Bay and adjacent shelf. These current vectors are then used in a drift model, LARTREK, which tracks the path of drifters, such as plankton or pollutants. The initial testing period for the integrated system, 10-24 April 1982, was selected because of the availability of satellite imagery for the Bay region.

Satellite data have been used in this integrated approach to set boundary conditions in our circulation model. Two techniques were also developed to expand the use of satellite remote sensing to estimate concentrations of suspended sediments and plant pigments.

As part of the integrated approach, the LFM predictions provide timely estimates and broad coverage of wind fields. In marine applications, the LFM boundary layer forecasts are the best LFM estimators of the surface winds. We examined the accuracy of the individual 12-hourly LFM forecasts. Stepwise linear regressions of observed winds on predicted winds and predicted barometric pressures allowed the predicted winds to be successfully corrected to represent surface winds for input as forcing functions to the circulation model.

Another element in the integrated technique, the three-dimensional numerical model for estuarine and coastal circulation assessment, MECCA, was applied to the Chesapeake Bay and adjacent continental shelf for the selected period to learn more about currents and their effects on biological processes. The model was run for a spin-up time of 15 days prior to the period of interest. The total run period was 25 March - 24 April 1982. A new feature added to the model was heat flux across the sea bed. This flux, if neglected would result in a spurious heat build-up in the simulation of Bay temperature. This circulation model has been shown to be a useful tool for estuarine applications.

Executive Summary

The final component of the integrated method is the generalized drift model, LARTREK, that can be used to assess recruitment for commercial species that have planktonic larvae. Given an initial distribution of drifters within the geographic boundaries defined by MECCA, the drift model, LARTREK, can estimate the future position of the drifters using the current vectors supplied by MECCA. Our tests indicate the simulated drift tracks have small positional errors (less than 0.0075 percent of distance traveled) resulting from computational truncation errors. Verification of the drift model is not possible for the chosen time period because of the lack of corresponding field data, but for the several hypothetical cases chosen for analysis the model was judged to give accurate results.

Conclusions

1. This interdisciplinary approach successfully applies new and developing technology as an integrated system to increase our understanding of fisheries resources and to assess environmental impacts on the Chesapeake Bay economy.

2. Satellite imagery can be used to produce accurate and useful maps of sea surface temperature, turbidity and plant pigments. Selected temperature data were found to be useful as an environmental input for the circulation model. Turbidity and plant pigment estimation techniques require in situ data for additional refinement of the indices. Although satellite data can be collected daily, its use is somewhat limited because only near-nadir, cloud-free data can be used presently.

3. Predicted winds (12 hours in advance) from the National Weather Service may be successfully corrected to local observations and thus provide reasonable forcing functions for circulation modeling for fisheries (or ecosystems) affected by estuarine circulation. More study is needed to determine the feasibility of using longer range wind predictions (e.g., up to 48 hours in advance) as an input to the circulation model.

4. In simulations with the circulation model, MECCA, mean tide ranges at several stations throughout the Chesapeake Bay and adjacent shelf were calibrated to an accuracy of 10 cm and a mean time lag of half an hour. Mean tidal currents were calibrated to an accuracy of 0.3 m/sec or less. Further adjustment of the bathymetry, bottom friction coefficient, grid cell size, and the horizontal eddy viscosity may increase the accuracy. Surface water temperatures calculated by MECCA had respectively a root mean square error of 1.3 °C and 2.6 °C for tested Bay and shelf sites. The accuracies would be improved if spatial variations in water turbidity were considered.

5. Results from the use of the numerical circulation model to provide vectors for drift modeling indicate simulated drift tracks have very small positional errors resulting from computational truncation errors, and simulated drift tracks appear to be reasonable approximations of known drift patterns. This approach with slight modification also has application to other areas such as tracking pollutants and modeling sediment transport.

This interdisciplinary approach has several possible applications for future assessment of ecological events, but has immediate importance for increasing our understanding of fisheries resources. Completion of the present work and extension of the study period to more critical biological seasons will enhance our assessment capabilities.

1. INTRODUCTION

David F. Johnson and Kenneth W. Turgeon

This report presents work to date on development and testing of the integration of field observations, satellite data, and simulations from wind and circulation models into a synoptic assessment of Chesapeake Bay. The Chesapeake Bay is complex and dynamic, and no existing technique provides scientists and managers with a synoptic environmental perspective of changes within the Bay for specific environmental or ecological events. Yet, such a view is vital to an understanding of variations in the Bay system, such as fluctuations in fishery resources and the transport of pollutants. Existing shipboard and moored sampling methods are aimed at very finite problems and cannot provide the Bay-wide, three-dimensional oceanographic information necessary for a synoptic understanding of the system. A hybrid modeling-monitoring approach could provide a prognostic or diagnostic analysis of value to agencies and institutions charged with the management of the Bay's natural resources.

We have combined the outputs of three numerical models, three external data sources, and satellite imagery into an interdisciplinary methodology to provide assessments of environmental changes in the Chesapeake Bay (Figure 1-1). The LFM predicted winds are adjusted using observed winds at stations nearest to model grid points to provide a corrected-wind forcing function for the circulation model (MECCA). Using NOS temperature and salinity observations, USGS river flow data and AISC satellite imagery for boundary conditions, MECCA calculates current vectors throughout the Bay and adjacent shelf. Finally, these current vectors are used as forcing functions in a model (LARTREK) which tracks the path of drifters. The integrated model output will allow MEAD to assess recruitment for many commercial species as well as impacts resulting from long-term or short-term perturbations to the Bay system. With slight modification, this approach also has real-time application to other estuaries for tracking pollution, sediment transport and phytoplankton blooms. The initial testing period for the integrated methodology is 10-24 April 1982. This period was selected solely with regard for the availability of satellite imagery having minimal cloud cover of the Bay region, not for biological processes. We are expanding the testing to periods of biological importance.

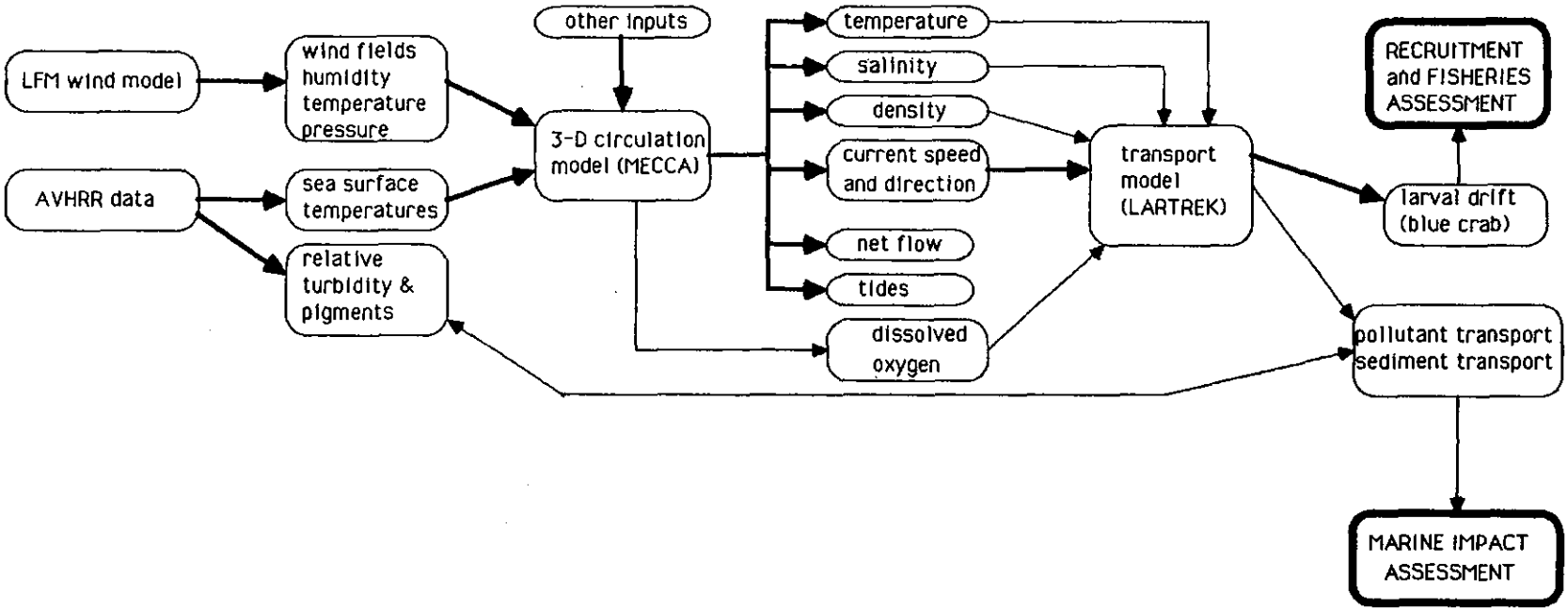

Figure 1-1. Flow chart of quantitative interdisciplinary assessment methodology for estuarine/coastal environments. Initial case study is Chesapeake Bay and the adjacent shelf region. Thick lines denote interactions incorporated into the model, thin lines denote interactions for future consideration.

2. WEATHER AND OCEAN CONDITIONS: April 1982

Peter J. Pytlowany and Martin C. Predoehl

The physical circulation of shallow coastal embayments, such as Chesapeake Bay, is strongly coupled to the regional weather. Fluctuations in weather conditions can elicit rapid responses, on the order of 1-2 days or less, in oceanic conditions. Atmospheric forcing of oceanic variability is most apparent during anomalous events, such as severe storms and strong fronts, and during the transitional seasons of spring and fall. Daily observations from a representative selection of meteorological and oceanographic stations in the Bay region were used to show the coupling that existed between the atmosphere and the Bay in April 1982 (Figure 2-1).

During the first two weeks in April 1982 a succession of cold fronts brought record low air temperatures to the Chesapeake Bay area (Table 2-1), inducing below normal surface water temperatures in the Bay (Figure 2-2). The first cold front to pass through the Chesapeake Bay region came on 3 April within a massive storm system moving northeastward across the Great Lakes. Temperatures fell by 7 to 8 °C producing readings as low as -1 °C in some Bay locations. Winds in thunderstorms along the cold front gusted to 34 m/sec in the Eastern Shore portion of Maryland, blowing down large trees and damaging buildings. Small craft and gale warnings were issued. After having declined in late March from above normal levels, streamflow increased temporarily to a peak on 5 April partially in response to widespread precipitation from the storm of 3 April.

Salt intrusions advanced upstream from their March locations more than 10 km in the James and Rappahannock rivers and 5 km in the Pamunkey River in response to a declining streamflow in late March and early April. The persistence of strong northwesterly winds behind the front in combination with the decreased freshwater discharge caused increased vertical mixing and greatly reduced the vertical stratification of Chesapeake Bay waters.

A second cold front embedded in a storm passing directly over the Bay on 6 April brought record low temperatures along with wind gusts to 18 m/sec and rain to most Bay locations; extensive snow accumulated in the northern reaches of the drainage basin. The strong northwesterly winds during 6-7 April produced the second lowest tide ever recorded at Royal Oak, MD on 7 April. The two cold fronts dropped air temperatures by approximately 11 °C Baywide. Bay surface water temperatures dropped by 2.5 to 3.0 °C (Figure 2-2). Record low temperatures followed, decreasing snowmelt and causing, in part, a steady decline in streamflow for the remainder of April (Figure 2-3). Additional snow occurred over the northern Bay early on 9 April from a low pressure system staying mainly south of the region. Abnormally cold temperatures persisted over the Bay from 4-12 April and were accompanied by a marked decrease in surface salinity in the mid-Bay region (Figure 2-4).

A third cold front passed over the Bay on 13 April, bringing strong northwesterly winds, with gusts up to 16.5 m/sec, recorded at Patuxent, MD. Daily low temperatures dropped -1.1 to 6.7 °C on 15 April with a strong wind flow from the northeast.

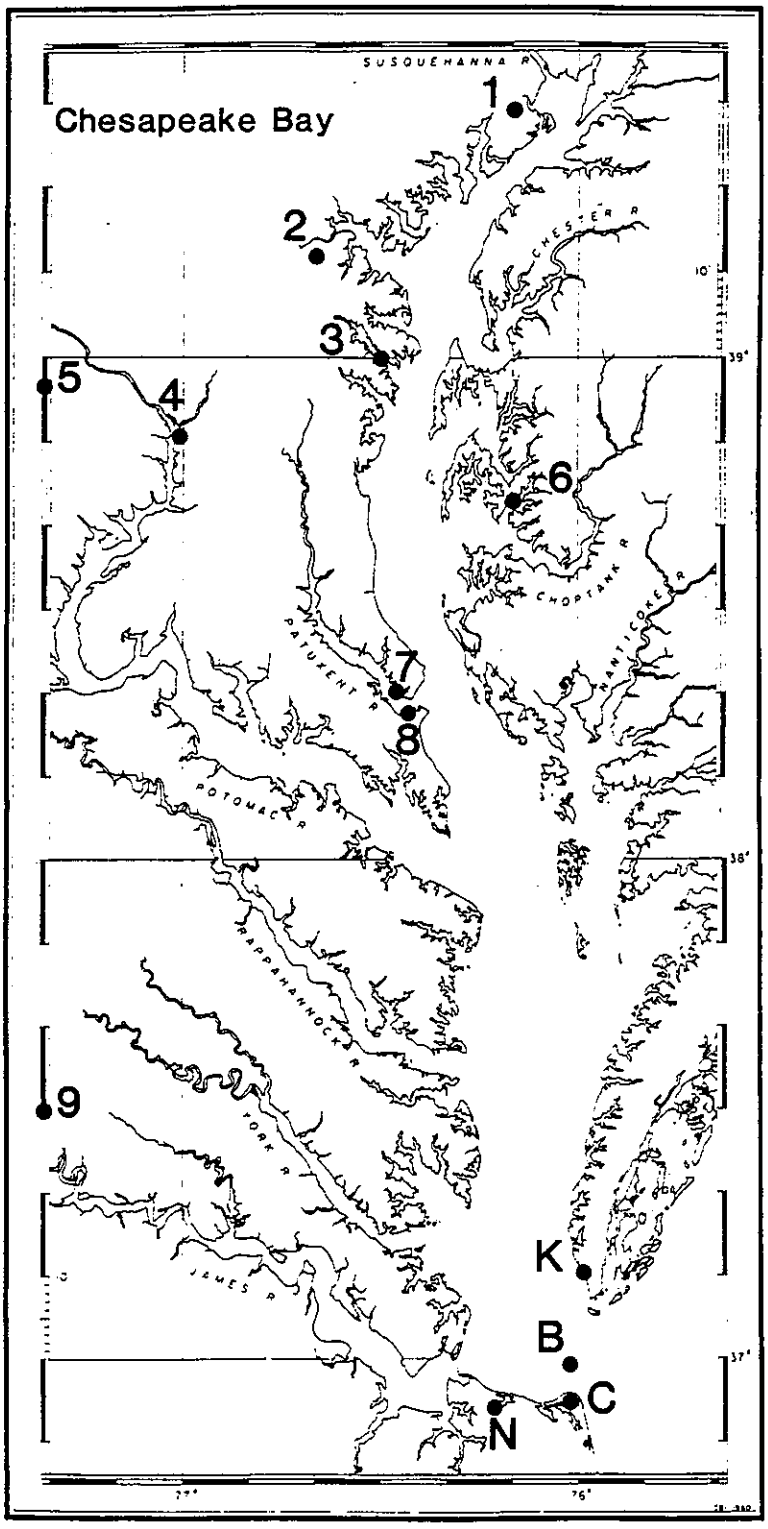

LEGEND

1	ABERDEEN
2	BALTIMORE
3	ANNAPOLIS
4	WASHINGTON
5	CHANTILLY
6	ROYAL OAK
7	SOLOMONS ISLAND
8	PATUXENT
9	RICHMOND
K	KIPTOPEKE BEACH
B	CHESAPEAKE BAY BRIDGE-TUNNEL
N	NORFOLK
C	CAPE HENRY

Figure 2-1. Selected meteorological stations and National Ocean Service (NOS) temperature and density stations in the Chesapeake Bay area. Chantilly and Richmond, VA are, respectively, 7 and 12 minutes (longitude) farther west than indicated. (Modified Chesapeake Bay Institute Map).

Table 2-1. April 1982 precipitation and temperature summary for selected stations in the Chesapeake Bay area. Departures from normal are deviations from the 30 year average of 1951 through 1980.

Station	Total Precipitation/ Departure from Normal (cm)	Daily Average Air Temperature/ Departure from Normal (°C)	Dates/Record Temperatures (Day/°C)
Aberdeen, MD	12.7/4.9	11.1/-0.9	
Baltimore, MD	9.2/1.4	10.4/-1.7	6th/-2.8 7th/-5.6 8th/-3.3 23rd/-0.6
Washington, DC	8.1/0.8	12.2/-1.3	
Chantilly, VA	7.2/-0.4	10.7/-1.0	
Royal Oak, MD	14.4/5.7	11.6/-1.6	7th/-5.0
Patuxent, MD	10.0/2.9	11.7/-1.3	
Richmond, VA	7.5/0.5	13.3/-1.1	
Norfolk, VA	4.3/-2.5	12.8/-1.6	7th/-2.2
Average	9.2/1.7	11.7/-1.3	

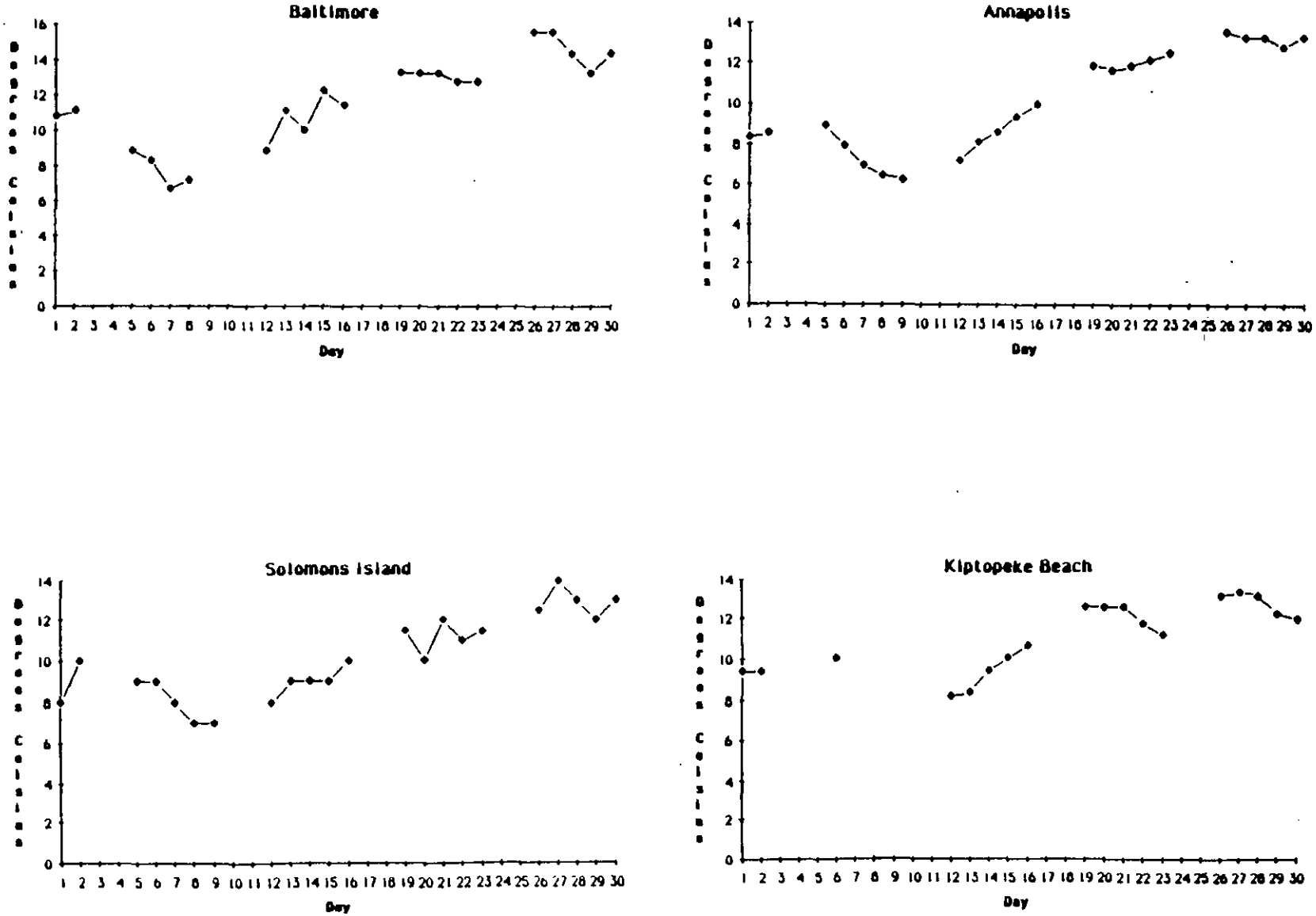

Figure 2-2. Surface water temperatures for locations in the upper (Baltimore, Annapolis), middle (Solomons Island), and lower or Bay mouth (Kiptopeke Beach) regions of Chesapeake Bay for April 1982.

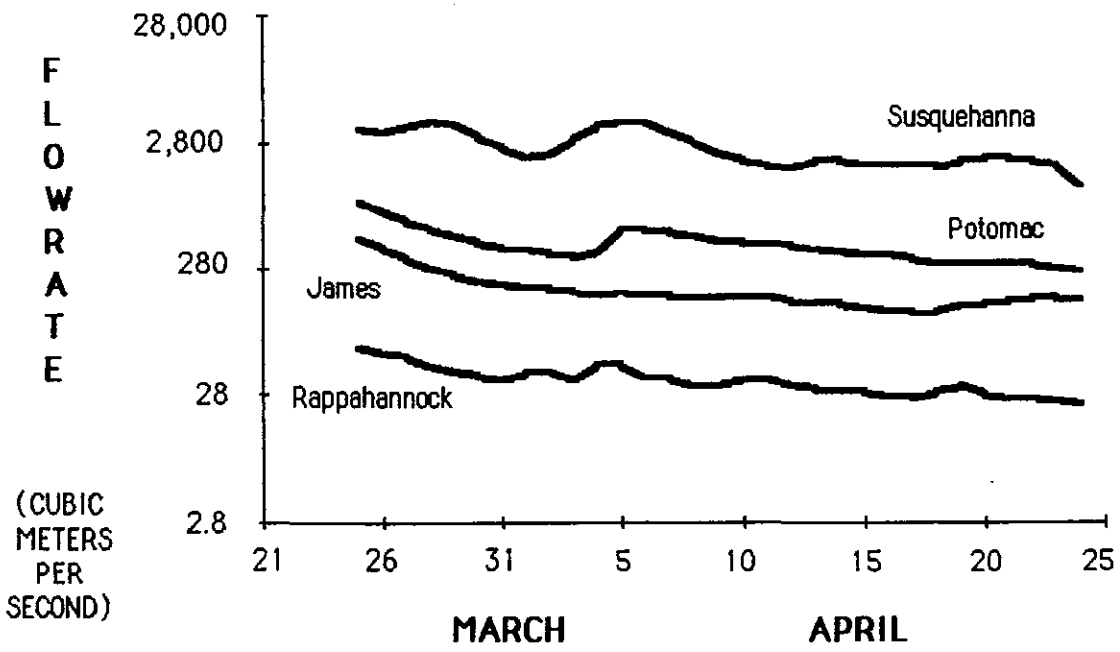

Figure 2-3. Daily mean flowrates of freshwater into Chesapeake Bay from major rivers for 25 March - 24 April, 1982.

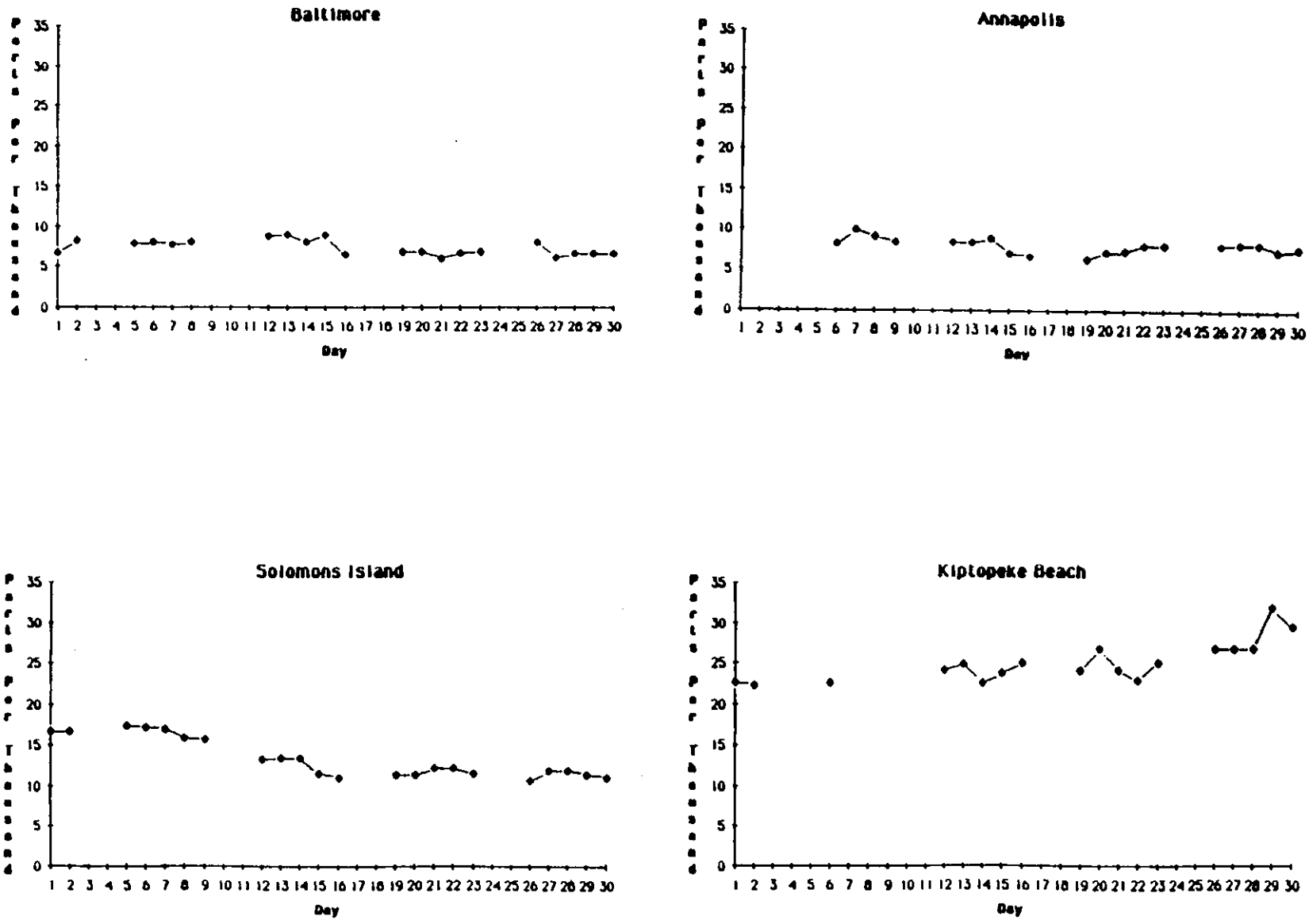

Figure 2-4. Daily surface salinities computed for locations in the upper (Baltimore, Annapolis), middle (Solomons Island), and lower or Bay mouth (Kiptopeke Beach) regions of Chesapeake Bay for April 1982.

A gradual warming throughout the Bay occurred on 16-17 April with a wind flow from the south bringing monthly high temperatures to several stations on 17 April. Surface water temperatures increased from 2 to 3 °C Baywide.

Another cold front passed through the Bay on 18 April, bringing widespread precipitation and winds from the northwest gusting to 13.5 m/sec. An occluded front passed on 21 April dropping low temperatures -1.1 to 10 °C over the Bay from 22-24 April with daily highs from 15.6 to 21.1 °C. Surface seawater temperatures ranged from 10.0 to 13.5 °C for the period and salinity readings remained relatively unchanged Baywide.

Moderate wind flow from the south brought warming temperatures on 25 April, preceding a warm frontal passage on 26 April. Surface water temperatures increased by 0.5 to 1.1 °C throughout the Bay. Thunderstorms occurred over the Bay on 27 April before a cold front pushed through from the west very early on 28 April, bringing widespread precipitation and northerly winds. Small craft advisories were issued Baywide on 27 April and over the southern Bay on 28 April. In the wake of the front, temperatures on 29-30 April were lower. A slight cooling of approximately 0.5 to 1.1 °C occurred in surface seawater temperatures through the remainder of the month. A gradual increase in salinity was evident in the lower Chesapeake Bay for the last week of April.

Only Norfolk and Chantilly received below normal precipitation for the month. Aberdeen, Royal Oak, and Patuxent all received over 2.5 cm in excess of normal precipitation. Much of the precipitation within the Chesapeake Bay drainage basin for April did not result in an increase in streamflow due in part to the freezing temperatures for the period.

For the April 1982 period, surface water temperature anomalies varied between 0.0 and -1.6 °C, with middle and southern Bay areas having the highest deviations. Surface salinities varied from 0.7 to 2.2 ppt above average, with the middle and northern Chesapeake Bay regions experiencing the highest positive anomalies (Table 2-2). Streamflow was normal for March and slightly below normal for April.

Table 2-2. April 1982 surface salinities and surface water temperatures for selected stations in the Chesapeake Bay area. Departures from normal are deviations from the long-term monthly averages.

Station	Surface Salinity/ Departure from Normal (ppt)	Surface Water Temperature/ Departure from Normal (°C)
Baltimore, MD	7.4/1.2	11.7/ 0.0
Annapolis, MD	7.9/0.7	10.2/-1.6
Solomons Island, MD	13.4/2.2	10.2/-1.2
Kiptopeke Beach, VA	25.1/0.7	11.1/-0.6

3. SATELLITE METHODS AND APPLICATIONS

Fred G. Everdale and Richard P. Stumpf

3.1 Introduction

Satellites can provide important data for the study and monitoring of transport in water because of their synoptic and repetitive coverage. Conventional oceanographic data, such as that collected from isolated moorings or from individual cruises, have substantial spatial or temporal limitations. Synoptic data can be collected only at great expense. Spatial variability cannot be properly observed from a limited number of discrete stations or tracklines and cruises cannot often be repeated. Satellites, however, collect data at thousands of points over the surface of the Chesapeake Bay, thereby providing essentially continuous coverage. Certain sensors, such as those on the NOAA weather satellites, provide coverage as often as two to four times a day, permitting the detection of temporal changes over large areas. In producing this detailed and virtually synoptic coverage, satellites can aid substantially in the study of spatial variability and in the modeling of dynamic estuarine and coastal processes. However, they cannot provide information on the vertical structure of the water column; therefore, a combination of in situ measurements, remotely sensed data, and modeling results are needed in the study of estuarine and oceanic processes.

At present, data obtained from satellites yield information on temperature, turbidity, and water color. Each of these characteristics can be used to identify certain water masses or water parcels and to estimate the surface concentrations of sediment and pigments. Therefore, satellites may aid in monitoring fronts and plumes and in identifying circulation patterns in the Bay and on the adjacent shelf.

There are three satellite sensors of potential use in estuarine waters: the NOAA-n series Advanced Very High Resolution Radiometer (AVHRR), Nimbus-7 Coastal Zone Color Scanner (CZCS), and Landsat Multispectral Scanner (MSS) (Tables 3-1 and 3-2). These sensors are on polar-orbiting satellites; i.e., the satellites have orbits oriented north-south in order to allow coverage of the entire globe. The sensors measure the radiance of the reflected visible and near-infrared light and the thermal infrared energy emitted by the earth and atmosphere. Each sensor system has different characteristics, which provide different advantages.

Landsat was designed for use over land, which has greater and more variable reflectance than does water. Accordingly, Landsat data has been shown to provide a good measure of suspended solids in turbid water. However, the satellite sensor is insensitive to slight changes in the reflectance of clear water. Landsat also has very high resolution, 80 m. To achieve this high resolution, the satellite has an overpass period of 16 days, thus limiting the temporal resolution.

The CZCS samples every three to five days in the mid-Atlantic with a resolution of 800 m. It has five reflected light bands and one thermal-IR band, all specifically designed for oceanic waters. It is quite sensitive to variations

Table 3-1. Spectral bands measured by AVHRR, CZCS, and Landsat MSS. Numbers denote sensor channels.

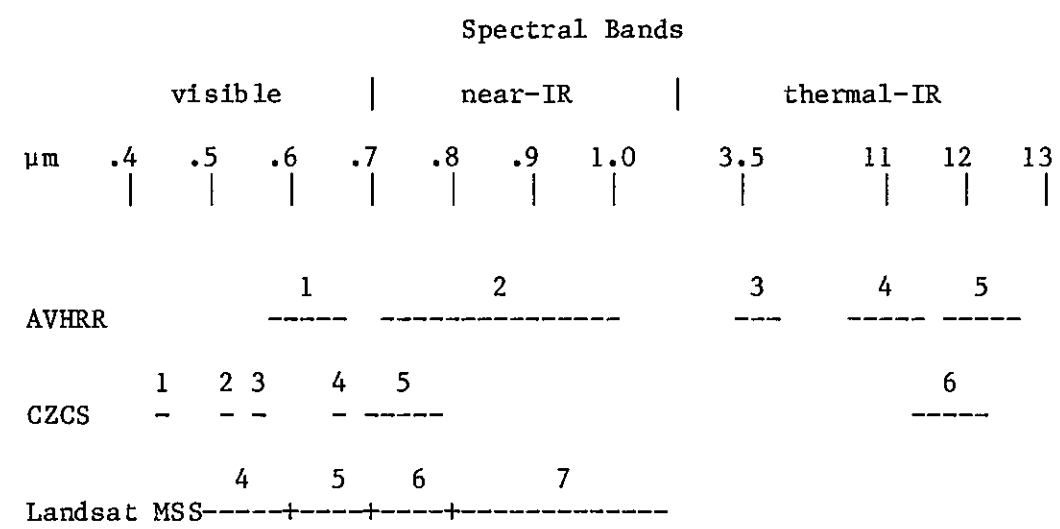

Table 3-2. Characteristics of Satellite Sensors.

	Spatial Resolution (km)	Maximum Scan Angle from vertical	Image Width (km)	Coverage Period (days)
AVHRR	1.1	56	2000	1/2
CZCS	0.82	38	1500	6
Landsat MSS*	.08	6	180	18**

* Landsat Thematic Mapper, which has a spatial resolution of 30 m, began operating in fall 1982.

** In 1979, the period was 9 days. Starting with Landsat 4 in fall 1982, the period between images changed to 16 days.

in water brightness, but is not always usable for turbid waters, like those found in the upper Chesapeake Bay, that reflect enough radiance to saturate some channels on the radiometer. Algorithms for the CZCS data have produced estimates of oceanic chlorophyll content accurate to within 30 percent (Gordon et al., 1983) (Figure 3-1). These results have permitted analysis of biomass on the shelf and in the Gulf Stream, and detection of some eddies and other features of circulation. Unfortunately, the error in these algorithms increases with turbidity, making them highly unreliable in many estuaries. Nonetheless, because the sensor's spectral bands were designed to collect measurements over water, this satellite sensor can provide useful information on estuaries. The CZCS is eight years old, well beyond its expected lifespan, and is beginning to fail. Thus, we cannot depend on it as a future source of data.

The AVHRR sensor is on the NOAA-n polar orbiting satellites. It measures radiance in two reflected (visible and near-infrared) bands and two or three thermal infrared bands. NOAA has developed regression equations to calculate sea surface temperature (SST) using data from the thermal channels (Strong and McClain, 1984). The sensors are intermediate in sensitivity between those of Landsat and CZCS, making them useful in estuaries (Gagliardini et al., 1984). This satellite is designed for frequent sampling of the globe, twice per day with one satellite, and with two operational satellites, four overpasses (two daytime and two nighttime) may be recorded. The resolution of the AVHRR is 1.1 km, making it useful for delineating the larger estuarine and oceanic features.

For application to Chesapeake Bay, the AVHRR and the CZCS systems are preferable because either sensor can include the entire Bay in one scene, and because either system has a high enough sampling frequency to aid in analyzing coastal dynamics and in verifying modeling. Biweekly sampling, like that done by Landsat, supplies more limited information on the dynamics of an estuary.

3.2 Satellite Techniques

3.2.1 Temperature

Using Planck's Law, we can calculate a temperature from the thermal infrared radiation detected by the satellite sensor. Due to atmospheric absorption and emission (primarily by water vapor), the thermal radiance reaching the satellite is not the same as that emitted by the surface of the water. Often the calculated black body temperature is lower than the surface temperature. A technique for atmospheric correction and calibration is required to determine the true surface temperature from the satellite data. The most accurate atmospheric correction entails the use of two or more thermal channels. Because CZCS has only one thermal-IR band, atmospheric corrections for CZCS are less accurate, although we can obtain reliable data on temperature gradients.

The AVHRR, through the use of regression equations developed at NOAA (Strong and McClain, 1984), provides excellent estimates of sea surface temperature using channels 3 and 4, and also channel 5, when available. These

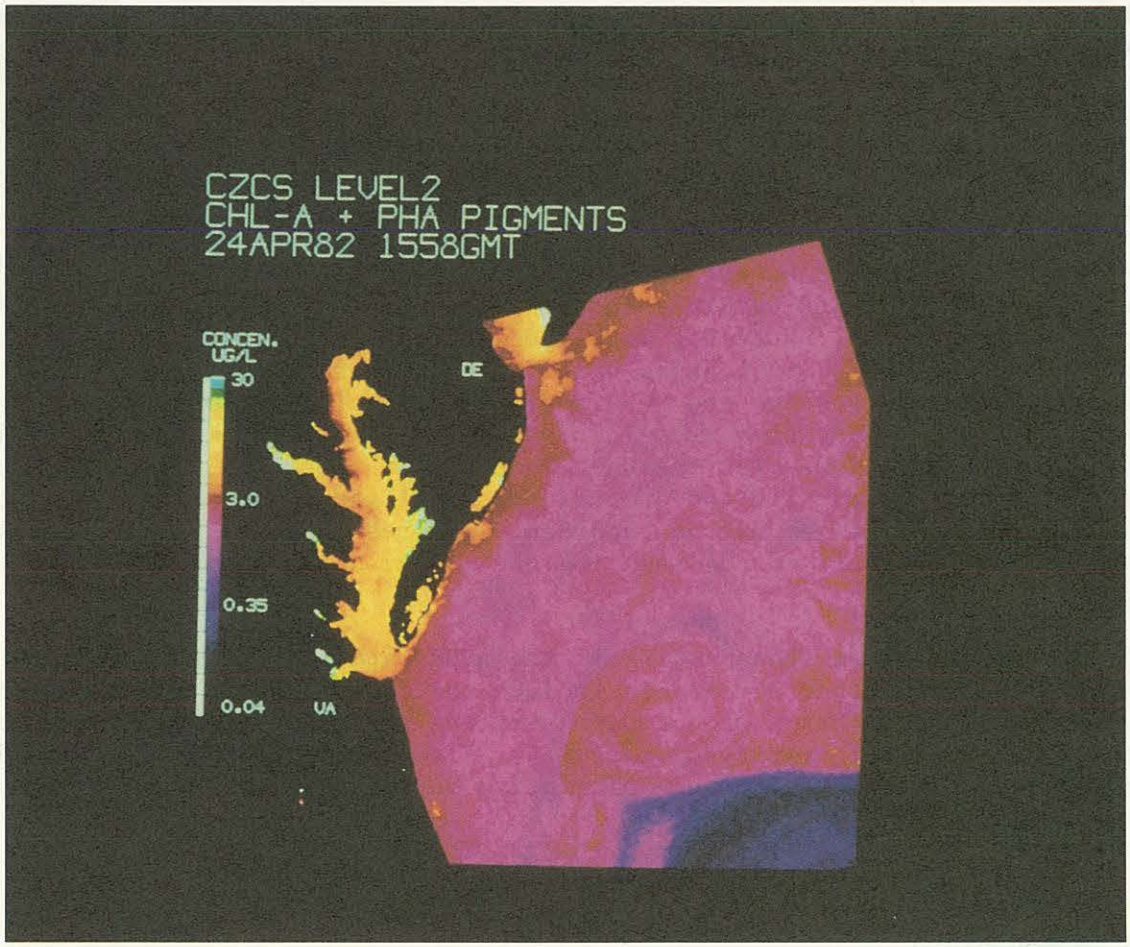

Figure 3-1. CZCS level 2 data showing concentrations of Chlorophyll-a + Phaeophytin, Middle Atlantic, 24-Apr-82. Data from the estuaries are not reliable.

calculated temperatures, "multi-channel sea surface temperatures" (MCSST), are accurate to within 1 °C when compared to ship and buoy data. Much of this 1 °C difference probably results from differences in the measured property; buoys measure bulk temperatures of the upper 0.5-1 m of water, whereas satellites receive radiation from the top millimeter or less of the water (skin temperature). Errors can also result from incomplete correction for the atmospheric effects, particularly for the effects of dust, fog, or thick haze. Because NOAA-6's channel 3 thermal data were noisy prior to September 1982, and the satellite did not have channel 5 (found only on NOAA-7 and NOAA-9), MCSST equations were not available for the April 1982 NOAA-6 imagery. Therefore, in this study, sea surface temperatures for the NOAA-6 imagery were determined by linear regression of channel 4 brightness temperatures against MCSST calculated from NOAA-7 data for the same day. The NOAA-6 temperatures matched the NOAA-7 temperatures to within 1 °C (95 percent confidence level).

3.2.2 Turbidity

Suspended materials provide useful tags of water parcels, and they indicate the extent of runoff, land erosion, and nutrient discharge. Visible or reflected infrared light provides an indication of the quantity of suspended materials by showing the turbidity of the water. However, monitoring and comparing imagery from different days requires a consistent and quantifiable property such as reflectance, or suspended sediment concentration. Determination of these quantities from the raw data requires several corrections of the total measured brightness.

Processing an image first requires the elimination of areas covered by clouds or showing discernible sunglint. Sunglint is the specular (mirror-like) reflection of sunlight off the surface of the water. It may provide useful information on surface phenomena, such as wave fields, but it prevents us from obtaining information on materials in the water, by masking the water column reflectances. The effect is similar to trying to see out a window at night and seeing only your own reflection. Water is a highly effective absorber of near-infrared radiation, therefore, both clouds and sunglint can usually be detected through the increased brightness they produce in near-infrared bands. In the areas not containing clouds or sunglint we can obtain the reflectance of the water column. To obtain reflectance in these areas, we must correct for both the radiance of the atmosphere between the earth and the satellite--known as path radiance--and the amount of total radiance reaching the surface (the incident irradiance).

Over water, path radiance frequently constitutes 50-90 percent of the total visible radiance detected by the satellite. It changes with the dust and water vapor content, and therefore can vary from one image to the next. In addition, the total path radiance generally increases toward the limbs of the image because of the greater thickness of atmosphere. To obtain only the radiance leaving the water, we must subtract the path radiance from the total radiance observed at each pixel by the satellite. The path radiance is usually determined as the radiance observed from the darkest pixels in the locale. In estuarine work, the path radiance is assumed uniform over the study area--a functional, albeit not ideal, correction. Areas near the limbs of the images are generally not usable.

The amount of radiance leaving the water depends on the amount entering; hence, there is need to correct for the incident irradiance. The incident radiance depends on the sun's elevation. Thus, water with a given sediment content will appear darker in the morning than at noon, and darker in the winter than in the summer. In contrast to the atmospheric correction, a calculation of the sun's elevation can be made quite precisely throughout the image, thereby allowing an estimate of the incident irradiance, using the solar constant multiplied by the sine of the solar elevation (Gordon et al., 1983). By dividing the atmospherically corrected water radiance by the incident irradiance, we obtain a form of reflectance that can be compared from one scene to the next with the same sensor band. Early morning and early afternoon scenes for the same day are shown in Figure 3-2. Without the correction to obtain reflectance, the morning scene would show about 60 percent of the turbidity of the afternoon scene. With the corrections, the turbidity becomes comparable in both scenes.

In the estuarine surface waters, reflectance (R) tends to vary directly with the common logarithm of the sediment concentration (n_s),

$$R \propto \log_{10}(n_s) \qquad (1.1)$$

so that a determination of reflectance can also show the amount and variability of suspended materials in the Bay (Munday and Alfoldi, 1979). For the study period, we do not have data on the concentrations of suspended solids, hence the results are shown as reflectance and not as concentrations. However, comparisons of reflectance (corrected turbidity) on different days can help show distribution patterns and paths of transport of suspended materials. In modeling, the suspended material may itself be of interest, or it may serve as a surrogate for other substances or organisms.

3.2.3 Pigments

As described earlier, algorithms developed for the CZCS have given very good estimates of chlorophyll in oceanic and shelf waters. However, the techniques do not provide valid information in many estuaries, because the water's turbidity interferes with the atmospheric correction (Gordon et al., 1983). An algorithm developed in AISC does permit the estimation of relative variations of the chlorophyll concentrations and the detection of algal blooms in turbid water such as found in Chesapeake Bay (Stumpf and Tyler, 1986). The technique is applicable to both AVHRR and CZCS data, although the CZCS, owing to its narrower bands and greater sensitivity, would tend to give results that are more specific to chlorophyll-a. The AVHRR, having broader bands, would respond to variations in other pigments, although it would be principally sensitive to chlorophyll. The corrected radiance as described in the previous section is necessary in these calculations.

Sample results for April 1982 for AVHRR and CZCS appear in Figures 3-3 and 3-4. Blooms appear in the western tributaries, the Rappahannock, Potomac, and Patuxent Rivers. The upper Bay, in the region of the turbidity maximum (Figure 3-2), contains low pigment concentrations. The frequent overpasses of the sensors permit study of diurnal variations in phytoplankton blooms. Many of

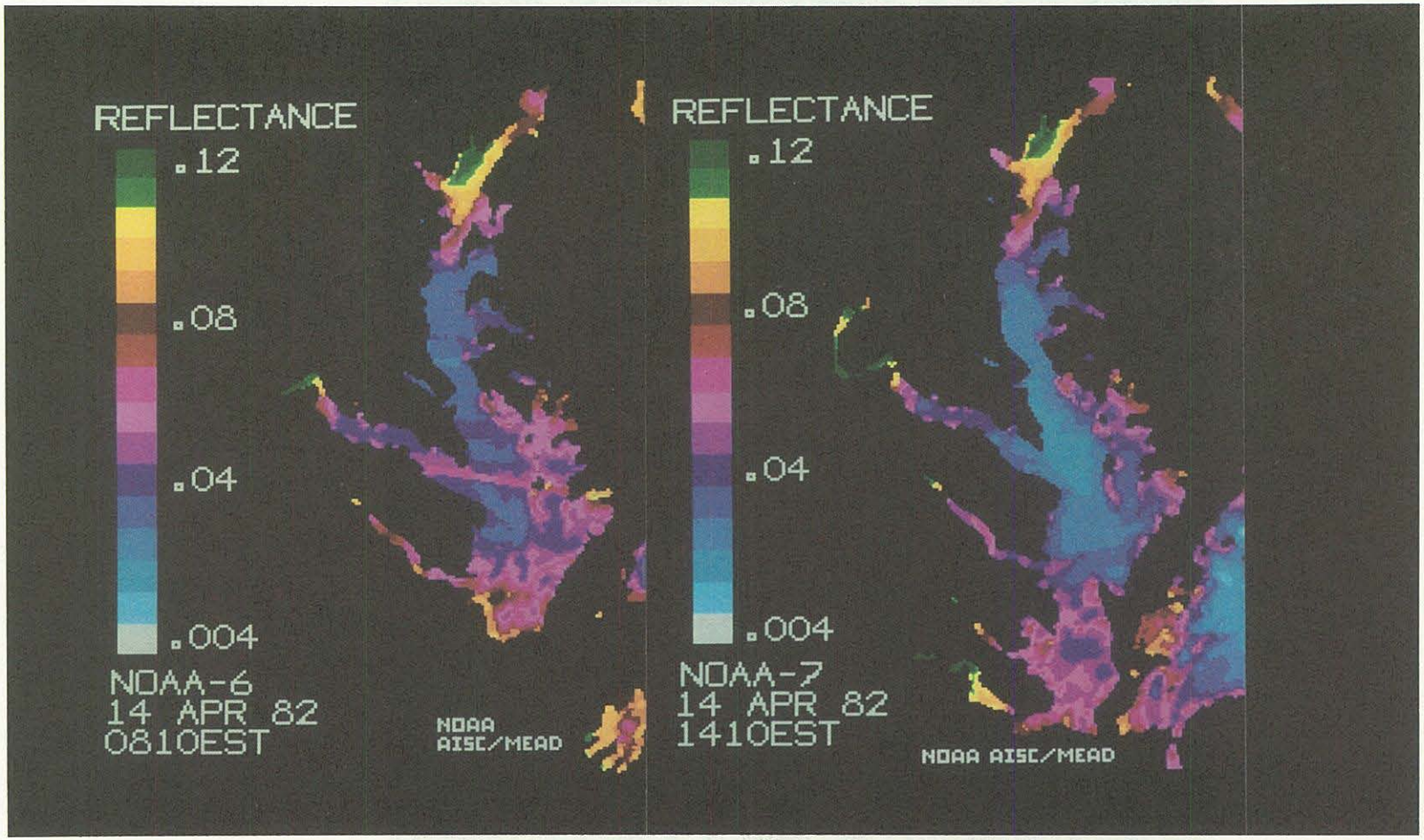

Figure 3-2. Reflectance in Chesapeake Bay from NOAA-6 AVHRR (early morning) and NOAA-7 AVHRR (early afternoon).

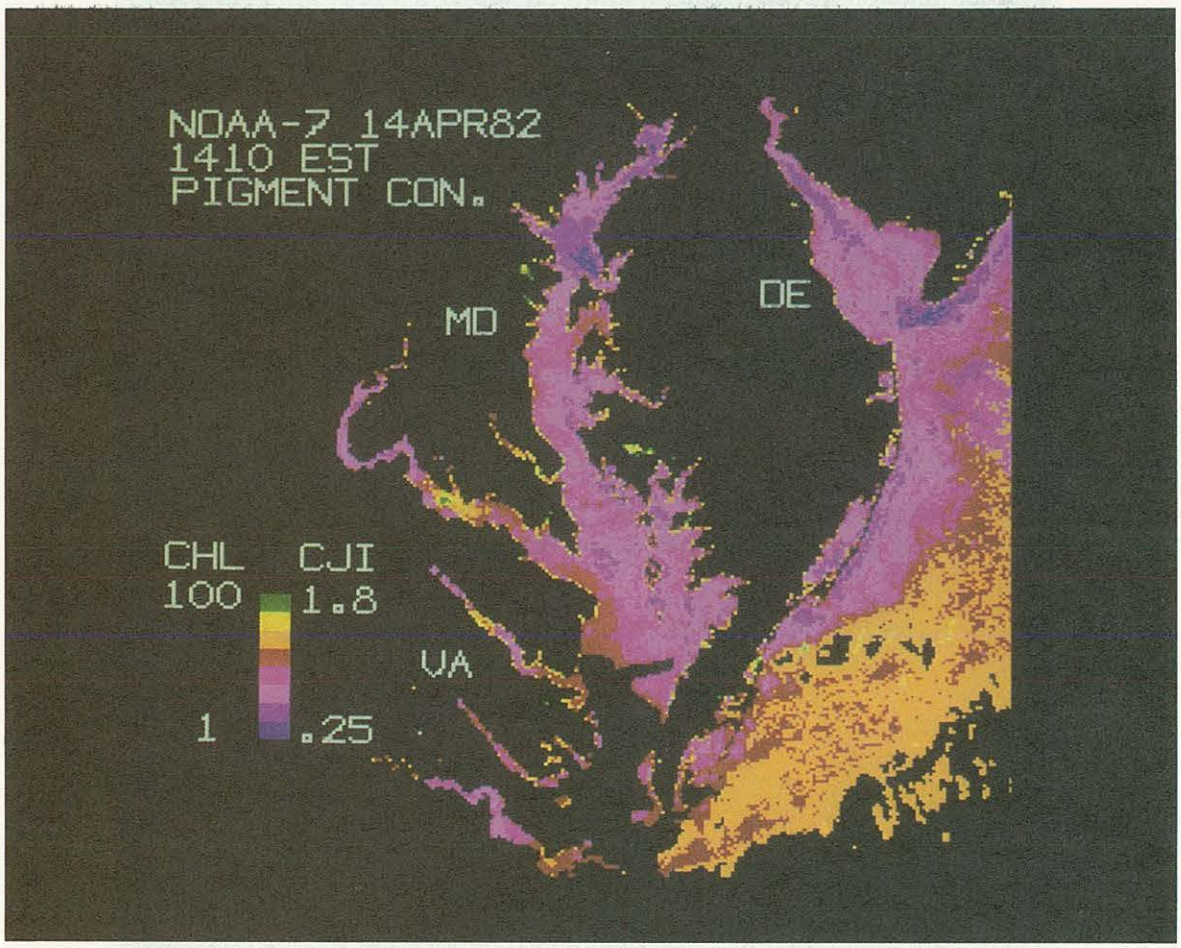

Figure 3-3. Relative pigment concentration, NOAA-7 AVHRR, Chesapeake Bay, 14-Apr-82. Clouds interfere with data at and below Rappahannock River. Offshore data are not reliable.

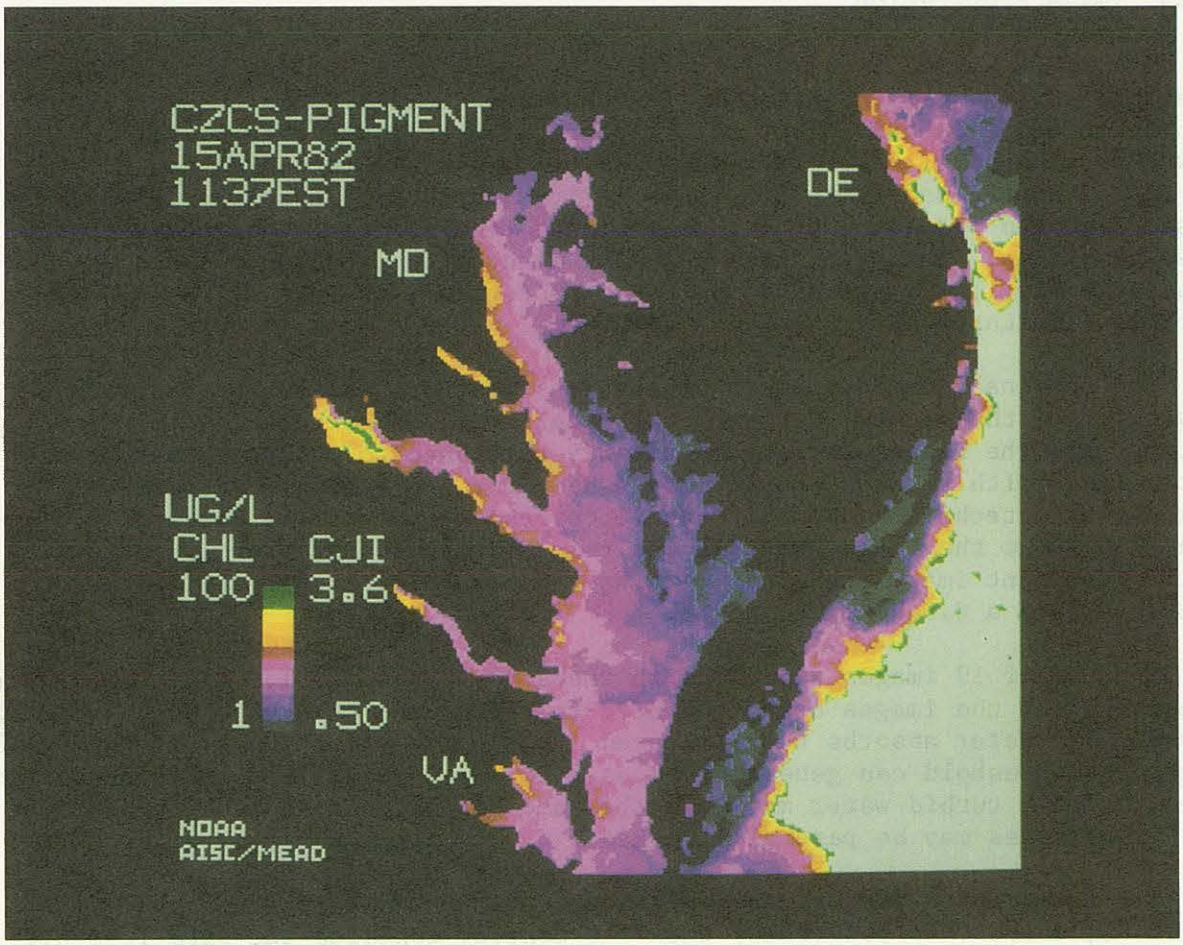

Figure 3-4. Relative pigment concentration, CZCS, Chesapeake Bay, 15-Apr-82. Offshore data are not reliable.

the blooms result from algae transported into the area, so that modeling the drift would be helpful in predicting the onset of these blooms. Conversely, detection of blooms with satellites can provide data to aid the calibration of drift models.

3.2.4 Image Preparation

The AVHRR and CZCS collect the data by scanning in a line across the satellite's path, collecting about 2000 radiance measurements on each line. Each measurement is called a pixel (picture element); the area of the earth viewed in each pixel determines the resolution, 1.1 km for AVHRR and 0.8 km for CZCS. As the satellite continues in its orbit, each scanline is slightly offset from the preceding one, thus an image results from the accumulation of these scanlines. The satellites take 1-2 minutes to produce an image of Chesapeake Bay. An image differs from a photograph, wherein all points are recorded simultaneously.

The original images contain distortions that are caused by the earth's curvature and the viewing angle of the satellite. To correct for the distortion, all the images were geometrically stretched to match certain points in the image with reference points on a Mercator projection. Because this commonly used technique does not assure correspondence with a Mercator projection throughout the image, we call the result a pseudo-Mercator projection. On the resultant image the AVHRR data have a 1.2 km/pixel projection, and the CZCS data have a 0.9 km/pixel scale.

A total of 19 images were used in the study (Table 3-3). Land and clouds were masked in the images using the near-infrared band (AVHRR channel 2, CZCS channel 5). Water absorbs near-infrared light quite effectively; therefore, a brightness threshold can generally be used to distinguish land and clouds from water. Highly turbid water may have the same reflectance as land, therefore some tributaries may be partially masked.

The temperature images were color-contoured in 1 °C intervals between 7 and 18 °C, where (for reference) the 7 °C contour contains the data from 6.95 to 7.95 °C. Temperatures outside that range were not distinguished.

The reflectance (turbidity) data were grouped into 16 classes and colored. Small values of reflectance should be interpreted as water that is relatively clear, i.e., the water does not contain large quantities of material, either organic or inorganic in suspension. Larger values of reflectance denote increasing quantities of suspended material in the upper water column. Reflectance indicates only the degree of water clarity or the relative quantity of materials in the water and does not indicate the composition of those materials.

3.3 Satellite Imagery Analysis and Interpretation

The distributions of temperature and turbidity (reflectance) in the satellite imagery are used to infer some of the circulation dynamics and water

Table 3-3. Imagery of Chesapeake Bay used in this study.

Date	Time (EST)	Satellite	Orbit Number
10 April 82	0800	NOAA-6	14477
	1148	CZCS	17475
12 April 82	0805	NOAA-7	04134
	1045	CZCS	17502
	1429	NOAA-7	04141
14 April 82	0239	NOAA-7	04162
	0810	NOAA-6	14534
	1410	NOAA-7	04169
15 April 82	0230	NOAA-7	04176
	0740	NOAA-6	14548
	1137	CZCS	17544
	1400	NOAA-7	04183
16 April 82	1157	CZCS	17558
	1345	NOAA-7	04197
18 April 82	0810	NOAA-6	14591
	1050	CZCS	17585
23 April 82	0755	NOAA-6	14662
	1400	NOAA-7	04296
24 April 82	1058	CZCS	17668

quality of the Bay and the adjacent shelf and slope region. The region contains four principal water masses: the Bay waters, the shelf water, the slope water, and the Gulf Stream. Temperature imagery for the study period can be used to discern variations in all four. Reflectance, however, provides information only on the Bay waters; the sensitivity of the sensor and the quality of the atmospheric correction cannot discern variations in the reflectance of the comparatively clear offshore waters during this period.

3.3.1 Chesapeake Bay

Insolation can significantly influence the surface skin temperature of the Bay. In the satellite imagery, the Bay cools by 1 to 4 °C at night, and warms throughout the day. Reduced vertical mixing during periods of reduced wind speeds may promote this variability. Figure 3-5 (12 April) shows the low nighttime temperatures in the Bay. The surface temperatures fall below 8 °C in the upper Bay, and below 7 °C in the lower Bay (below the Rappahannock River). By early afternoon (Figure 3-6), diurnal heating has greatly increased the temperatures. The entire Bay has warmed by as much as 4 °C. *In situ* data taken in the Bay on this day correspond to the satellite-derived daytime temperatures. The shelf waters have warmed to a lesser extent (1 to 2 °C), while negligible changes appear in the slope and Gulf Stream waters. The difference between the day and night temperatures observed during the study period may result from either diurnal variations in the skin temperature or fog and mist over the Bay at night. If the variation is in the skin temperature, it does not necessarily indicate temperature fluctuations in the upper meter of the water column, because the skin temperature can react rapidly to changes in air temperature and sunlight.

The seasonal increase in surface temperature is evident during the study period. Some warming is evident on 15 April (Figure 3-7). By 23 April (Figure 3-8), the Bay and shelf have warmed substantially, about 4 °C throughout the area. Shallow waters, such as those in the sounds and tributaries, respond relatively quickly to changing insolation and air temperatures, while the deeper waters of the Bay and shelf respond more slowly. Thus, the western tributaries and eastern shore of the Bay contain warmer water than does the central Bay. Similarly, the lower Bay has warmer water than the adjacent shelf. Therefore, temperature can be used to infer transport of tributary water in the Bay and certain characteristics of the exchange of water between the Bay and the shelf.

The flows from the four largest tributaries, the Susquehanna, Potomac, Rappahannock, and James appear to hug the western shore. This is particularly evident on 12 April (Figure 3-6), where cool northern Bay and Susquehanna water follows the western shore, as does the 9 °C water leaving the Potomac River. The warm waters associated with the Rappahannock, York, and James Rivers appear to flow along the western shore down the Bay and out the mouth around Cape Henry (Figures 3-6 through 3-8).

The reflectance is generally highest in the upper reaches of the Bay and its tributaries, decreasing with distance downstream (Figure 3-9, 3-10; cf. Figure 3-2). The main Bay, Potomac River, and James River show turbidity maxima at the upper reaches with a rapid decrease in reflectance and fairly clear water

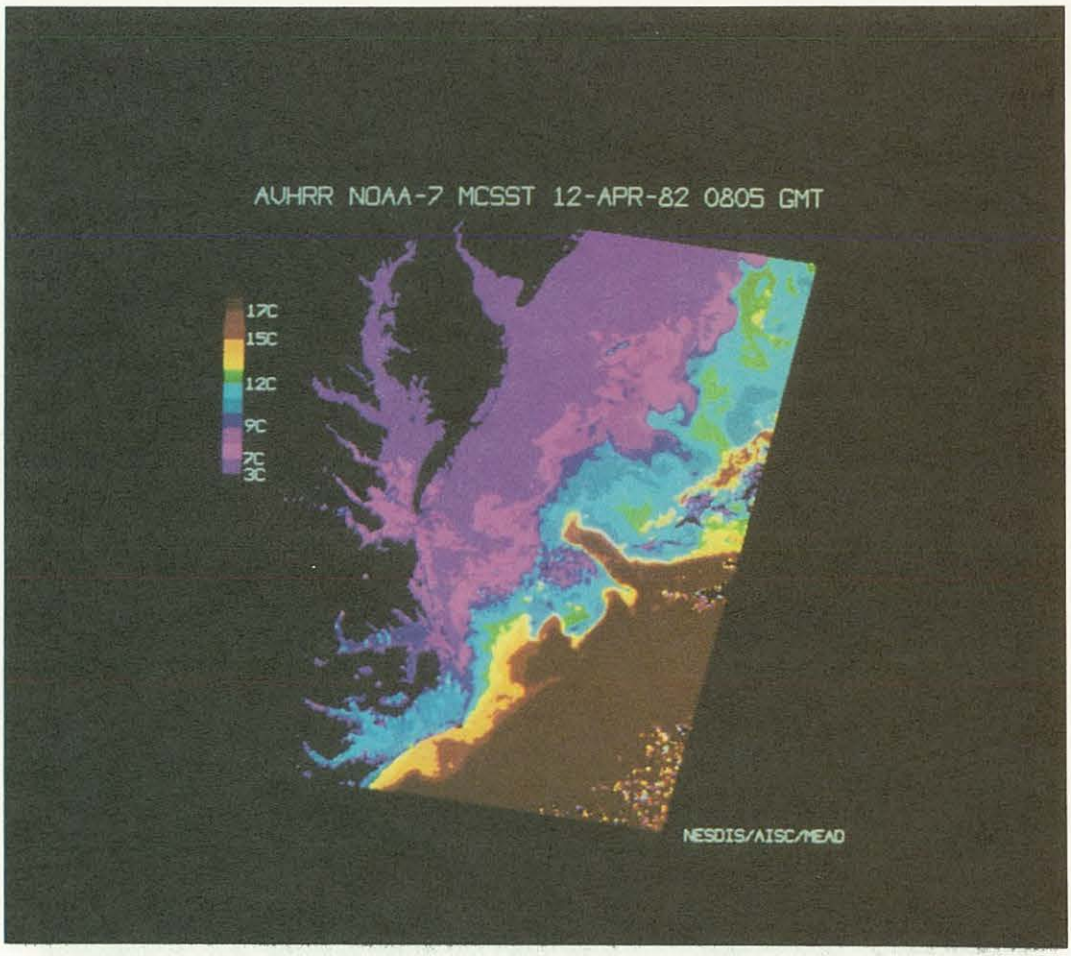

Figure 3-5. Sea surface temperature 12-Apr-82 0805 GMT (0305EST), pre-maximum ebb at Bay mouth. Wind 6.0 m/sec (12 kn) to ESE.

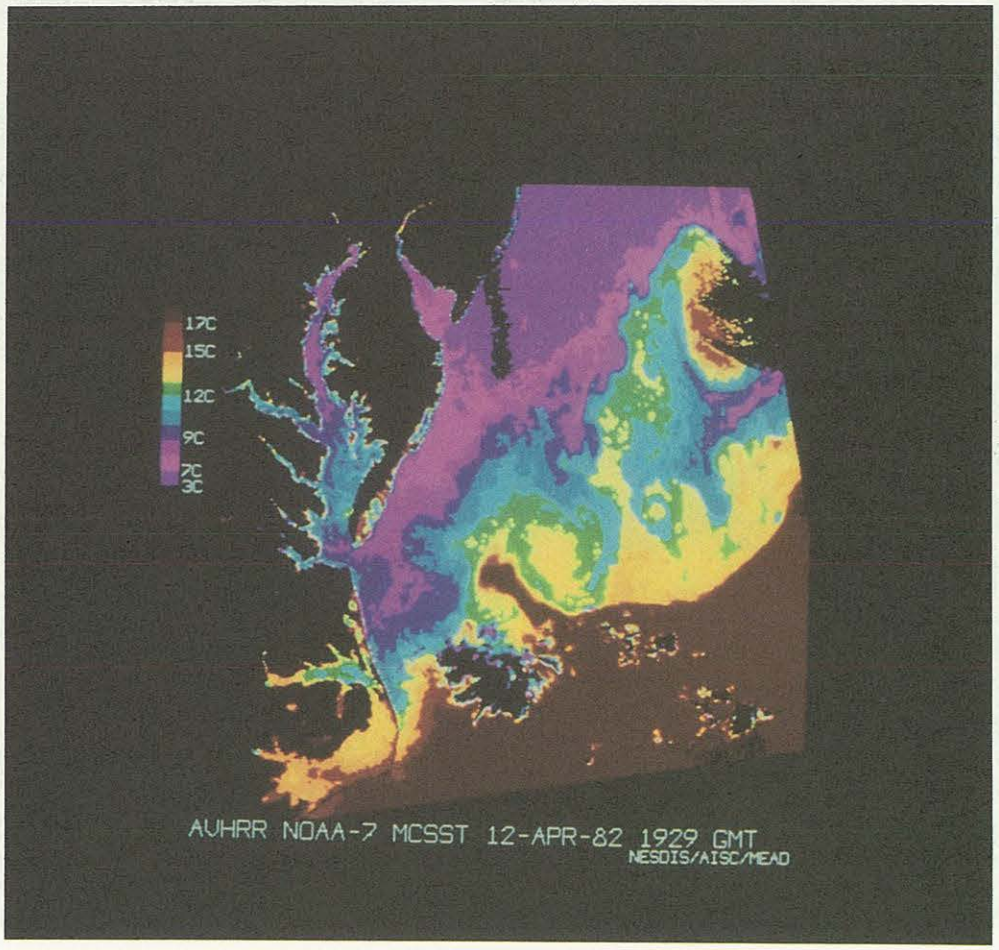

Figure 3-6. Sea surface temperature 12-Apr-82 1929 GMT (1429EST), pre-maximum ebb at Bay mouth. Wind 1.2 m/sec (2.5 kn) to E. A smoke plume from a power plant on the Bay just above the James River has distorted the measurements, producing a patch of invalidly low temperatures across the Bay at the mouth.

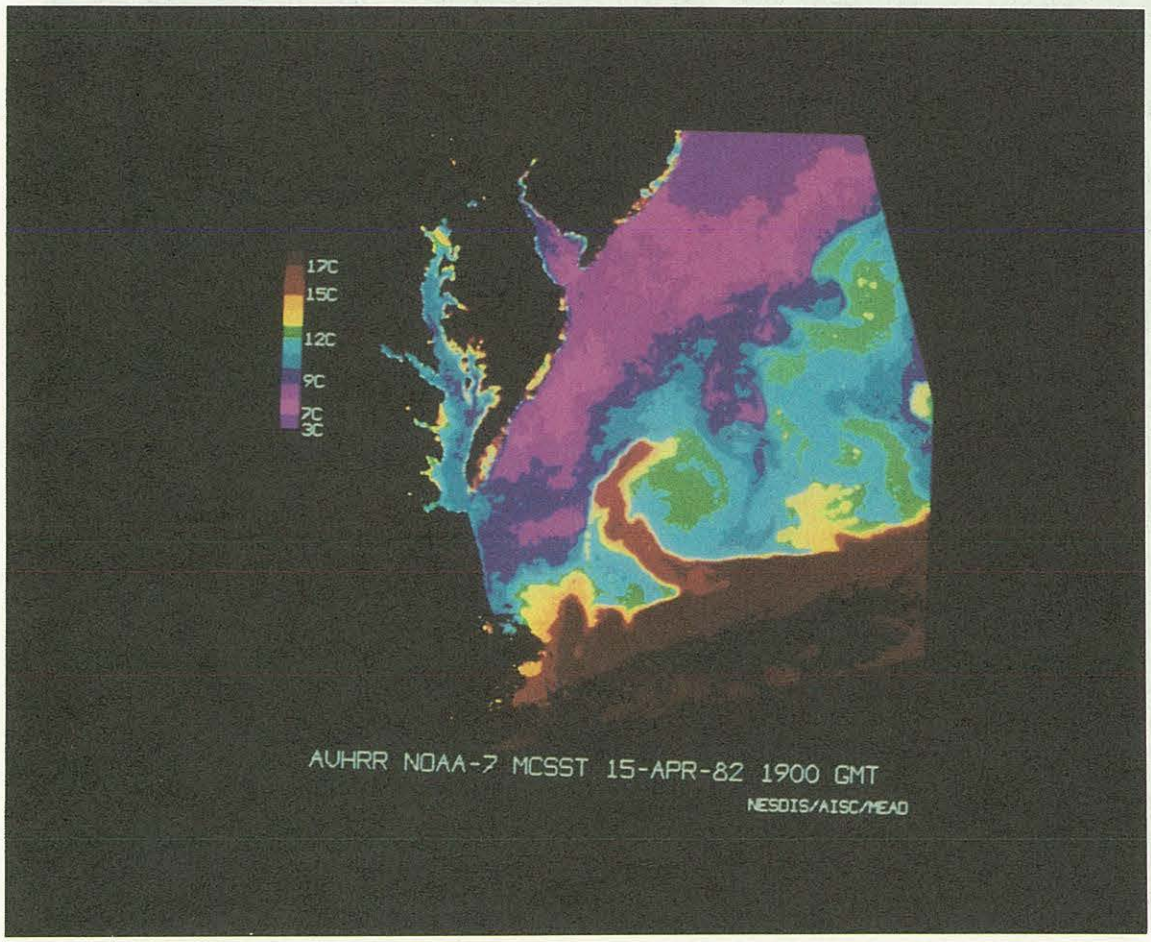

Figure 3-7. Sea surface temperature 15-Apr-82 1900 GMT (1400EST), maximum flood tide stage at Bay mouth. Wind 4.2 m/sec (8.5 kn) to W.

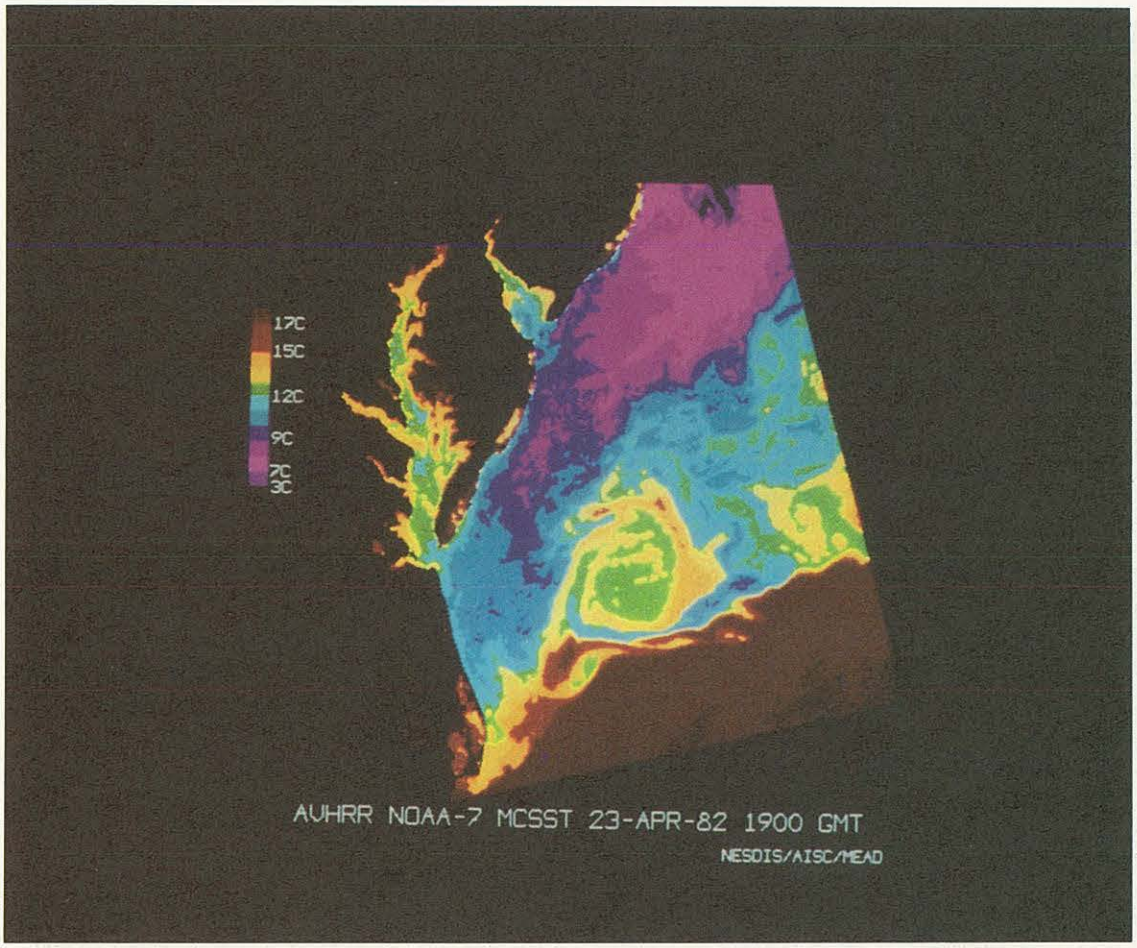

Figure 3-8. Sea surface temperature 23-Apr-82 1900 GMT (1400EST), maximum ebb tide stage at Bay mouth. Wind 7.6 m/sec (15 kn) to SE.

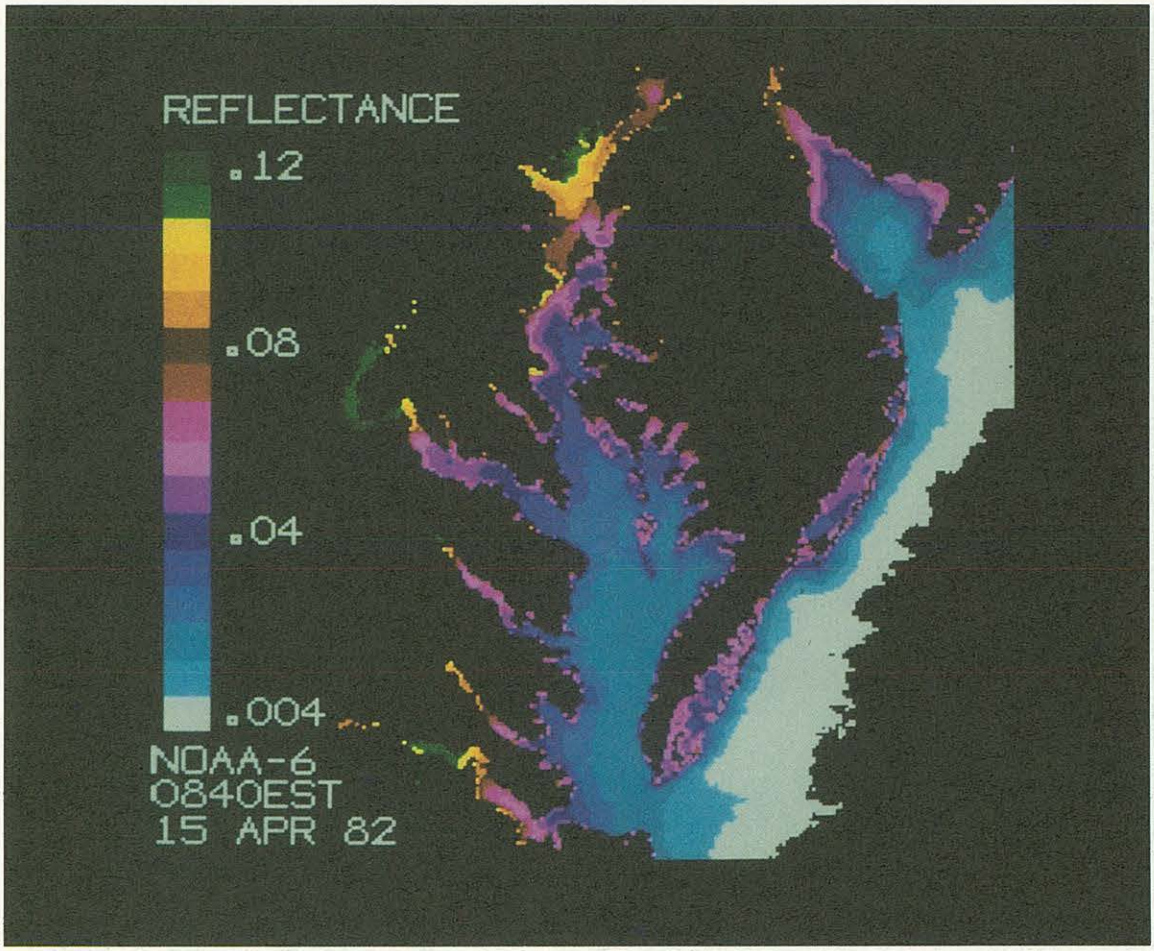

Figure 3-9. Reflectance (turbidity) 15-Apr-82 1240 GMT (0740EST), maximum ebb tide stage at Bay mouth. Wind 3.6 m/sec (7 kn) to W.

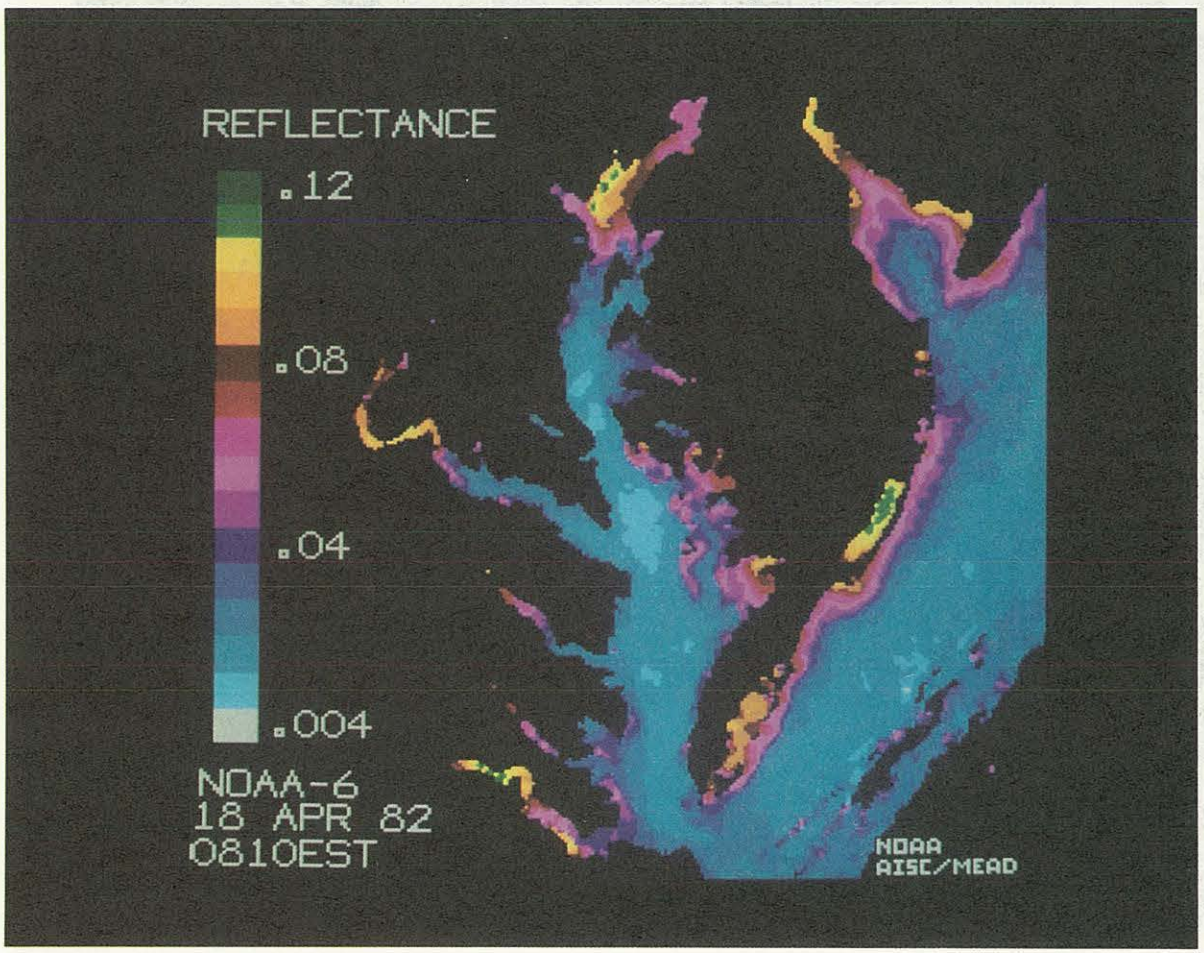

Figure 3-10. Reflectance (turbidity) 18-Apr-82 1310 GMT (0810EST), post maximum flood tide stage at Bay mouth. Wind 5.6 m/sec (11 kn) to E.

downstream, as material supplied by the rivers settles from the surface. In the main Bay, lateral variations appear in the turbidity maximum. A slanting (SSW-NNE) front appears, particularly in Figure 3-9. This front coincides with a temperature front (Figure 3-7). Similarly, the James River shows a marked cross-stream gradient (Figure 3-9).

The water of the central Bay, off the Potomac and Rappahannock Rivers is clearer and colder than the adjacent waters. These differences result from the greater depth of the water, which reduces both warming and sediment resuspension, and the greater distance from riverine and shoreline sources of sediment.

The thermal and turbidity fronts at the mouths of the Rappahannock, York, and James Rivers coincide (Figures 3-7 and 3-9). The Bay mouth plume shows a more complicated structure. The temperature and turbidity plumes do not always coincide, although the turbidity plume, owing to its low reflectance, is less pronounced than the plumes and fronts within the Bay.

The thermal plume's position is highly variable. Early on 12 April (Figure 3-5), the warmer Bay water appears to branch; one limb hugs the coast to the south for some 100 km, the other limb moves directly offshore, suggesting intense mixing. This structure may result from the 12 kn winds from the west pushing water offshore. In the afternoon the plume is oval (Figure 3-6), although tending southward. A bulge of turbid water appears off the mouth of the Bay at this time (Figure 3-9). A thermal plume is distinct, despite the maximum flood tide at the mouth of the Bay. Small detached pools of 10 °C water are observed offshore. Two or three elongated filaments suggest intense mixing. Again, as on 12 April, the plume extends to the south. The 10 °C ribbon of water along the North Carolina coast may be simply warm nearshore water and not water from the Bay.

3.3.2 Offshore Waters

The water masses of the shelf, slope, and Gulf Stream show strong mixing and marked spatial variability in temperature during the period. The shelf waters, are cooler (3 to 11 °C) than the other water masses. Diurnal fluctuations in observed surface temperature occur in the shelf waters (Figures 3-5 vs. 3-6), but to a lesser degree than in the Bay. Near Cape Hatteras, the warm Gulf Stream (>15 °C) pinches off the shelf waters of the mid-Atlantic Bight. The Gulf Stream veers to the northeast from Cape Hatteras. Because the slope water originates as a mixture of shelf and Gulf Stream waters, it has intermediate temperatures to shelf and Gulf Stream waters. Thermal fronts sharply delineate the three water masses: the shelf break front between the slope (blue-green) and shelf (purple) waters, and the north wall of the Gulf Stream (Figure 3-6).

Gulf Stream eddies also can be tracked with the imagery. A warm core eddy, Eddy 12, having clockwise rotation, lies about 180 km off the mouth of the Bay. The eddy becomes increasingly evident through the study period because a filament of warmer Gulf Stream water wraps around it. The filament of 15 °C water

develops on the SW side of the eddy (the eddy center is green) (Figure 3-5). On the NE side, cold shelf water is apparently being advected onto the slope by the eddy. By 15 April, the filament has partially encircled the eddy and the cold water (10 °C) has moved around the eddy almost to the Gulf Stream (Figure 3-7). On 23 April, the filament has encircled the eddy and the cold water has moved between the eddy and the Gulf Stream (Figure 3-8). The eddy also appears in the chlorophyll pigment image (Figure 3-2). As the Gulf Stream has much lower chlorophyll than the slope or eddy, the filament appears as a ring of lower chlorophyll water.

3.3.3 Summary

Data collected by satellites can show spatial and temporal changes in temperature, reflectance, and color (pigments) in the Bay and offshore. The high sampling frequency of the NOAA-n series and CZCS permits detection of daily and weekly variations in temperature. Temperature contrasts during the period were strong, the imagery showing fronts of 4-5 °C and a temperature range of 15 °C. Although turbidity showed slight changes over the study period, spatial variability in turbidity is quite evident in the images. The images show the turbidity maxima near the heads of the Bay and the major tributaries, and the clear water in the lower central Bay and offshore.

The Bay mouth temperature and turbidity plumes were neither well defined nor (apparently) persistent, thus movement during the period could not be inferred from a set of images. The greater temperature contrast offshore and the persistence of distinct features such as Eddy 12 did allow tracking of these features by satellite. This indicates that the movement of comparably distinct features within the Bay (such those produced by floods) could be traced.

Analysis of the imagery allows us to infer characteristics of the Bay's surface circulation for the conditions of the study period. The Susquehanna River waters produce a southward flow along the western shore, probably because of Coriolis force. As the Susquehanna and northern Bay waters move southward, they become less turbid. The temperature also changes because increasing time is available for mixing, sensible heat exchange and solar insolation. From the Patuxent River to the Rappahannock, a pool of clear and cooler water persists. This region is relatively deep and furthest from sources of suspended sediments and freshwater; hence it has low turbidity and the uniform and cooler temperatures. Plumes emanating from the Rappahannock and York Rivers are advected southward along the western shore. This water appears to merge with the James River plume and the combined unit moves seaward along the coast around Cape Henry.

Most of the exchange of water with the shelf probably involves the central and eastern portions of the lower Bay. This Bay water closely resembles the shelf water in turbidity and temperature, hence the exchange cannot be readily seen in the images.

3.4 Conclusions

Satellites can provide important environmental information on Chesapeake Bay and the adjacent shelf. Using the satellite data, we can obtain a synoptic view of sea surface temperatures, particularly during the day, calculate the reflectances caused by suspended solids, and determine the presence and strength of phytoplankton blooms. Some characteristics of surface circulation can be inferred from the distributions of temperature and reflectance. With the presence of well defined features, the satellite data can be used to determine actual circulation, as shown by the movement of Eddy 12 on the shelf.

At present, satellites can provide accurate temperatures within 1 °C. Reflectance values give an indication of the relative concentration of suspended solids; however, estimates of actual concentrations will depend on our ability to calibrate in situ data against remote measurements of reflectance. Similarly, the pigment index requires additional calibration in order to make it more widely applicable. However, the use of reflectance and a pigment index show the potential ability of satellites in studying and monitoring estuaries.

The temperature data can be used to initialize the surface temperature component of the MECCA circulation model. In addition, it can be used to verify the temperature distributions predicted by the model (section 6.6.3). Similarly, when material transport is added to the model, bloom and reflectance distributions could be compared with the model predictions. The synoptic coverage and availability of satellite data fill a void caused by the logistics and expense of conventional oceanographic measurements.

3.5 References

Gagliardini, D.A., H. Karszenbaum, R. Legeckis, and V. Klemas. 1984. Application of Landsat MSS, NOAA/TIROS AVHRR, and Nimbus CZCS to study the la Plata River and its interaction with the ocean. Remote Sensing of Environment 15:21-36.

Gordon, H.R., D.K. Clark, J.W. Brown, O.B. Brown, R.H. Evans, and W.W. Broenkow. 1983. Phytoplankton pigment concentrations in the Middle Atlantic Bight: comparison of ship determinations and CZCS estimates. Applied Optics 22: 20-36.

Munday, J.C. and T.T. Alfoldi. 1979. Landsat test of diffuse reflectance models for aquatic suspended solids measurement. Remote Sensing of Environment 8:169-183.

Strong, A.E. and E.P. McClain. 1984. Improved ocean surface temperatures from space--comparisons with drifting buoys. Bulletin American Meteorological Society 62(2):138-142.

Stumpf, R.P. and M.A. Tyler. Satellite detection of bloom and pigment distributions in estuaries. (submitted to Limnology and Oceanography).

Satellite Applications

U.S. Department of Commerce. 1982. Tidal Current Tables, Atlantic Coast of North America. NOAA, National Ocean Survey, Rockville, Md.

4. SATELLITE IMAGERY AS AN INPUT TO A CIRCULATION MODEL

Marlene K. Stern

4.1 Introduction

Satellite imagery of the Chesapeake Bay can be a valuable source of data for the verification and calibration of MECCA (Hess, 1985). Each image contains thousands of pixels which can serve as data for comparison with the circulation model. In order to take advantage of this data source a method must be developed to accurately sample the block of pixels which corresponds to the 11.2 x 11.2 km sized grid cell of MECCA. This chapter describes a preliminary investigation into such a technique. Emphasis is placed on sampling pixels within a grid cell, matching the location of a pixel in an image with its correct location on the model grid, and determining the spatial resolution obtainable by this method.

4.2 Methods

Sea surface temperature images of the Chesapeake Bay from 12-23 April 1982 were displayed on the image processor screen. The model grid, which was photocopied onto a transparency, was then placed against the screen of the image processor and aligned with the coastline of the selected image. Because the Chesapeake Bay images were not identical in size, reductions of the grid were made until each image had an adequate grid overlay. This arrangement allowed a match of pixels with grid cells. Each grid cell includes approximately 84 pixels and each pixel has an intensity value which is converted to a temperature. Temperatures are incremented in quarter degrees Celsius.

The method for sampling pixels from the north, south and deep water boundaries of MECCA (Figure 4-1) is as follows. First, the intensities of two pixels, from diagonally opposed corners of a MECCA cell, were determined. When the temperature gradient in a cell was 1 °C or less, two pixels near the center of the cell were selected because it was quicker than selecting pixels from diagonal corners. If the intensity difference between the two pixels was 4 (1 °C) or less, the intensities were averaged and that average used as the intensity for the cell. If the intensity difference between the two diagonal pixels was 5 or 6, a third pixel was sampled from the center of the grid cell. If the value from the third pixel fell within the range of the first two, all three pixel values were averaged to calculate the cell's intensity. If the value from the third pixel fell out of the range of the first two, then a 7 by 7 pixel "window" was fitted over the cell and the average intensity of 49 pixels within the cell was calculated with an image processor-library routine. If the intensity difference between the first two pixels was 7 or greater, the window average was also used. These dimensions, 7 by 7, were selected because the window fitted easily into the cell yet greatly increased the number of points sampled. The surface area covered by the window was 59.29 km^2, approximately half the area covered by a model grid cell. While the window allows for a more accurate determination of a cell's intensity, it was not used for each cell because it takes much longer for the image processor to calculate an average than to read back an intensity for a single pixel.

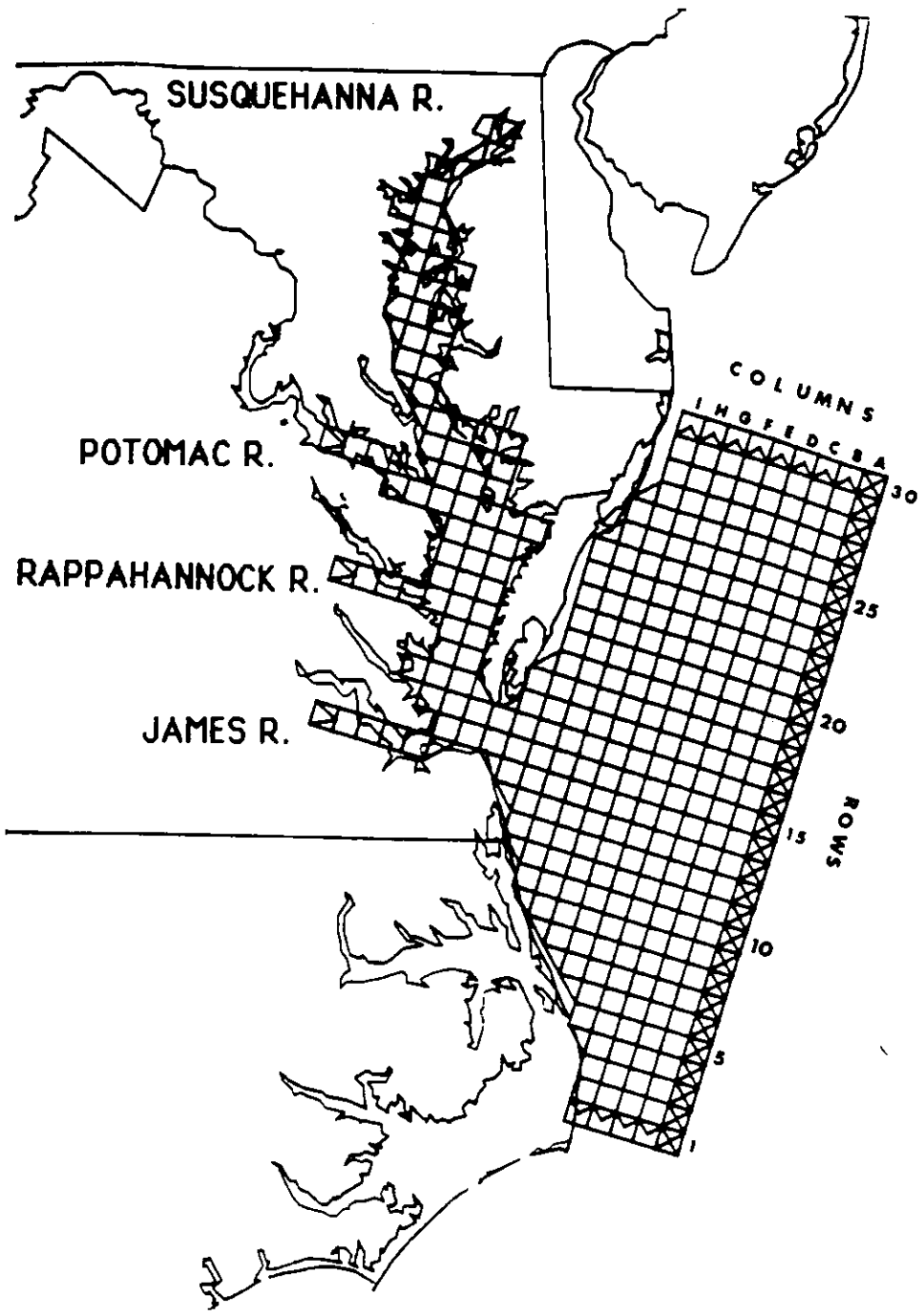

Figure 4-1. MECCA grid showing cell labeling scheme used in this chapter. Columns are assigned letters and rows are assigned numbers.

For a quantitative evaluation of the sampling scheme, the following method was used. On the image of 12 April at 0805 GMT, temperatures of all cells in the northern half of the offshore portion of the grid were determined using both a 7 by 7 pixel window and the average of two pixels in diagonally opposed corners of a cell. A total of 179 cells were sampled and the temperatures were compared between methods.

The results of the comparison of sampling with a window versus sampling with two pixels are shown in Table 4-1. Of the total number of comparisons, 95 percent had intensity differences between 0.5 and -0.5. The category for zero difference between sampling methods had the greatest number of occurrences of all categories and accounted for 43 percent of all the comparisons. A regression of window values versus pixel values (Figure 4-2) had a slope of 1.01 and an R^2 value of 0.95 with an F-value that was significant at the 0.0001 level, reflecting excellent agreement between the sampling methods.

In the course of sampling the satellite imagery, difficulties in correctly matching pixels with the proper grid cells became apparent. Part of the problem was due to parallax. Depending on the angle from which one viewed the screen of the image processor, the cursor shifted with respect to the overlay. The spatial error associated with this is no more than a quarter of a grid cell (2.75 km) in any direction. Another factor contributing to the difficulty in correctly pairing pixels and grid cells was that when the Atlantic Coast was in alignment with the overlay, the shoreline of the Bay was not. This was due to the fact that the grid overlay was mapped using a Mercator projection, while the images were processed using an image stretching technique. Consequently, the overlay had to be repositioned depending on whether the Bay or nearshore Atlantic Ocean was to be sampled, and its position on the screen might be slightly different each time it was readjusted. The spatial error associated with this is approximately one grid cell (11.2 km) or less.

The method used to determine intensity for MECCA's river boundary cells differs from the method used for offshore boundaries because the river boundary cells do not always overlap the actual rivers. A segment of each river was therefore selected to represent the boundary cell. Rivers were first enlarged on the image processor to make viewing easier and to ensure that the same area was sampled on each image. Because the rivers were enlarged the grid overlays could not be used; however, geographic features provided adequate means for identifying river segments in each image. After the segment was enlarged, a new window (not necessarily square) was made to cover the maximum number of water pixels possible in the boundary segment, and no land pixels. The average intensity in the window was then used to determine the temperature of each river boundary.

4.3 Results and Discussion

Temperatures of the boundary cells obtained from the images are displayed in Table 4-2. Each cell is identified by a letter designating its column, and a number designating its row in the grid (Figure 4-1). Column letters ascend

Table 4-1. Distribution of differences between average window values and average two pixel values. Differences were calculated by subtracting the pixel average from the window average.

DISTRIBUTION OF DIFFERENCES

DIFFERENCE	COUNT
-1.50	1
-1.25	0
-1.00	1
-0.75	4
-0.50	17
-0.25	48
0.00	77
0.25	24
0.50	4
0.75	1
1.00	1
1.25	0
1.50	1

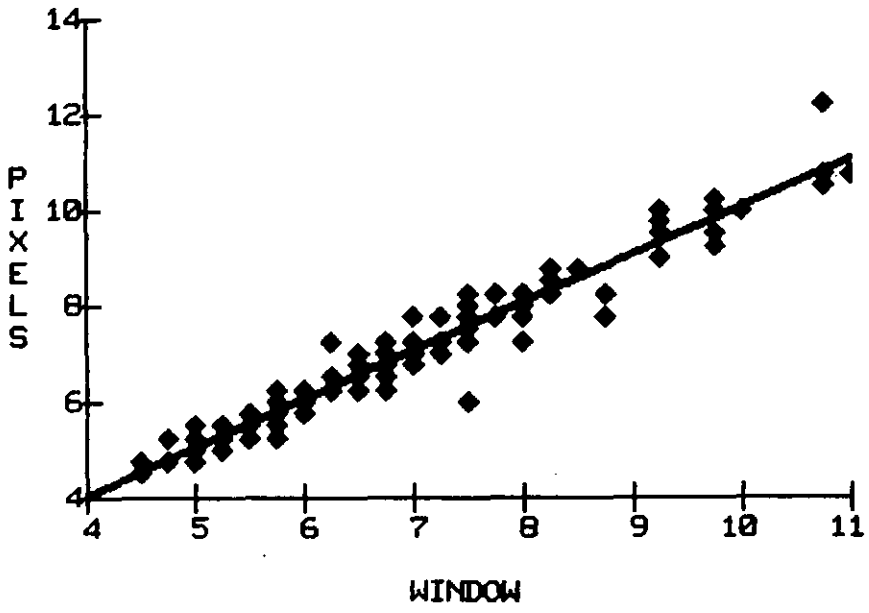

Figure 4-2. Regression of two-pixel averages versus window averages for 179 cells. Best fit line: $y = 1.01\ (x) + .03$.

the alphabet moving inland, and row numbers increase from south to north. The deep water boundary is along column A. The four corner cells of the offshore portion of the grid correspond to the labels in Figure 6-1 as follows: Point 1 in Figure 6-1 is labeled E1 in Table 4-2, Point 2 is labeled A1, Point 3 is labeled A30 and Point 4 is labeled I30. River boundary cells are designated by the first three letters of the river name.

The boundary cells show temperatures increasing from north to south and over time. The passage of a cold front over the Bay on 13 April, mentioned in Chapter 2, was reflected by decreased water temperatures in most cells on 14 April. The warming trend which followed on 15-16 April is also present in the data (Table 4-2, Figure 4-3). The tendency for the nearshore stations to experience greater diurnal changes than offshore stations, mentioned in Chapter 3, is quite apparent (Table 4-3). The fact that these trends are discernible indicates the method detects large-scale variation.

In an effort to further assess the spatial resolution obtainable with this technique, a portion of the temperature data extracted from the image for 23 April at 1900 GMT (Figure 3-8) was plotted (Figure 4-4) to see which features were evident. Only data from the deep water boundary were plotted. The boundary cuts across the western portion of Eddy 12 (Chapter 3). Cell A1 is in the Gulf Stream and is one of the warmest in the boundary (Table 4-2, Figure 4-4). Temperatures decrease with distance north. Cells A2 - A7 are in water inshore of the Gulf Stream and so have lower temperatures than A1. Cells A8 - A11 have higher temperatures because they cross a pool of water as warm as the Gulf Stream (visible in Figure 3-8 as a filament of deep red-brown located north of the Gulf Stream but south of the eddy). Temperature drops sharply from A11 - A14 as the boundary begins to cross Eddy 12. The temperature of cell A14 is lowest because it lies in the cooler (blue) water south of the eddy. This cooler water is apparently shelf water which has been advected around the eddy from the north (see description in Chapter 3). Temperatures rise in cells A15 - A21 as the boundary cuts across the warm core of the eddy. Cell A22 shows a sudden drop in temperature because it lies near the northwestern edge of the eddy where a filament of shelf water has been entrained in the eddy currents. Temperatures in cell A23 rise sharply because that cell lies over the water encircling the eddy (orange), which is warmer than the core. Temperatures decrease from A23 - A30 because the boundary there is out of the eddy and into the cooler slope waters.

Distinct features covering relatively small areas were detected. For example, the advected shelf water (at A14) measured 8.4 km from north to south in the place where the boundary grid crossed it. The shelf water entrained in the northwest edge of the eddy (at A22) measured 7.2 km in width where the boundary crossed it. This degree of spatial definition is acceptable because the grid cells have an area of about 121 km^2.

Table 4-2. Sea surface temperatures (°C) of boundary cells from AVHRR images. Date in April 1982, and time of image (GMT) are given at the head of each column. Blanks denote missing data (grid obscured by clouds).

GRID CELL	4/12 805	4/12 1929	4/14 1310	4/14 1910	4/15 730	4/15 1240	4/15 1900	4/16 1845	4/23 1255	4/23 1900
E1	10.00	14.75			10.25	13.00		16.75	12.50	13.00
D1	13.50	13.50	10.50		12.25	14.50	15.50		13.25	13.25
C1	14.50	15.00	12.50			15.00	16.50		14.00	14.00
B1	14.25	17.25				15.00	17.25		14.25	14.25
A1	16.00	17.50				15.00			17.00	18.75
A2	15.00	17.25				15.00		20.50	15.75	17.00
A3	14.75	19.75				15.00		16.75	14.75	16.50
A4	14.25	19.25				15.00	17.75		15.50	15.75
A5	14.25		14.00			15.00	18.00	18.75	15.00	16.25
A6	15.00		16.25		16.00	16.00	18.00	18.75	15.00	17.75
A7	15.50		16.75		16.25	16.00	18.00	18.75	13.75	14.25
A8	14.75		16.00		15.75	16.00	17.75	18.75	13.00	17.75
A9	14.25		13.25		13.25	16.00	17.00	18.00	13.00	19.25
A10	13.75					16.00	13.75	18.00	13.50	16.50
A11	12.50	14.50				13.00	13.50	15.75	13.50	19.00
A12	11.00	12.75	7.25		8.00	13.00	12.00	12.25	13.00	14.25
A13	11.25	12.75				12.00	11.50	11.75	13.00	12.25
A14	10.75	13.00				11.00	11.00	12.75	13.00	11.50
A15	9.25	14.00				12.00	12.25	9.75	13.00	12.00
A16	13.25	17.25				11.00	15.50	10.25	13.50	12.25
A17	10.50	18.25				12.50	16.00	10.75	12.50	12.25
A18	11.00	15.25				14.50	16.50	12.00	13.50	12.75
A19	10.75	14.50				16.00	15.50	12.00	13.50	12.50
A20	11.00	13.25				16.00	14.50	10.25	12.50	13.25
A21	10.75	12.75				15.00	14.25	10.75	11.50	13.75
A22	10.00	12.75			6.00	11.50	15.50	11.25	13.00	12.50
A23	9.25	12.25			3.25	9.50	16.75	11.25	11.50	14.25
A24	9.25	12.25	8.50		7.25	9.00	13.25	11.75	11.00	12.75
A25	9.25	11.00	9.25	6.75	10.00	10.00	10.50	10.75	10.50	13.00
A26	8.00	10.00	9.50	9.25	10.50	10.00	11.00	9.25	9.50	12.75
A27	8.25	10.50	10.00	10.50	10.00	9.50	10.75	8.75	10.00	12.00
A28	7.50	9.75	9.50	10.50	9.25	8.50	10.50	8.75	10.00	10.75
A29	6.75	9.75	9.00	9.25	9.00	8.00	9.00	7.50	9.00	11.00
A30	6.50	9.75	8.75	9.25	9.00	8.00	9.25	11.00	9.00	10.00
B30	6.50	8.75	8.00	8.00	8.00	8.00	8.75	10.00	8.00	8.75
C30	6.25	8.75	7.75	6.75	7.50	7.50	8.75	9.50	8.00	8.25
D30	5.75	8.75	7.50	5.50	7.00	7.50	8.50	9.00	8.00	8.75
E30	5.25	8.00	6.00	7.25	4.75	7.00	8.25	8.75	8.00	9.00
F30	4.50	7.25	3.25	6.25	3.00	7.00	7.75	8.50	8.00	9.00
G30	4.75	7.25	3.00	5.75	3.50	7.00	7.75	6.75	8.00	9.00
H30	5.00	6.75	6.75	7.00	6.50	7.00	8.25	7.25	8.00	9.00
I30	5.25	7.25	6.75	7.25	7.00	7.00	8.50	7.50	8.00	
sus	3.60	8.00	4.00	9.75	6.50	7.00	10.25	14.50	11.00	15.75
pot	5.50	10.00	9.00	11.00	8.60	8.25	10.80	12.10	11.00	15.40
rap	6.60	11.50	10.00	13.75	9.17	10.00		17.00	12.00	14.00
jam	8.00	11.25		13.50	10.67	11.00			13.00	

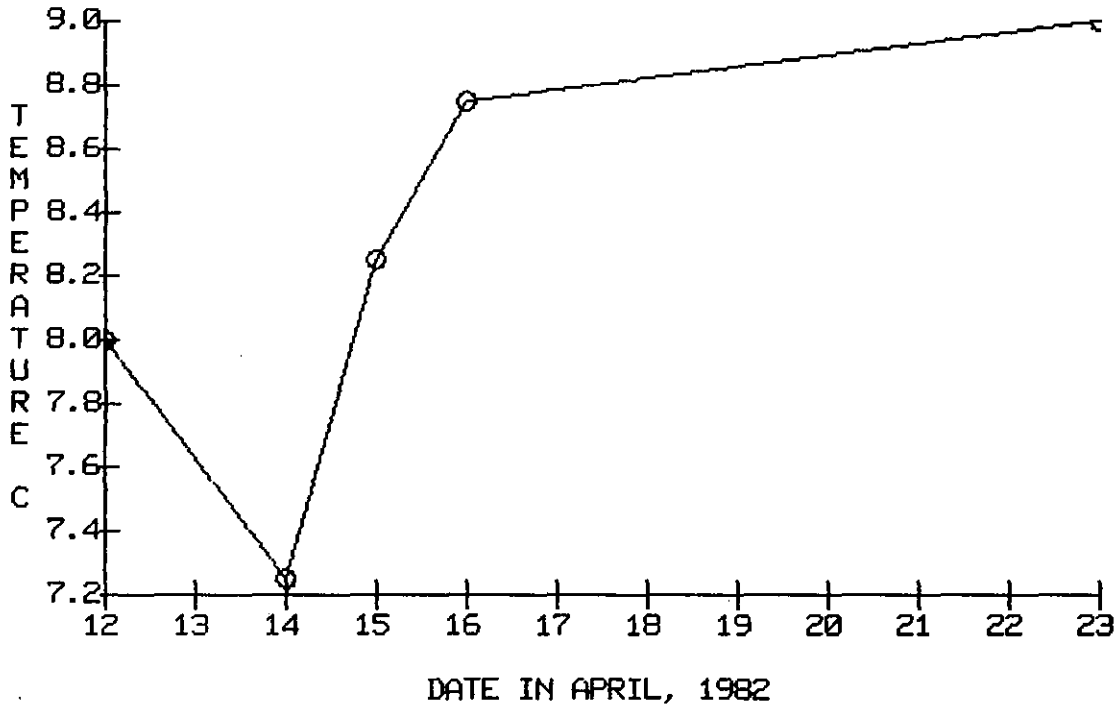

Figure 4-3. Graph of sea surface temperatures from cell E30. Only afternoon temperatures (at approximately 1900 GMT) are shown to eliminate diurnal variation.

Table 4-3. Temperature changes (°C) of river and corner boundary cells from AVHRR data. Date and time period are given at the head of each column. Total change over the study period, from 12 April at 1900 GMT to 23 April at 1900 GMT, is given in column 1. Other columns show daily changes.

BOUNDARY CELL	4/12 4/23	4/12 805-1900	4/14 1310-1910	4/15 730-1900	4/15 1240-1900	4/23 1255-1900
SUS	7.75	4.40	5.75	3.75	3.25	4.75
POT	5.40	4.50	2.00	2.20	2.55	4.40
RAP	2.50	4.90	3.75			2.00
JAM		3.25				
E1	0.63	4.75				0.50
A1	1.59	1.50				1.75
A30	1.31	3.25	0.50	0.25	1.25	1.00
I30	1.85	2.00	0.50	1.50	1.50	

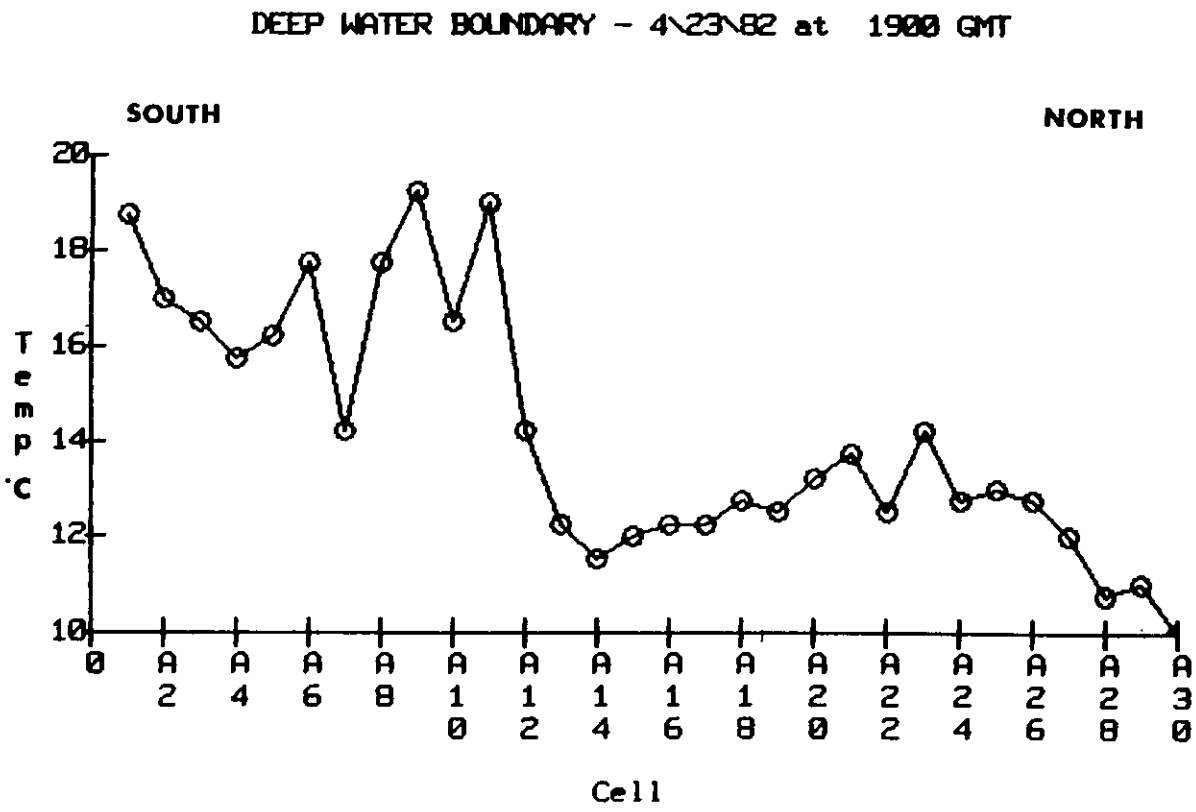

Figure 4-4. Sea surface temperature for cells A1-A30 for the image of 23 April at 1900 GMT showing south to north temperature gradient.

4.4 Conclusions

The preliminary sampling and analysis of satellite imagery presented here demonstrates that this technique can obtain accurate temperatures at a spatial scale appropriate for use with MECCA. However, two limitations in the technique should be addressed.

The first is the tendency of the temperature obtained from window samples to be slightly higher than temperatures from the average of two pixels. However, the difference between the two sampling sizes was small, as was demonstrated by the fact that 95 percent of the comparisons had differences of between 0.5 and -0.5 °C. The estimated accuracy of the algorithm used to calculate satellite sea surface temperatures is $\pm$ 1 °C, so the sampling discrepancy falls within this error range, indicating that either sampling technique is sufficiently accurate (assuming the 49-pixel average equals the average of all pixels in a cell to within half a degree). The two-pixel sampling method has the additional benefit of decreasing sampling time.

The second limitation is the difficulty in accurately pairing pixels and grid cells due to parallax and the use of different projections for the grid and images. Possible errors could be minimized by digitizing the grid so it could be projected as part of the image. An initial attempt to do this, using a video digitizer, indicated the process might be very time-consuming because the images were processed at different scales and orientations. Furthermore, because the image and model grid projections are different, each image would require that two digitized overlays be made, one with the Bay in alignment to sample Bay cells and one with the coastline in alignment to sample offshore cells. Also, the grid lines lacked definition after being digitized. It is possible that the resolution of the grid could be improved by plotting only the grid cell centers or plotting the grid with a finer pen. Another possible solution to the pairing problem is to combine the grid and the reflectance data in the same image using latitude and longitude. This would require new software for the image processor.

4.5 References

Hess, K. W., 1985. Assessment model for estuarine circulation and salinity. NOAA Technical Memorandum NESDIS AISC 3, National Environmental Satellite, Data, and Information Service, NOAA, U.S. Department of Commerce, 39 pp.

5. LFM WINDS AND MASS TRANSPORT

Peter J. Pytlowany

5.1 Introduction

Reliable estimates of surface winds are an important consideration to studies of the dynamics of marine circulation, particularly those effects induced by wind-driven currents. The interactions between shelf circulation patterns and water levels within Chesapeake Bay are reflected by inflow and outflow at the mouth of the Bay. In addition, water levels and turbulent mixing are dependent on surface winds. Mass transports of the larvae of some commercial species are strongly related to the surface wind flow (Johnson, et al., 1986). The advection and dispersion of industrial pollutant discharges or oil spilled in tanker mishaps can affect these species and have broader economic implications.

One source of near-surface wind values is the National Weather Service's (NWS) Limited-area, Fine-mesh Model (LFM). Unlike the observations collected by buoys deployed by the NOAA Data Buoy Center (NDBC), the LFM predictions provide coverage at regularly spaced grid positions every 6 hours up to 48 hours in advance. The LFM is a 7-layer numerical model with three tropospheric, three stratospheric and one boundary layer, defined as the lowest 50 mb of the atmosphere. The LFM output consists of predictions of meteorological parameters such as precipitation, pressure, humidity, and winds in the seven layers. In deriving the predictions, buoy measurements, radiosonde observations by balloons, weather station, radar, aircraft, ship and satellite data serve as input to the LFM. Coverage extends over the North American continent and to coastal and offshore areas. LFM output in the form of weather maps and charts is an important tool used by private and NWS weather forecasters.

In marine applications, the boundary layer forecasts are the best of the LFM estimators for the surface winds. Wind values are regarded as the "mean" winds for the boundary layer of the atmosphere, centered at approximately 200 m above the Earth's surface. In the Bay and shelf area, the horizontal size of an average LFM cell is approximately 165 km. Unlike *in situ* observations given at a buoy or weather station, the LFM grid provides synoptic coverage, enabling the detection and recognition of areal circulation patterns.

Efforts to analyze the accuracy of LFM forecasts inevitably require comparisons with site-specific measurements. Comparisons of LFM forecasts with buoy or station observations can be interpreted in the context of some inherent differences between numerically modeled variables and *in situ* measurements. The LFM grid point may be relatively distant from the nearest sensor used in model initialization and is rarely collocated. Furthermore, an LFM prediction is made over a uniform grid mesh and is subject to the continuity equation. In contrast, a site-specific measurement need not conform with observations taken elsewhere, and is typically representative of both synoptic and localized conditions. Near the west side of Chesapeake Bay, a wind toward the northeast or east would be slowed by land induced drag. Winds blowing toward the west or southwest would have different characteristics, depending on the local topography, and the measurements or LFM forecasts reflect these effects. Discrepancies between LFM

predictions and winds measured by buoys will arise because of the differences in the nominal heights of the predictions (200 m) and the observations (10 m). Other discrepancies could occur because the geographic locations of the predictions and observations are not the same. Errors in LFM forecasts could also affect the comparisons. These effects and variabilities were modeled statistically to facilitate the analysis of errors and formulation of corrections.

5.2 Analysis and Results

Weekly averages of LFM winds are reasonable estimates of actual winds (Reeves and Pytlowany, 1985). The weekly average LFM-buoy vector differences were found to be 0.9 to 1.6 m/sec, only marginally higher than typical wind instrumental biases. The standard deviations were 0.9 to 1.6 m/sec. Weekly vector averages of LFM winds have been postulated as "building blocks" for transport studies involving time periods of a week to several weeks and for climatological applications (Reeves and Pytlowany, 1985).

5.2.1 Calibration of LFM Forecasts

We examined the accuracy and correctibility of the individual 12-hourly LFM forecasts in order to use the data as input to the circulation model of the Chesapeake Bay and shelf region. We compared daily LFM wind predictions for 0600 and 1800 GMT for April 1982 with station data observations for Norfolk Naval Air Station (NGU), Patuxent Naval Air Station (NHK), and Baltimore Washington International Airport (BWI) for the coastal/estuarine environment. We compared the offshore LFM grid locations with NDBC buoys B41001 and B41002 for the period September 1977 through December 1981 (Figure 5-1). NGU station observations were taken as most indicative of the surface wind flow for the mouth of Chesapeake Bay. For each of the comparisons, the station data and the buoy observations were regarded as the reference data defining the wind regime.

The comparison of Chesapeake Bay LFM predictions and station observations showed LFM winds to average 3 m/sec (60 percent) faster than observed winds. Direction differences (LFM - station) averaged -17 degrees for NGU comparisons (Bay mouth), 6 degrees for NHK comparisons (mid-Bay), and -3 degrees for BWI comparisons (upper Bay). The root-mean-square (rms) differences, however, were sufficiently high (50 - 68 degrees) to warrant an attempt to correct the LFM winds. To formulate corrections of the LFM winds, stepwise linear regressions of observed wind u and v components, and speeds were run against the equivalent LFM parameters and LFM pressures at the four LFM grid points surrounding each of the three stations, for a total of 16 possible variables. The coefficients from the speed regressions provide unbiased correctors for the LFM speeds directly. In contrast, unbiased correctors for the LFM directions must be derived by first performing regressions on the u and v wind components. The coefficients from the u and v component regressions can then be used to correct the LFM components from which the estimates of wind direction can be computed (Glahn, 1970).

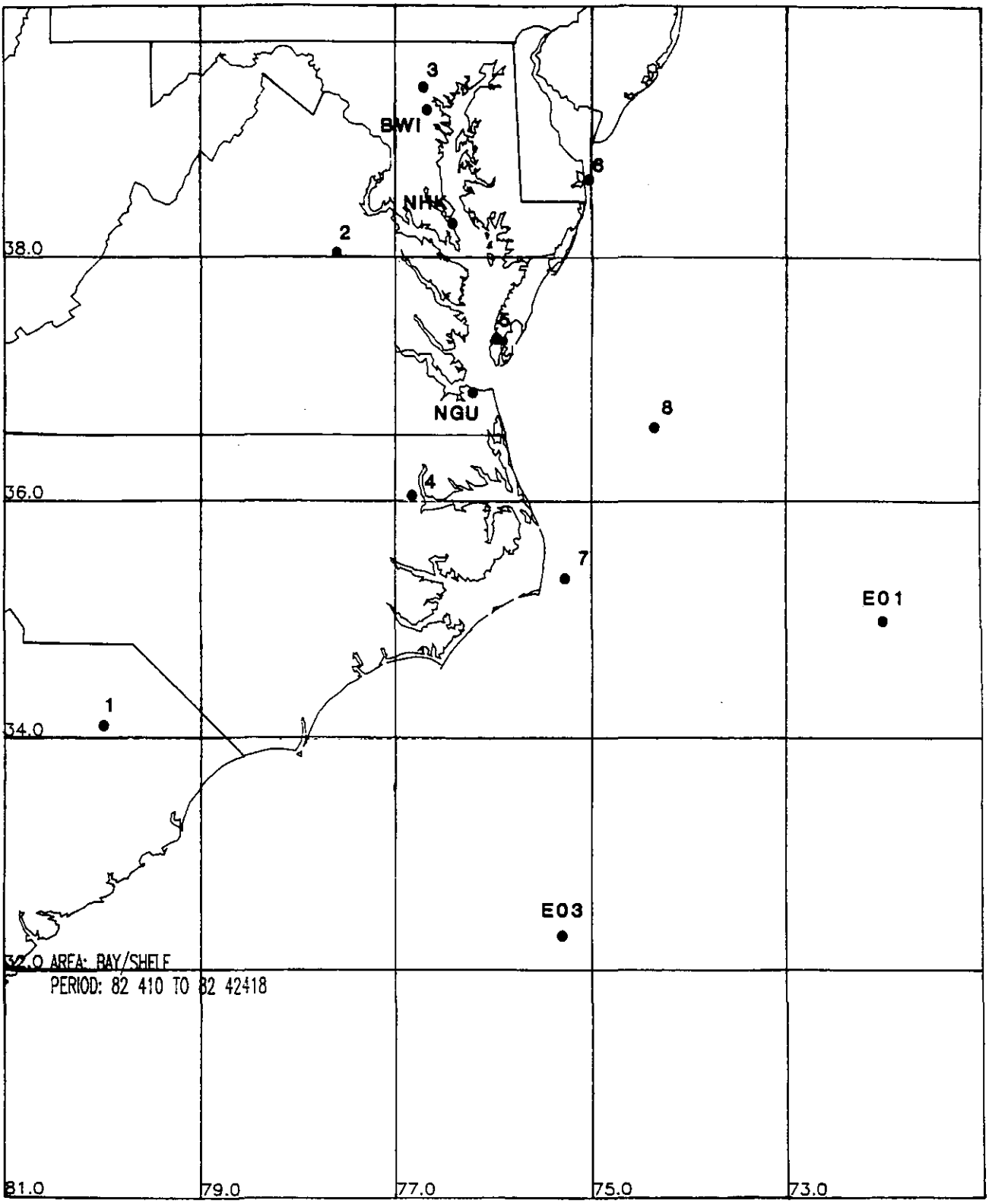

Figure 5-1. Chesapeake Bay-shelf map depicting weather stations at Norfolk (NGU), Patuxent (NHK), and Baltimore/Washington International Airport (BWI). Also shown are NOAA buoys B41001 (E01) and B41002 (E03) and LFM points 1 to 8.

The regression models were chosen that produced unbiased parameter estimates, significant variables, and explained variances lower by less than one percent than those models having an additional variable (Table 5-1). For the 12 regressions, the number of variables required to explain approximately 55 to 80 percent of the variance ranged from three to eight. All regressions were significant at alpha less than or equal to 0.0001 and the independent variables had F-values significant at alpha less than or equal to 0.05. The comparisons revealed that the LFM speeds required the greatest number of regression variables to correct (6 to 8) and these tended to explain the least variance of the three variables modeled (Figures 5-2 to 5-4). Frictional drag from local terrain effects, highly dependent on wind direction within the Bay, are believed to have caused consistently lower observed wind speeds.

For the comparisons of buoys and LFM estimates at offshore locations, the nearest LFM point to each buoy was chosen. The mean speed biases were 0 m/sec for each buoy and direction biases were -2 to -4 degrees. However, regressions analogous to those for the station data were needed due to the root-mean-square (rms) differences in the individual 12-hourly comparisons of approximately 3 m/sec for speed and 45 degrees (one octant) for direction. Plots of buoy versus LFM u and v components and speeds supported the use of linear regression models to correct the LFM estimates (Figures 5-5 to 5-7). Four LFM parameters (u and v components, speeds, and mean sea level pressures) were used as independent variables for each regression. Model coefficients were derived for each buoy and for the combined data. Approximately 50 to 70 percent of the variance was explained with four or less of the independent variables (Table 5-2).

5.2.2 Wind-Induced Mass Transport

Another application of LFM wind predictions in offshore physical oceanography is the estimation of averages of wind-driven mass transport for weeks, months, or any other specifiable periods. Because the LFM predicts winds over a large geographic area, mass transports can be computed and displayed on a map to show large-scale circulation features. The mass transport estimates are not intended as a measure of the absolute component magnitudes, but as relative transport magnitudes and directions. Units are expressed as cubic meters per second per meter of baseline length normal to the LFM wind vector.

A mass transport map for 10-24 April 1982 was derived (Figure 5-8). A progressive vector diagram of corrected LFM winds for Point 5 in Figure 5-1 was also constructed (Figure 5-9).

5.3 Summary and Conclusions

The results indicate that the LFM winds can be successfully corrected and used as predictors of surface winds in studies requiring individual 12-hourly forecasts as input. Further studies analyzing the use of LFM forecasts extending out to 48 hours from model initiation at 0000 and 1200 GMT daily are needed. The LFM wind predictions as used in a climatological sense enable the identifi-

Table 5-1. Linear regression models for LFM/station comparisons. LFM variables are (a.) wind: speed (S), u (+ toward East) component, v (+ toward North) component, and (b.) mean sea level pressure (P) at numeric locations given in Figure 5-1.

Component	R-Square	LFM Variables (x) Coefficients	Intercept
Norfolk Naval Air Station			
u	0.72	U5 S1 P4 P2 .4 .22 .871 -.885	11.93
v	0.80	V4 S1 P5 P2 .21 -.18 1.546 -1.495	-50.98
s	0.64	S1 U1 V5 P5 .61 .17 .31 -1.559 P2 P1 1.422 .208	-71.26
Patuxent Naval Air Station			
u	0.70	U3 S3 V2 S5 .23 -.25 .07 .46 P5 P6 1.056 -1.112	53.98
v	0.77	V2 S3 U6 .46 -.16 -.21	1.8
s	0.71	S5 U5 U6 V3 .35 -.73 .41 -.48 U2 V2 P3 P6 .55 .80 .681 -.645	-35.92
Baltimore/Washington International Airport			
u	0.76	U6 V6 V5 P5 .41 .66 -.91 1.056 P3 -1.173	115.77
v	0.67	V2 P3 P6 .20 -.868 .992	-127.04
s	0.53	S3 U3 U2 U6 .25 -1.13 1.0 1.19 U5 V6 V5 -.76 .75 -.79	2.03

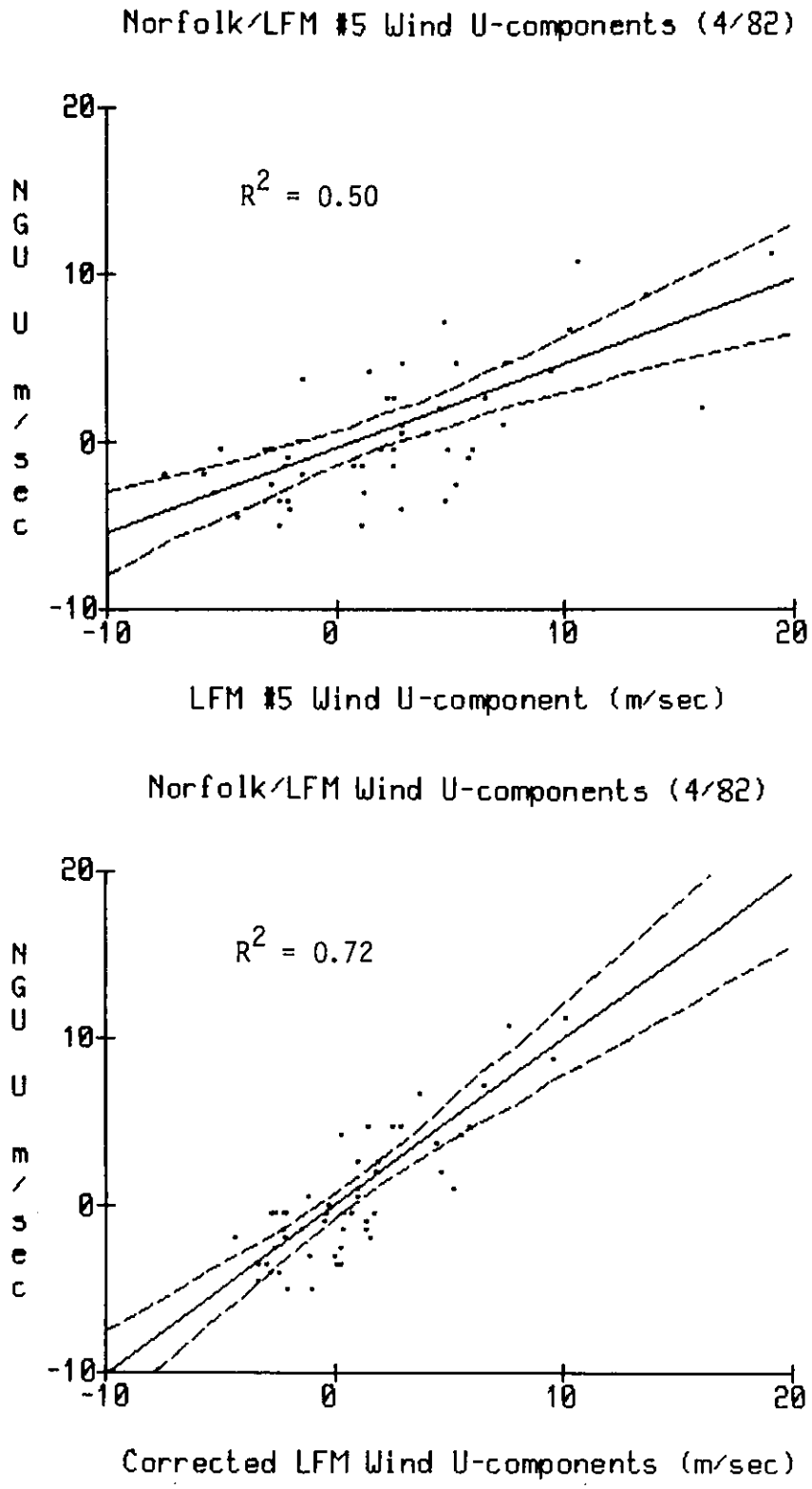

Figure 5-2. Linear regression with upper and lower 95 percent confidence levels of (a) uncorrected wind u-components predicted for the LFM point (No. 5, Figure 5-1) nearest Norfolk (NGU) versus NGU observations, and (b) corrected LFM u-components versus NGU observations for April 1982 (n = 53).

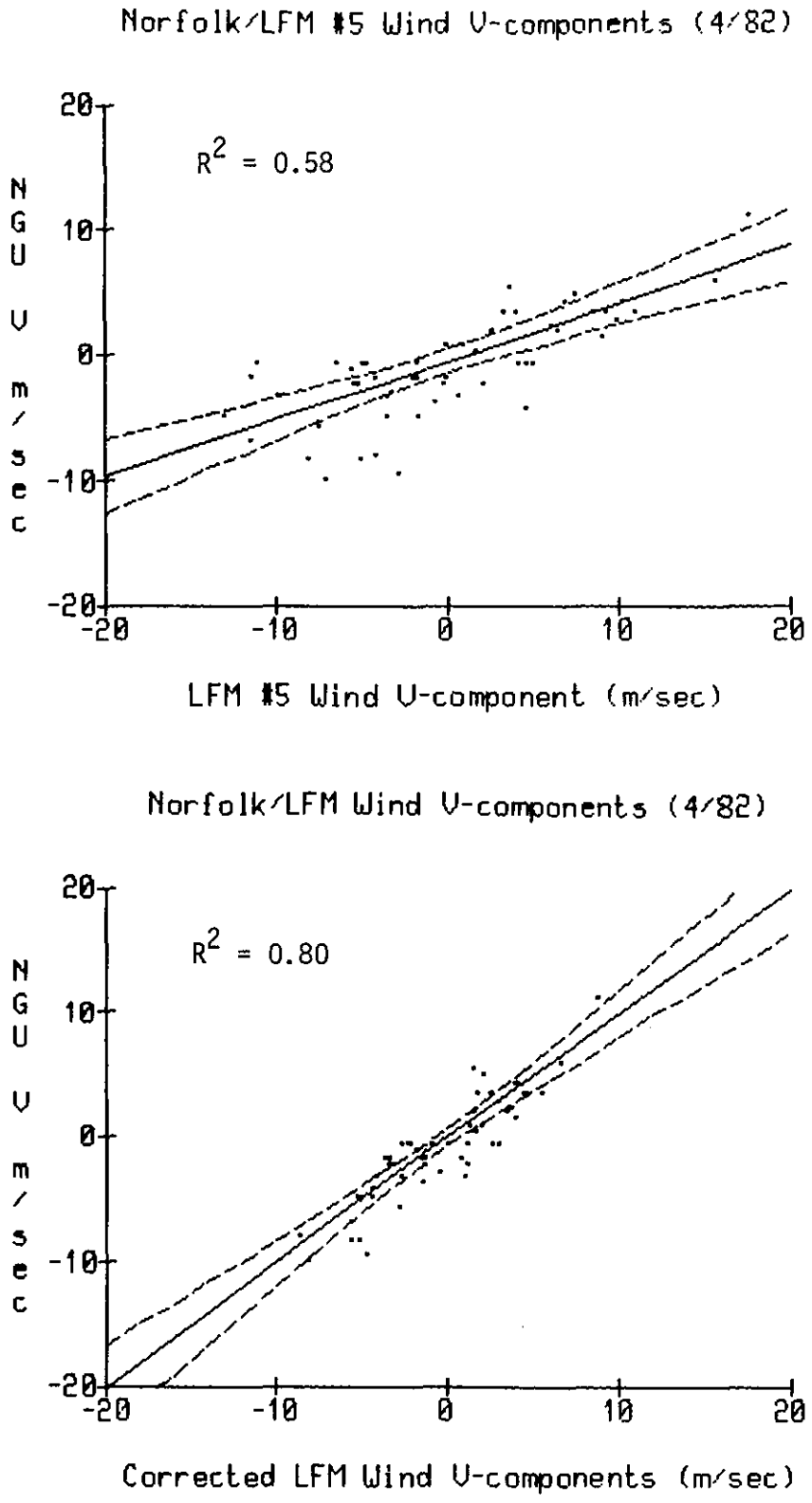

Figure 5-3. Linear regression with upper and lower 95 percent confidence levels of (a) uncorrected wind v-components predicted for the LFM point (No. 5, Figure 5-1) nearest Norfolk (NGU) versus NGU observations, and (b) corrected LFM v-components versus NGU observations for April 1982 (n = 53).

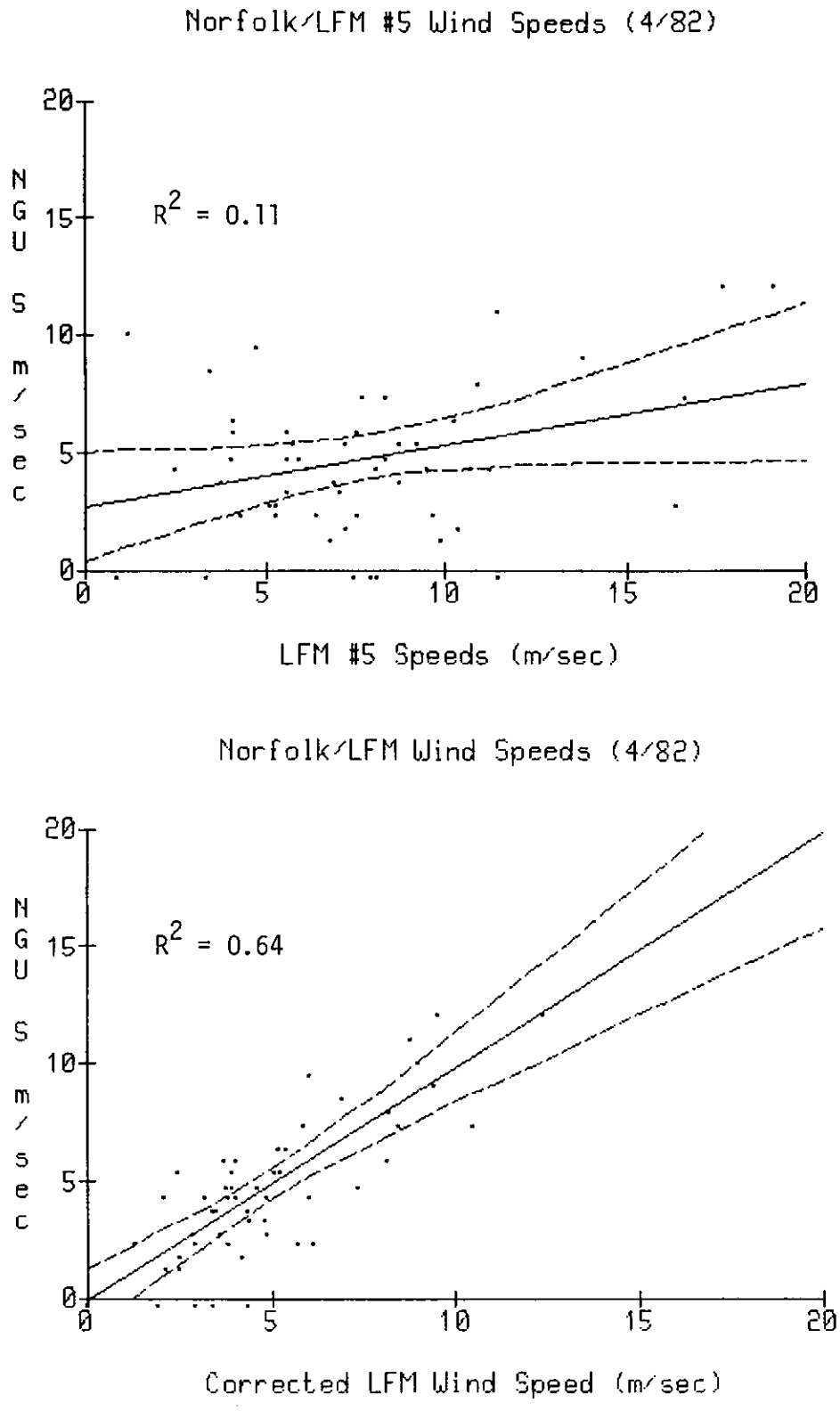

Figure 5-4. Linear regression with upper and lower 95 percent confidence levels of (a) uncorrected wind speeds predicted for the LFM point (No. 5, Figure 5-1) nearest Norfolk (NGU) versus NGU observations, and (b) corrected LFM speeds versus NGU observations for April 1982 (n = 53).

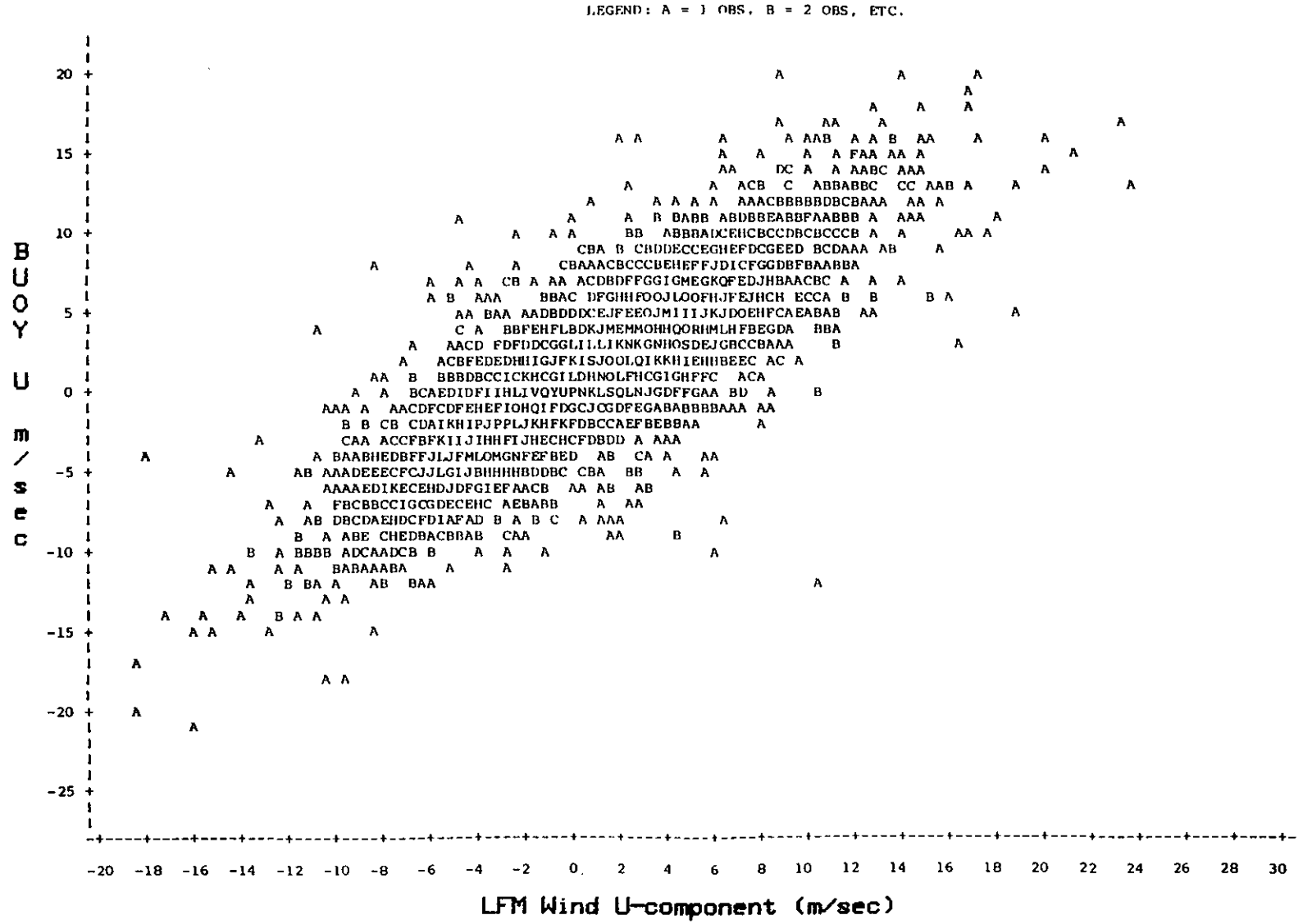

Figure 5-5. Wind u-components from NOAA buoys B41001 and B41002 versus u-components from the nearest LFM grids to each buoy for 0600 and 1800 GMT daily comparisons (n = 3778) between September 1977 and December 1981.

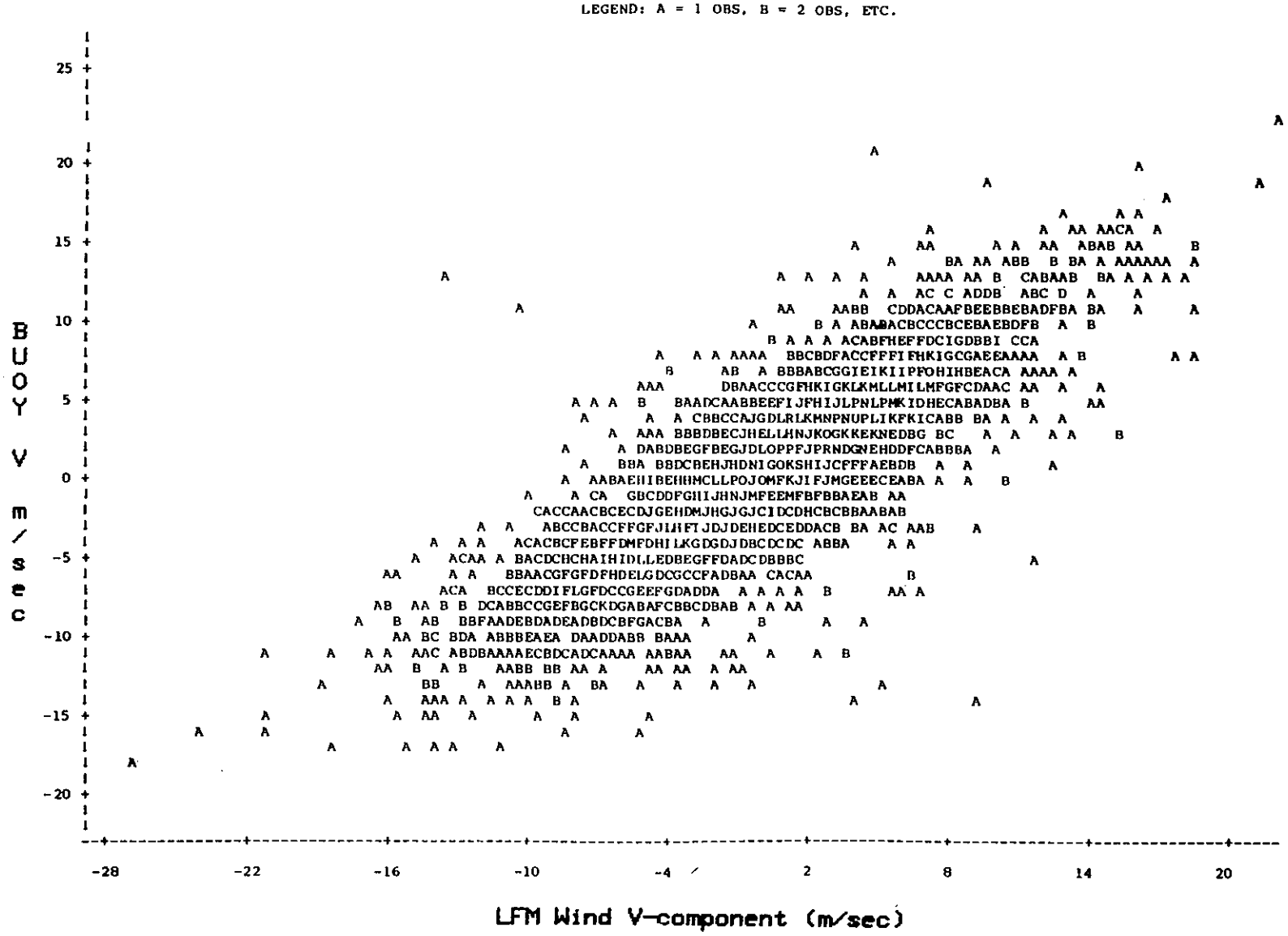

Figure 5-6. Wind v-components from NOAA buoys B41001 and B41002 versus v-components from the nearest LFM grids to each buoy for 0600 and 1800 GMT daily comparisons (n = 3778) between September 1977 and December 1981.

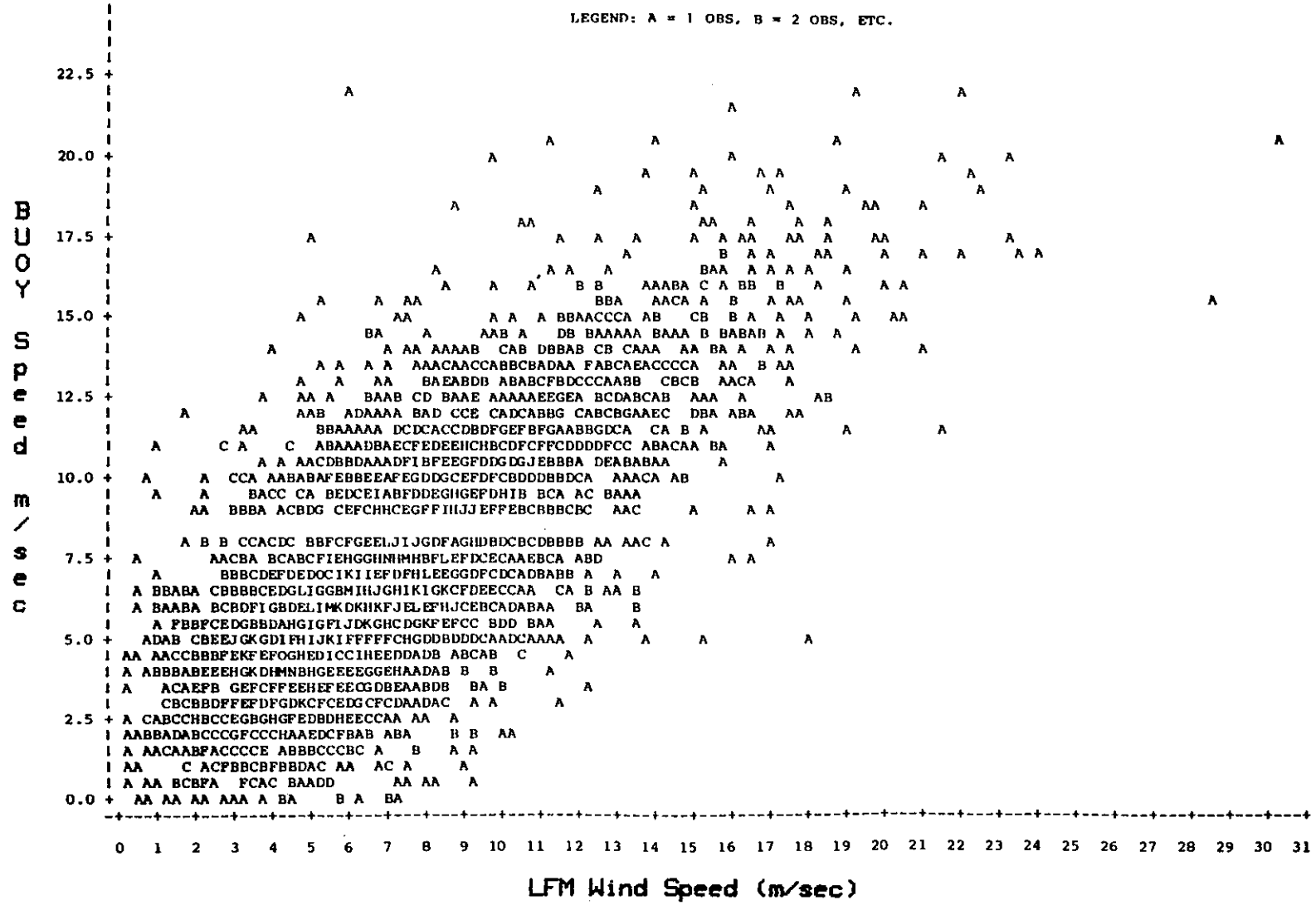

Figure 5-7. Wind speeds from NOAA buoys B41001 and B41002 versus speeds from the nearest LFM grids to each buoy for 0600 and 1800 GMT daily comparisons (n = 3778) between September 1977 and December 1981. Break in buoy data at 8.5 m/sec is probably due to an instrumental anomaly in processing and recording the observations.

Table 5-2. Linear regression models for LFM/buoy comparisons offshore. LFM variables are (a.) wind: speed (S), U (+ toward East) component, V (+ toward North) component, and (b.) mean sea level pressure (P) predicted at grid points nearest each buoy.

Component	R-Square	LFM Variables (x) Coefficients	Intercept	No. of Obs.
		Buoy B41001		
u	0.64	U V S .76 .38 .04	0.4	1403
v	0.73	V U P .83 -.10 .108	-109.3	1403
s	0.61	S V P .70 .05 -.106	109.8	1403
		Buoy B41002		
u	0.68	U S .83 .08	-0.01	2375
v	0.71	V U S P .83 -.04 .07 .0588	-59.77	2375
s	0.51	S U V P .69 .02 .03 -.111	114.83	2375
		Combined Buoys B41001 and B41002		
u	0.67	U V S .80 .02 .06	0.18	3778
v	0.71	V U S P .84 -.07 .03 .0811	-82.3	3778
s	0.56	S U V P .69 .02 .04 -0.1	108.3	3778

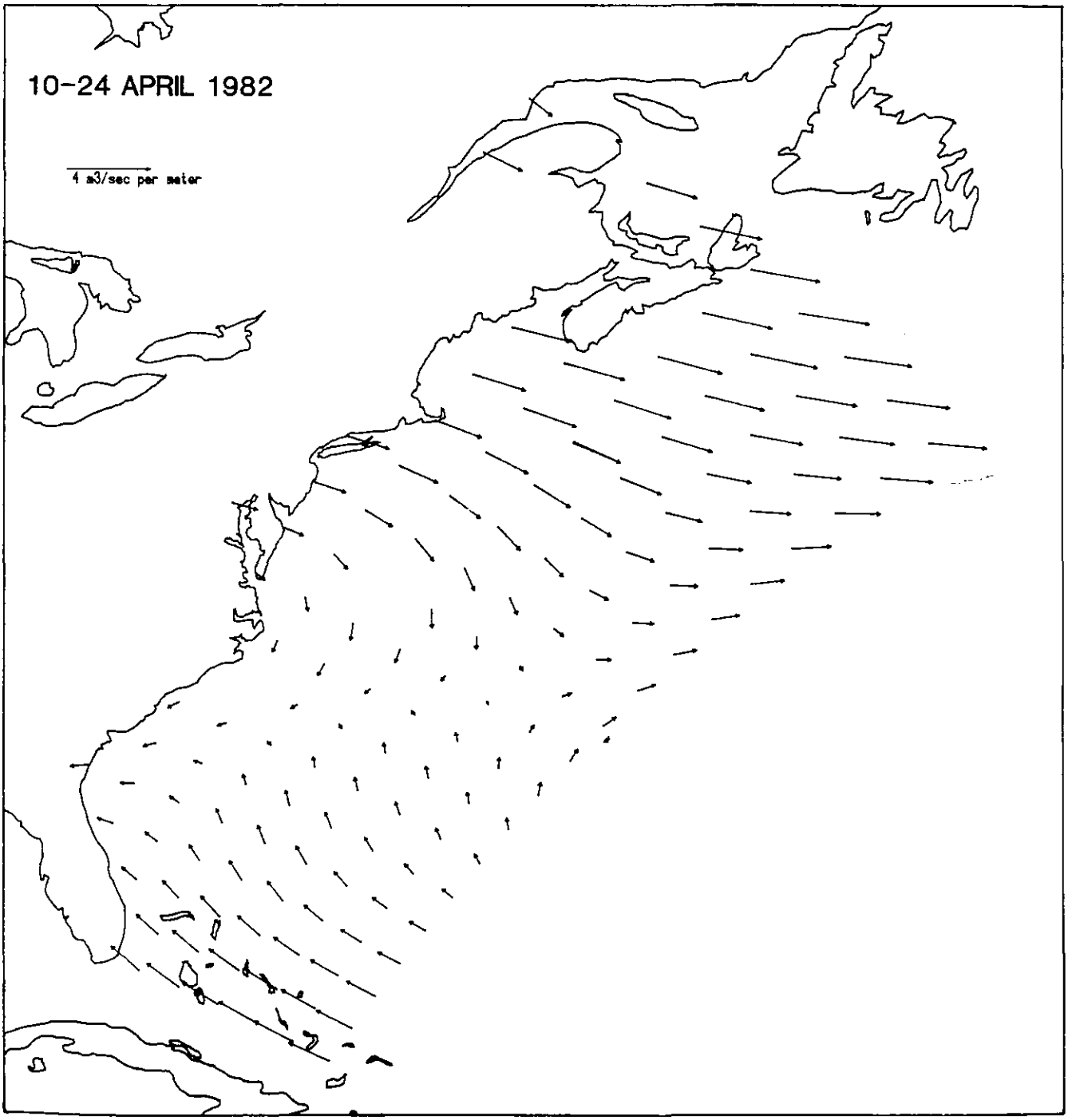

Figure 5-8. Mean vertically-averaged mass transport derived from uncorrected LFM wind predictions for 10-24 April 1982.

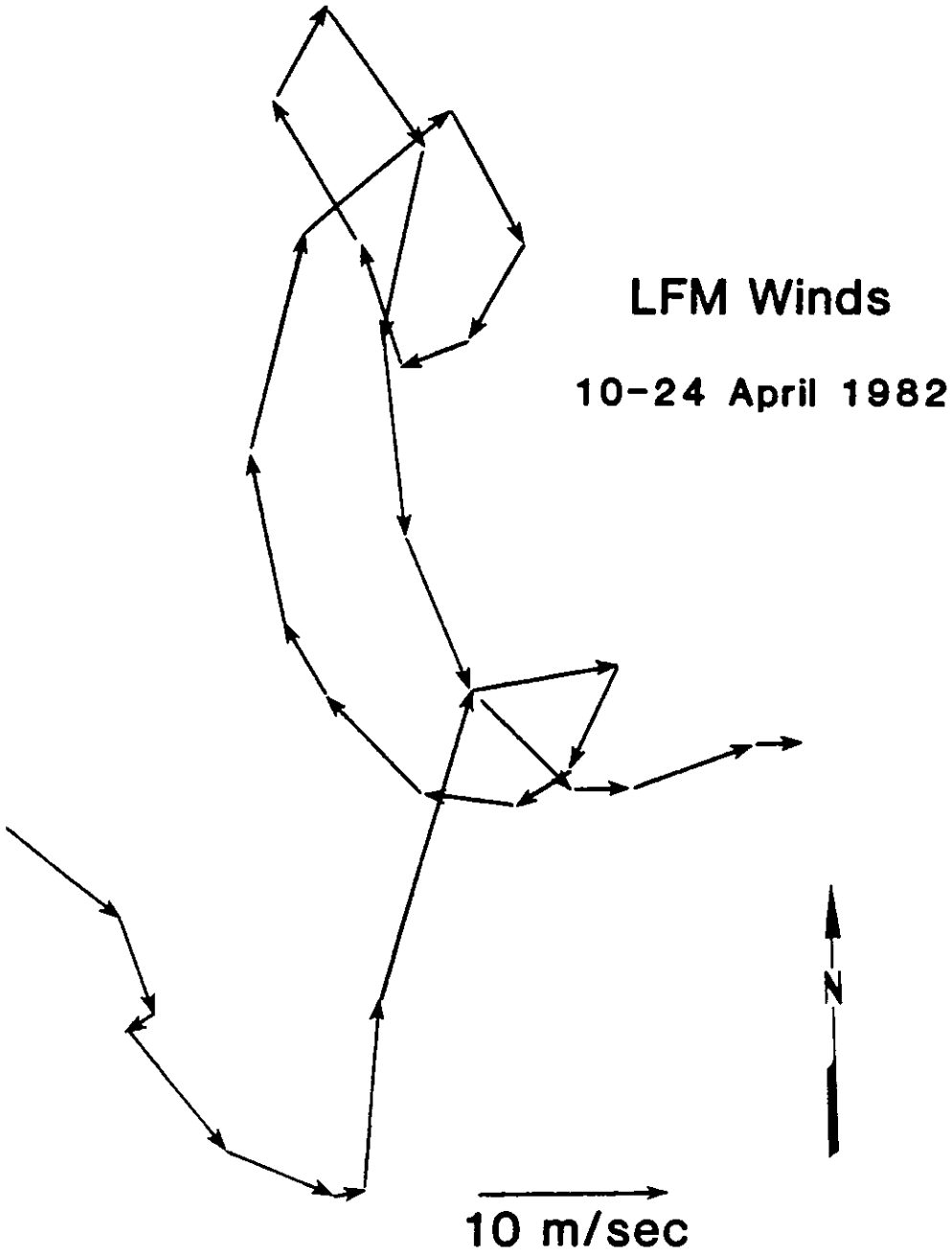

Figure 5-9. Progressive vector diagram of corrected LFM winds (Point 5, Figure 5-1). Winds are plotted for each 12 hour interval from 0600 GMT, 10 April 1982 to 1800 GMT, 24 April 1982.

cation of large-scale circulation features of coastal waters and comparison with long term climatic averages. The potential exists to identify climatological anomalies in their early stages.

5.4 References

Glahn, H. R. 1970. A Method for Predicting Surface Winds. ESSA Technical Memorandum, WBTM TDL 29, Environmental Science Services Administration, U.S. Department of Commerce, Washington, D.C., 15 pp.

Johnson, D. F., L. W. Botsford, R. D. Methot and T. Wainwright. 1986. Possible influence of wind on the cycles of Dungeness crab catch. Canadian Journal of Fisheries and Aquatic Sciences, 43:838-845.

Reeves, R. W., and P. J. Pytlowany. 1985. Comparison of Boundary Layer Winds from NWS LFM Output and Instrumented Buoys. NOAA Technical Memorandum, NESDIS AISC 2, NOAA, U.S. Department of Commerce, Washington, D.C., 43 pp.

6. NUMERICAL MODELING OF CIRCULATION AND TEMPERATURE

Kurt W. Hess

6.1 Introduction

A numerical model for the three-dimensional coastal and estuarine circulation (Hess, 1985a) was applied to the Chesapeake Bay and local continental shelf to learn more about currents and their effect on the biological productivity of the region. The specific modeling tasks to be completed for the study were (1) refining the model to include temperature calculations, (2) verifying the model with data on water levels, currents, salinities, and temperatures, and (3) simulating the oceanic variables of interest for the two-week study period in April, 1982.

6.2 The Numerical Model

The circulation model MECCA (Model for Estuarine and Coastal Circulation Assessment) used in this study was designed to simulate tidal, density-driven, and wind-driven currents such as those commonly found in the Chesapeake Bay and adjacent shelf waters. These currents are known to vary rapidly with time, and to change with horizontal position and with depth, i.e., they are three-dimensional and time-varying. MECCA has been applied previously to Chesapeake Bay proper to analyze the large-scale synoptic changes in salinity following the passage of Hurricane Agnes in 1972 (Hess, 1985a). MECCA was demonstrated to simulate the tides accurately, and to reproduce the major features in salinity reduction in the upper Bay reasonably well. A user's guide to running the model was also completed (Hess, 1985b).

For this study, the model was applied to the Chesapeake Bay and the adjacent continental shelf to simulate the currents for the period of 10-24 April, 1982. Inputs to the model include atmospheric forcing, river flowrates, and oceanic salinity and temperature. For the period of interest, atmospheric data was obtained from the National Weather Service, river data from the United States Geological Survey, and salinity data from various other sources. NOAA satellite imagery provided some of the water temperature data.

Model output consists of (1) water levels, vertically-averaged velocities, surface and bottom salinities, and surface and bottom temperatures each 24 hours (corresponding to midnight each day), (2) surface water temperatures each 24 hours (corresponding to noon each day), and at each of ten vertical levels (3) velocity, coefficients of vertical momentum and mass exchange, salinity, temperature, density, Richardson Number, and horizontal pressure gradient, and finally (4) time-averaged flowrates across the mouth of the Bay.

6.3 Temperature Calculations

MECCA has been updated to include temperature as a prognostic variable (Hess, 1985c). The numerical calculation for temperature is similar to that for

salinity, with the major difference being that there is a flux across the surface and bottom water interfaces.

The total surface heat flux is the sum of several terms. They are, in general order of importance, (1) the incoming solar short-wave (i.e., in the visible range) radiation, (2) the out-going long-wave (black body) radiation from the water surface, (3) the incoming long-wave radiation from the atmosphere, (4) the sensible heat flux, and (5) the latent heat flux. These last four are combined in a single term, Q, so that the surface boundary condition is

$$D_v T,_z = Q \tag{6.1}$$

where D_v is the vertical turbulent diffusivity (m^2/sec) and the subscript (,z) denotes the partial derivative with respect to z.

If heat flux across the bottom of the water column is ignored, the temperatures of shallow waters rise. Here we use, for the bottom condition,

$$T,_z = K(T_b - T_{sb})/H \tag{6.2}$$

where T_b is the water temperature just above the bottom, and T_{sb} is the temperature of the sea bed. There is some research that suggests that bottom heat flux may be an important factor in determining estuarine temperature changes (e.g., Smith, 1980).

With the exception of the solar short-wave radiation, all the fluxes are assumed to be absorbed in, or radiate from, the topmost model layer (the top 11 percent of the water column). The solar short-wave radiation, however, penetrates several meters into the water column, and is absorbed over that depth, although most of the absorption takes place near the surface. The amount of radiation reaching any depth decreases exponentially from the amount passing through the water surface. The depth at which the intensity is only 10 percent of that at the surface, D10, is taken to be either 6 meters or the total depth, whichever is smaller. The suitability of this value is discussed later.

The equation of heat conservation used in the model is

$$T,_t + (uT),_x + (vT),_y + (wT),_z - D_h(T,_{xx} + T,_{yy})$$

$$- (D_v T,_z),_z - R = 0 \tag{6.3}$$

where T is the temperature (°K), u,v, and w are the components of water velocity (m/sec), D_h is the horizontal thermal diffusivity coefficient (m^2/sec), and R is a source term accounting for the absorption of solar energy. The values used for diffusion coefficients are discussed in Hess (1985a).

6.4 Model Application to the Bay-Shelf Region

The first step in the application of MECCA to the Bay-shelf region was the generation of a grid representing the coastline, bathymetry, and water. The gridmesh used for this study covers the Bay proper, the lower portions of the major rivers, and part of the local continental shelf out to approximately the 80 m isobath (Figure 6-1).

The grid cell size is 11.2 km, and represents a compromise between requirements for adequate resolution of the relevant phenomena and the limit on computer time. The external-mode (i.e., vertically averaged) velocities are updated each timestep of 450 seconds. The internal-mode velocities (i.e., total velocity minus vertically-averaged velocity) and the salinities and temperatures are updated one-sixth as often, or each 45 minutes. Larger values were tried, but they produced instabilities manifested by unrealistically large salinities upstream of the mouths of some of the rivers. These salinity irregularities were the result of the numerical scheme trying to accommodate large horizontal salt fluxes. The 45-minute timestep eliminated most of the problems. The computer time required to simulate 15 days of currents, salinities, and temperatures with this grid mesh on a Sperry UNIVAC 1180 computer was approximately 3 hours and 20 minutes.

The gridmesh's open boundaries consist of four riverine (Susquehanna, Potomac, Rappahannock, and James rivers) entrances and three oceanic sections (the northern, deep-water, and southern boundaries) (Figure 6-1). Input values are necessary at all boundary grid cells.

6.5 Model Inputs and Initialization

At each open-boundary grid point we specify either a water level or a vertically-averaged transport, and also a velocity, temperature, and salinity value at each level. In addition, conditions at the air-water interface must also be specified. Model spin-up tests showed that an initial computation interval of 15 days was necessary to reduce transient solutions to a manageable level; the period of interest is thus extended to 25 March - 24 April. Each type of boundary is now examined in detail.

6.5.1 Oceanic Boundaries

At the deep-water boundary, the water level is made to vary sinusoidally in time to represent an average astronomical tide. The equation for water level is

$$h = A \cos(2 \pi t/T) \qquad (6.4)$$

where h is the water level above mean sea level, A is the tidal amplitude (half the range), t is time, and T is a mean tidal period (12.40 hours).

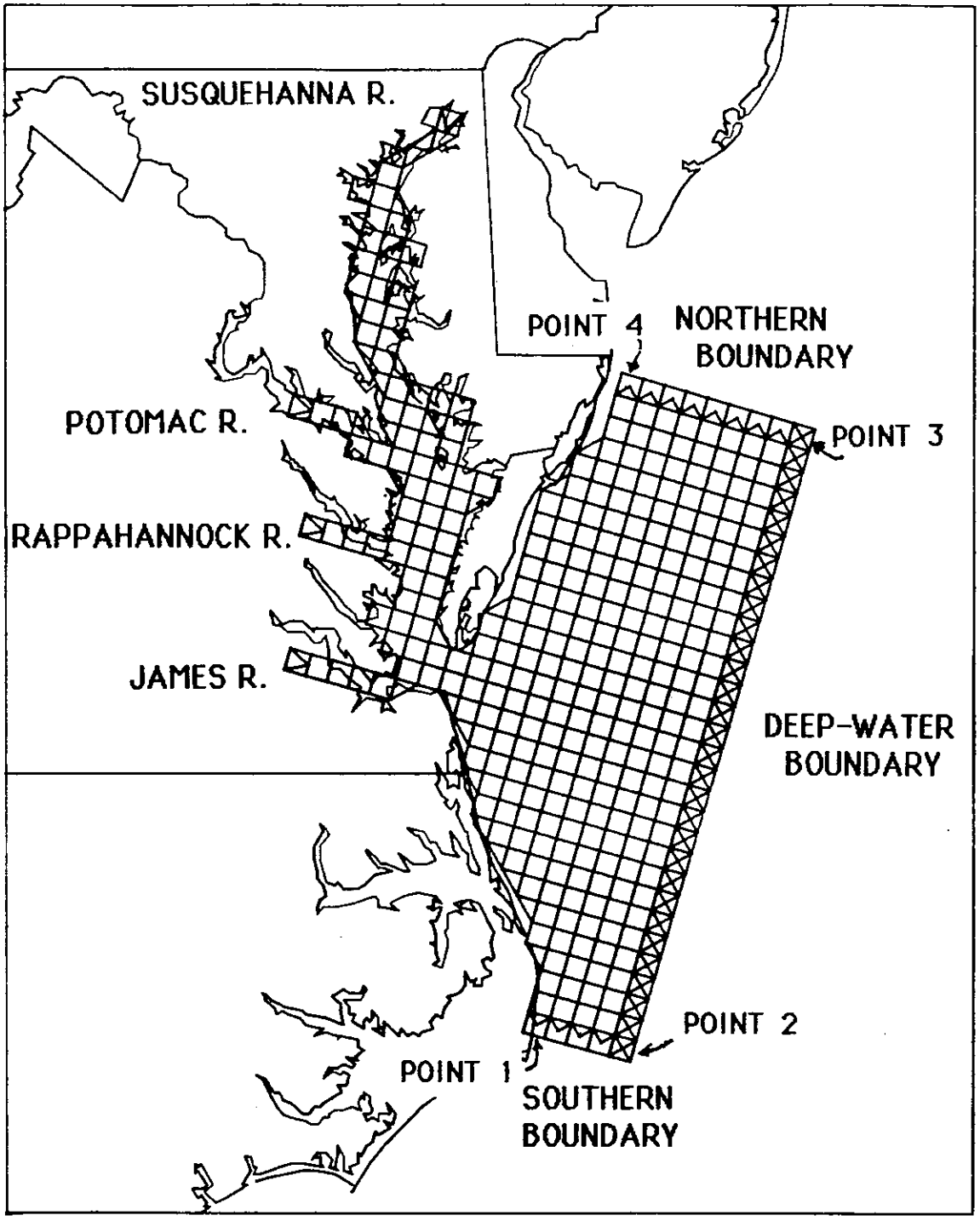

Figure 6-1. Local geography of the study area showing the numerical model gridmesh, the location of the oceanic boundaries, and the location of the river inputs. Grid cells measure 11.2 x 11.2 km.

The tide at each grid point along the deep-water boundary is computed by linear interpolation between the tides at each end (Points 2 and 3 in Figure 6-1). At Point 2, the tide has a range of 0.80 m, and at Point 3 the range is 1.0 m. These values were determined to best account for the changes in observed tide range along the Delaware, Maryland, and Virginia outer coasts. Subtidal variability can be included in the boundary conditions when more data become available.

At the northern and southern boundaries, the water level boundary value is computed from the internal flow field using a radiation outflow condition (Davies, 1983):

$$h = h' + U/c, \tag{6.5}$$

where h is the boundary water level, h' is tidal water level, U is the outward normal volumetric flowrate per unit width, and c is the shallow water gravity wave speed.

Surface temperatures in the oceanic region were determined solely from analysis of satellite imagery. The temporal progression of temperatures at five points along the grid boundary, indicating a gradual increase of about 0.09 °C per day, is shown in Figure 6-2.

Temperature and salinity distributions over depth for any one time are given at the four boundary end points (Points 1, 2, 3, and 4; Figure 6-1). At each of these points, data values represent the hypothetical coastal ocean's top three layers: the mixed layer, the pycnocline, and the deep layer. The salinity distribution, for example, is determined by the depth to the top of the pycnocline (equivalent to the mixed layer depth), the depth to the bottom of the pycnocline, and four salinity values: one each for the water surface, the bottom of the mixed layer, the bottom of the pycnocline, and the bottom of the water column (Figure 6-3). Intermediate salinities are determined by a linear interpolation between data values. The temperature distribution is represented by another set of four numbers, so that for each end point, at any time, there must exist a set of ten data values.

Actual temperature and salinity variations over depth are based on data from the NOAA Northeast Monitoring Program (NEMP) (NMFS, 1982). Observed variations over the vertical were quite small; the temperature decreased from surface to bottom by about 1 °C, and the salinity increased by about 1 ppt.

At each intermediate cell (i.e., between end points) along the northern, deep-water, or southern boundary, the local values of the ten parameters are determined by linear interpolation between end point values. Each set of ten numbers for each end point is referenced to a specific time, and a series of sets is given. At intermediate times, the instantaneous values are determined by either linear or cubic interpolation.

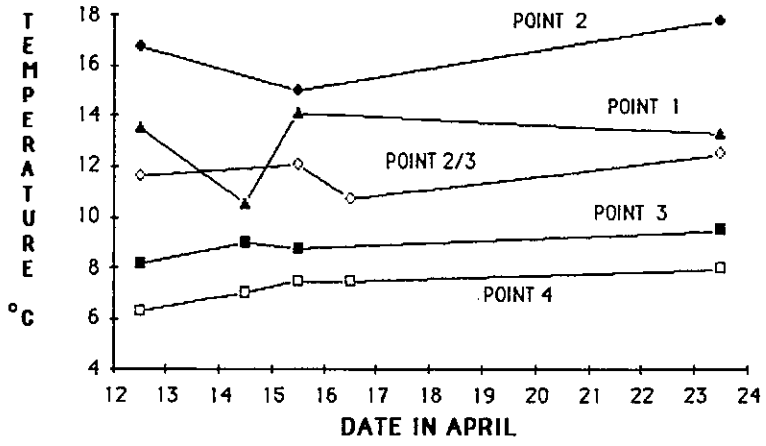

Figure 6-2. Temporal progression of surface water temperatures (°C) in April 1982 at five points on the gridmesh oceanic boundary (see Figure 6-1). Point 2/3 is halfway between Point 2 and Point 3.

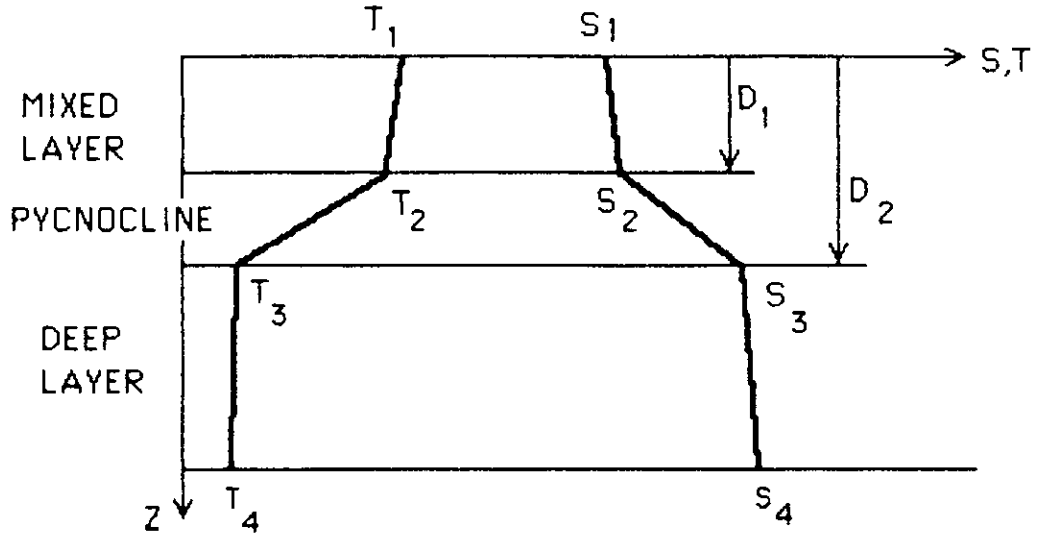

Figure 6-3. Schematic of variables that describe vertical variation in MECCA's oceanic salinity and temperature boundary conditions.

The temperatures and salinities determined this way are used for the computation (at each level and cell) when the total water velocity is directed into the mesh. When the total velocity is directed out of the mesh, the boundary value is determined by extrapolation of concentration within the domain.

6.5.2 Riverine Boundaries

At the river boundaries, the flowrates are specified from USGS observations (USGS, 1982a, b). The daily mean flowrate value is used to represent the instantaneous noon value in the model. Flowrates during the early part of April were high due to rainfall, and declined to fairly uniform levels during the later part of the month (Figure 6-4). By comparison, the 22-year mean April flowrate for the Susquehanna River is approximately 2300 cubic meters per second, so the flow during the study period can be characterized as near-normal.

River surface temperatures were taken from satellite images for the period of interest (Figure 6-5). Salinity data were compiled from several sources, primarily Birdsong, et al. (1983) and Tyler (1985). Salinities and temperatures at intermediate depths are found by interpolation as

$$S = S_s - (S_s - S_b)[1 - \cos(\pi z/H)]/2 \qquad (6.6)$$

where S_s is the surface value, S_b the bottom value, and H the total depth.

6.5.3 Air-Water Interfacial Boundary

Meteorological data were taken from the NWS's LFM forecasts. The sea-level pressure, boundary-layer potential temperature, wind speed and direction, and boundary-layer relative humidity are available as 6-hour forecasts, valid for 0100 and 1300 local time each day. Values for other times of day are found by interpolation. Although the LFM data are available for several points in the Bay-shelf region (Figure 5-1), we used only data from Point 5.

The LFM data are quite representative of the observed ground temperatures. Figure 6-6 shows the LFM boundary layer potential temperatures at Point 5 and the observed temperatures at Norfolk, Va. While the LFM values rarely coincide with the daily high and low, the values are representative of the 12-hourly means.

The LFM boundary-layer wind speed (m/sec) was adjusted to better represent the surface wind. The u (toward east) and v (toward north) 10 m wind was obtained from the LFM boundary layer winds (U, V) at LFM Point 5 by the regression formulae derived for the combined buoys in Chapter 5:

$$u = 0.18 + 0.80U + 0.02V + 0.06S \qquad (6.7)$$

$$v = -82.3 - 0.07U + 0.84V + 0.03S + 0.08111P \qquad (6.8)$$

where S is the magnitude of the LFM wind (m/sec), and P is the atmospheric pressure (mb).

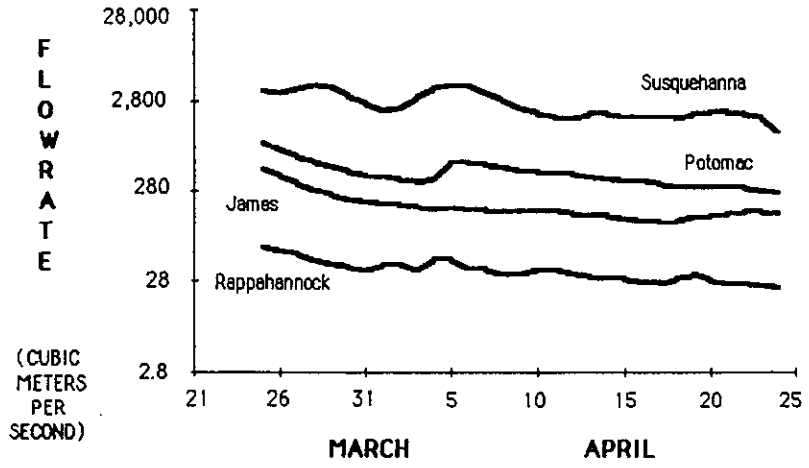

Figure 6-4. Daily means of river flowrates for 25 March - 24 April, 1982, for the principal tributaries of Chesapeake Bay.

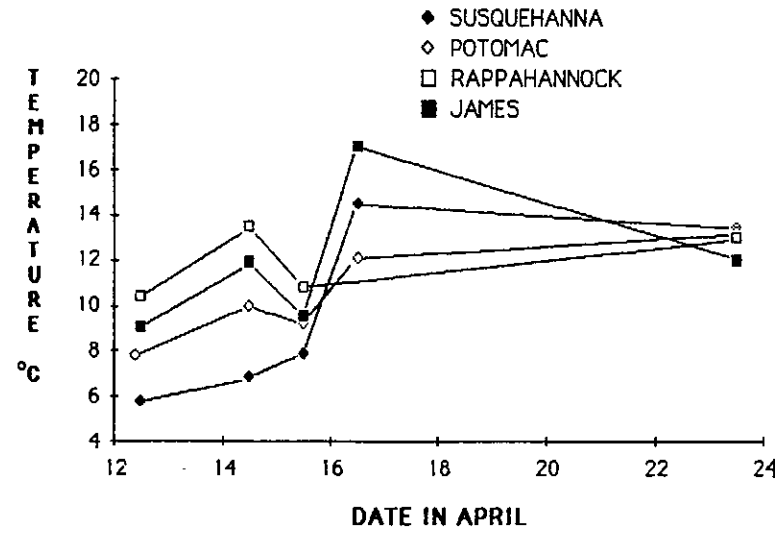

Figure 6-5. Temporal progression of surface temperatures at the heads of the major tributaries for several days in April, 1982.

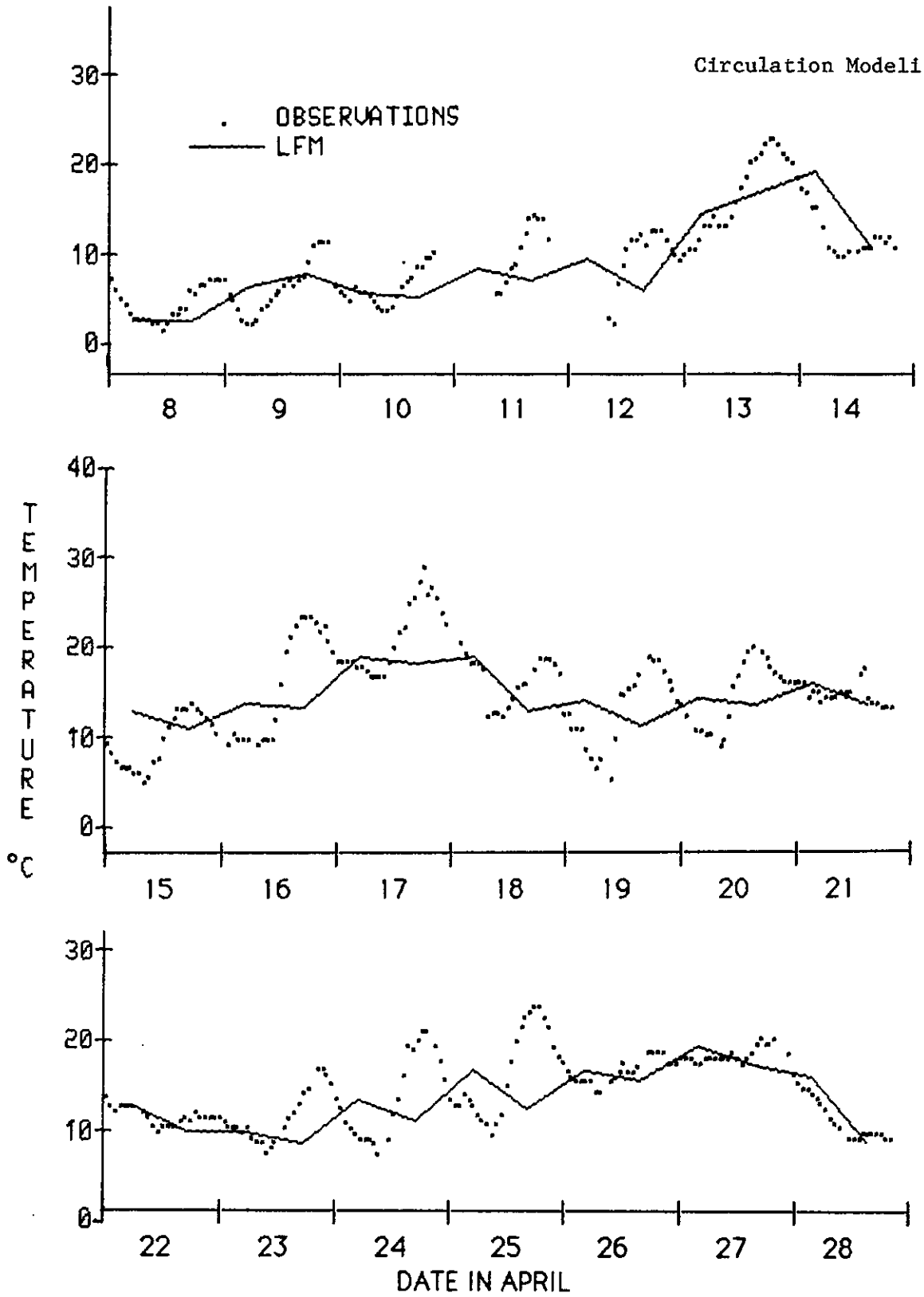

Figure 6-6. Hourly atmospheric temperature (°C) data for Norfolk, VA, and the 12-hourly boundary layer potential temperature (°C) from the National Weather Service's Limited-area, Fine-mesh Model, for 8-27 April 1982.

Only temperatures were used directly from the LFM. Throughout the simulation, the atmospheric pressure was held constant (1014.0 mb), as was the relative humidity (70 percent). Cloud cover, which is not available as a LFM forecast, was held constant at 10 percent.

6.5.4 Initialization Procedures

Initial conditions for the computational (non-boundary) grids included zero velocities and interpolated temperature and salinity fields. The temperatures and salinities were found by taking a weighted average of the values at the boundary. The weights were inversely proportional to the distance between the computational grid and the boundary grid.

6.6 Model Results

6.6.1 Spin-Up Experiments

Several tests of the model basin showed that, given periodic inputs, only a few tidal cycles were necessary before the water levels reached a stage of periodicity. The temperatures and salinities required a few months.

The spin-up temperature and salinity calculations were made with a 12.4-hr tidal period, winds of constant speed (7 m/sec) but cyclicly changing in direction over a 48-hr period, and diurnal solar and atmospheric heating cycles which do not vary in amplitude. Surface temperatures, both inside the Bay and on the shelf, approached periodicity after 15 days (Figure 6-7a). Bottom temperatures showed very small changes.

Salinities changed more slowly (Figure 6-7b). Surface values still showed some changes after 60 days. As a compromise, we chose 15 days for the spin-up period, primarily because we are more interested in temperature for this study.

6.6.2 Verification of Water Levels and Currents

MECCA was run numerous times to simulate the tides and tidal currents in the Bay-shelf region. A typical set of external-mode currents is shown in Figure 6-8. Mean tides at 11 NOS tide stations were simulated. MECCA was able to reproduce the mean tide ranges and times of high water (referenced to Hampton Roads) quite well (Figure 6-9a, b).

Mean tidal currents at four locations were compared to NOS data. The locations are at the entrance to Chesapeake Bay; off Smith Point, VA; off Sandy Point, MD; and at an offshore location on the continental shelf designated as MAB (Mid-Atlantic Bight). The flood and ebb magnitudes of the mean tidal currents are shown in Figure 6-9c. The model does reasonably well, except for Sandy Point, where model currents were approximately one-half the observed magnitude.

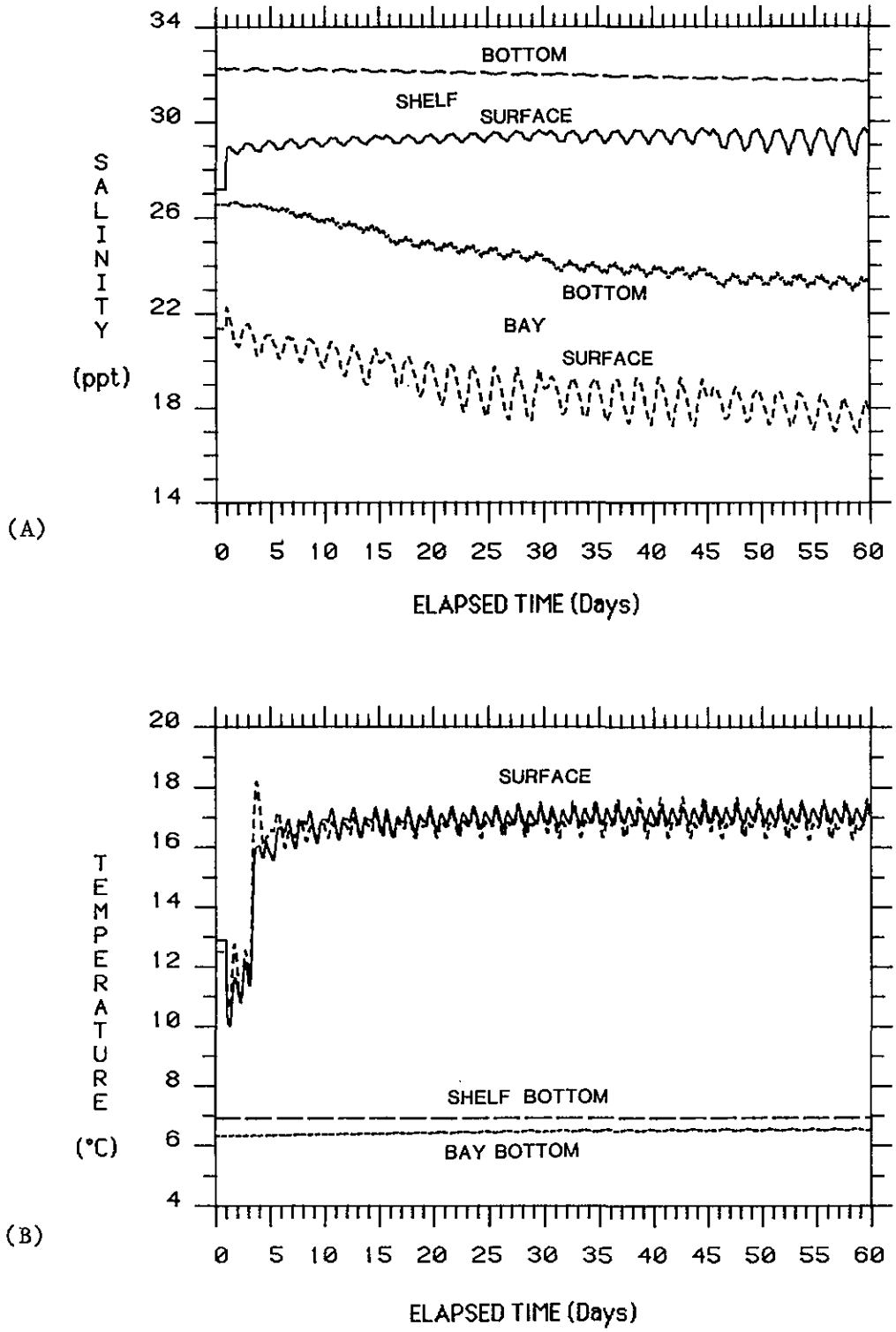

Figure 6-7. Results of spin-up tests showing 60-day variation of (A) salinity, and (B) temperature.

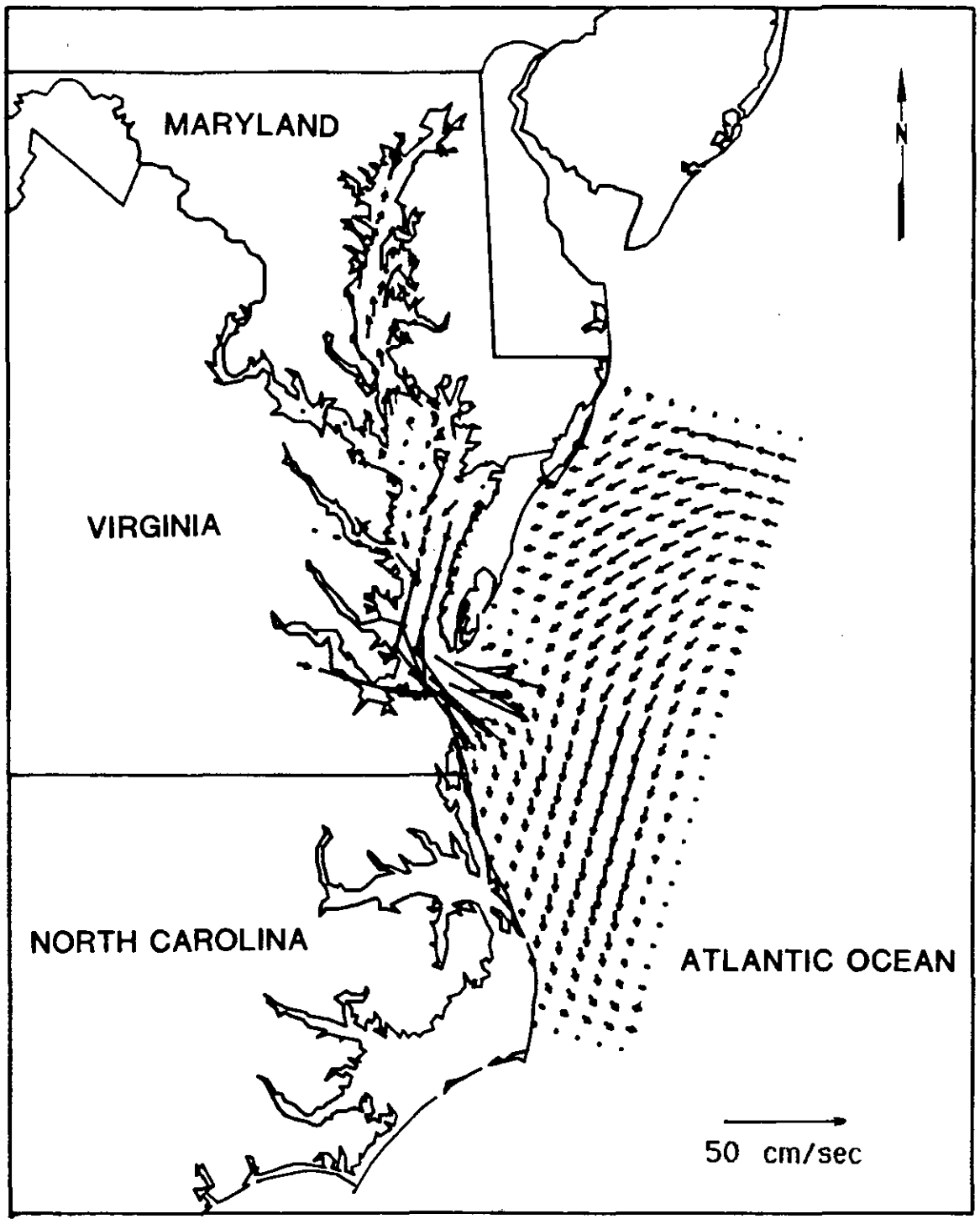

Figure 6-8. Barotropic (vertically averaged) currents as computed by MECCA for two hours before mean low water at Hampton Roads, VA.

(A)

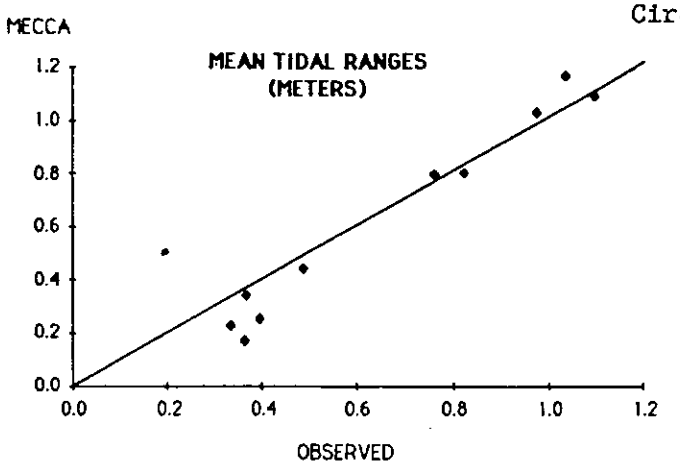

(B)

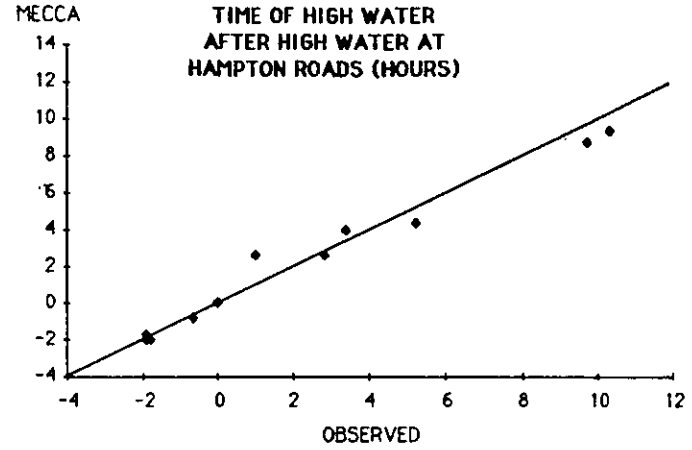

(C)

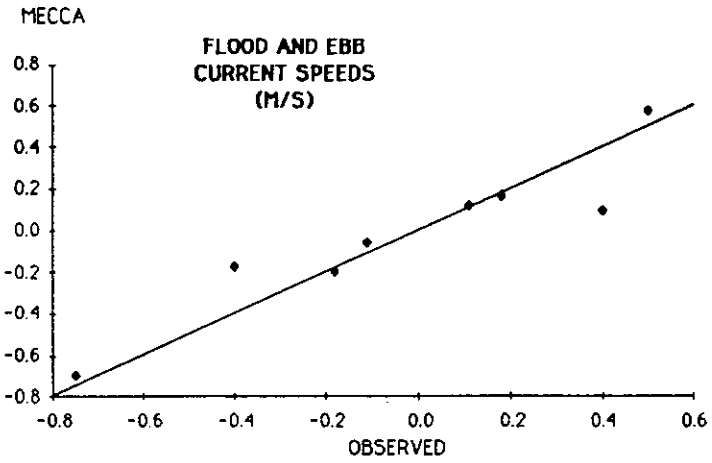

Figure 6-9. Comparison of observed and modeled (A) tide ranges (B) time lags, and (C) tidal currents.

6.6.3 Water Temperatures

We have compared the MECCA simulated temperatures with estimates obtained from satellite imagery. Satellite data are available from the NOAA-7 and the NOAA-6 satellites for the period 12-23 April. Although satellite imagery has a resolution of 1.1 km, the spatial resolution of the model is limited by the 11.2 km grid size.

A plot of the surface temperatures for a location near the main axis of the Bay at the same latitude as the Potomac River mouth is given in Figure 6-10. Temperature variation over time at that location is representative of changes in the rest of the Bay. The MECCA temperatures at the start of the period (9 April) were low, initially about 2 °C. The model's low temperatures resulted from the cold air which passed over the region during the first week of April. MECCA temperatures showed rapid increases on 13-14 April, and a smaller rise on 18 April, reflecting episodes of warmer air moving into the region. In general, surface water temperature rises lagged behind periods of atmospheric warming by 12 to 24 hours. Water temperatures never exceeded air temperatures during the study period.

Temperature estimates from satellite imagery were generally within 1 to 2 °C of the MECCA simulated temperatures, although occasionally (as on 12, 16, and 23 April) the imagery estimates were 2 to 4 °C higher. These high values are from afternoon satellite transits, so it is possible that either (a) MECCA is not adequately representing the daily heating cycle of the near-surface waters, or (b) because the imagery is a measure of only the topmost 0.5 millimeter, it is not representative of the upper layers.

Surface temperatures at a mid-shelf location is shown in Figure 6-11. The major features of the water temperature history closely match those of the mid-Bay location. The surface temperature here is initially warmer, by about 2 °C, than in the mid-Bay (Figure 6-10). Satellite estimates are generally within 1 to 2 °C of the MECCA result, although the extreme difference, about 2 °C, is much smaller than for the first case. One reason is that the mid-shelf region does not show the large diurnal changes evident in the mid-Bay area.

6.7 Summary and Conclusions

This extensive experimentation provided the opportunity to test many of the variables and formulations, and lead to the completion of a useful and flexible numerical scheme. The major task of verifying the model temperatures has just begun. There are extensive NOS data sets available for 1982 for many locations throughout the Bay, so that further refinement of the model should be possible.

The model was found to simulate the mean tide range to within about 10 cm. The time lags were simulated to within a half an hour. Tidal currents were also simulated to within 0.1 m/sec, with the exception of those at Sandy Point, MD. MECCA currents there were underestimated by a factor of three or four.

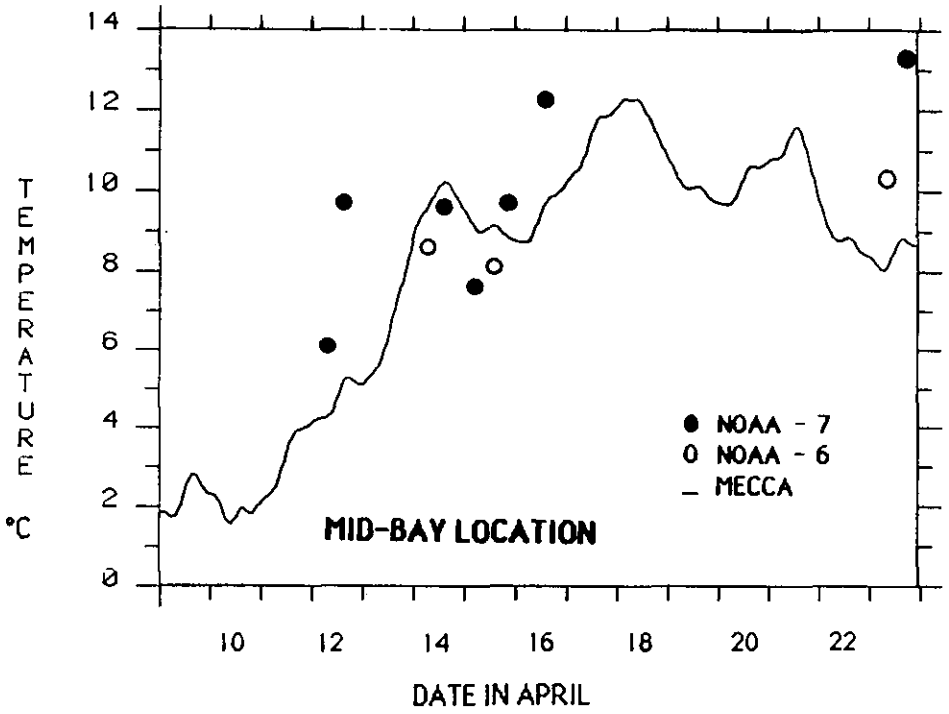

Figure 6-10. Twelve-hourly surface water temperatures (°C) at a mid-Bay location for 10-24 April 1982, as simulated by MECCA and from satellite imagery.

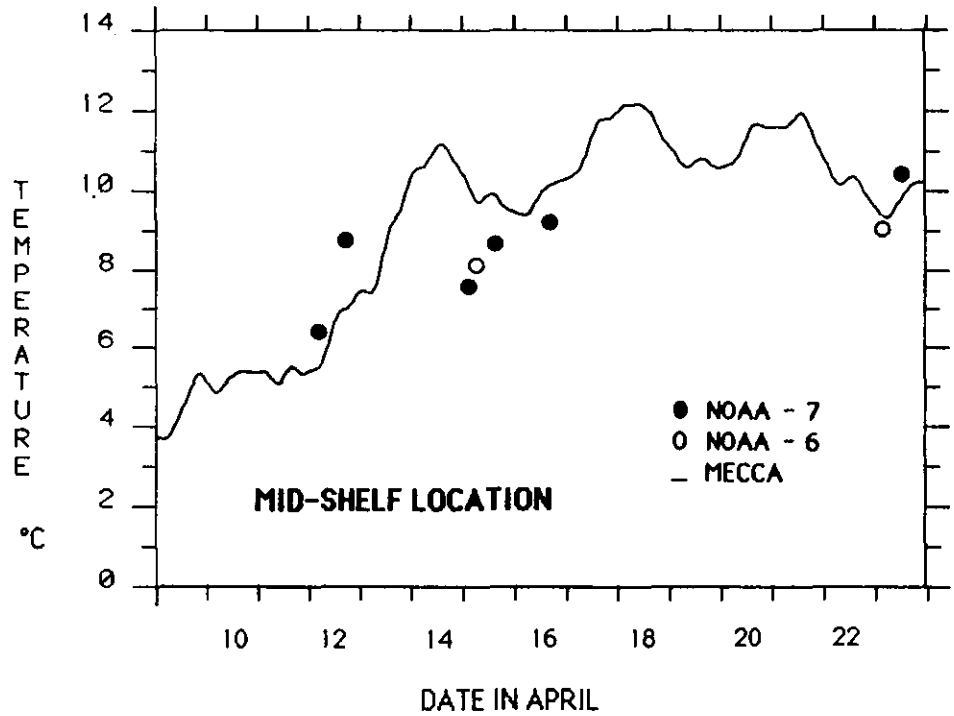

Figure 6-11. Surface water temperatures (°C) at a mid-shelf location for 10-24 April 1982, as simulated by MECCA and from satellite imagery.

The model's results followed the general trend of satellite imagery, and produced temperatures usually within 1 to 2 °C of the satellite estimates. The elapsed time between satellite estimates, however, was too large to permit accurate definition of the daily heating cycles.

The model grid was probably too coarse to allow a meaningful comparison of temperature features. A grid size in the range of 1 to 5 km would be more useful.

6.8 Future Plans

There are many possible areas of model improvement. One would be a change in the specification of the depth of solar shortwave energy penetration, D10. For example, in the turbid rivers, D10 is probably on the order of only a few tens of centimeters, while in the Bay itself, only a few meters. Specifying a spatial variation of D10 would improve the accuracy of the temperature calculations.

Another modification would be the inclusion of a spatially-varying horizontal eddy viscosity. Results for the tides and tidal currents indicate that the viscosity is too large inside the Bay, because tidal currents are overly dampened. Smaller viscosities would be anticipated because the horizontal scale of fluctuations is more limited in the Bay.

Close examination of the salinity field shows spurious values are being generated near land boundaries. The bottom boundary condition and the maximum allowable internal-mode time step will be investigated to find the cause of the difficulty.

In the near future, the numerical scheme will be revised to incorporate variable horizontal grid sizes. Then the continental shelf could be covered by a coarse mesh spacing (say 20 km) and the Bay by a finer spacing (say 1 or 2 km), with little additional computer time. This will resolve the smaller scales of motion within the Bay which are not presently modeled but which are important for understanding the Bay's dynamics.

6.9 References

Birdsong, R. S., R. L. Bedenbaugh, and R. D. Owen. 1984. Fin fish seasonality and utilization of Hampton Roads and the entrance channel. Applied Marine Research Laboratory, Old Dominion University, Norfolk, Va. (unpublished manuscript), 100 pp.

Davies, A.M. 1983. Application of a three-dimensional shelf model to the calculation of North Sea currents. North Sea Dynamics (J. Sundermann and W. Lenz, eds.), Springer-Verlag, New York, pp. 44-62.

Hess, K. W. 1985a. Assessment model for estuarine circulation and salinity. NOAA Technical Memorandum NESDIS AISC 3, National Environmental Satellite, Data, and Information Service, NOAA, U.S. Department of Commerce, 39 pp.

___. 1985b. User's guide to running MECCA on the AISC VAX 11/750 and the DAMUS UNIVAC 1100. Available from Marine Environmental Assessment Division, Assessment and Information Services Center, NESDIS, NOAA, 3300 Whitehaven St., NW, Washington, DC 20235, 41 pp.

___. 1985c. Numerical solution of the three-dimensional temperature equation. MEAD Office Note 85-4. Available from Marine Environmental Assessment Division, Assessment and Information Services Center, NESDIS, NOAA, 3300 Whitehaven St., NW, Washington, DC 20235, 13 pp.

National Marine Fisheries Service. 1982. Environmental conditions in the coastal and offshore zones of the northeastern U.S.A. - April through September 1982. Atlantic Environmental Group, NMFS, Narragansett, R.I., (unpaged).

Smith, N. P. 1980. Computer simulation of air-estuary thermal energy fluxes. Estuarine Perspectives (V. S. Kennedy, ed.) Academic Press, New York, 317-328.

Tyler, M. 1985. personal communication.

U.S. Geological Survey 1982a. Water resources data, Maryland and Delaware, water year 1982. U.S.G.S. Water-Data Report MD-DE-82; 63-65 and 250-253.

___. U.S. Geological Survey. 1982b. Water resources data, Virginia, water year 1982. U.S.G.S. Water-Data Report VA-82; 98-100, 113, 120, and 182.

7. LARVAL DRIFT MODEL

David F. Johnson and Kurt W. Hess

7.1 Introduction

The ability to identify temperature and turbidity patterns using satellite data, and to model winds and circulation in the Chesapeake Bay provides us with the tools to assess synoptically the effects of weather events and ocean circulation on the larval recruitment of many estuarine-dependent fishery species.

Dispersal of planktonic larvae is a common reproductive strategy for estuarine organisms (Table 7-1), yet estuarine circulation produces a net outward flow proportional to fresh water inflow. Numerous investigators have demonstrated that while larvae cannot swim fast enough to resist typical horizontal currents, larvae may make conspicuous vertical movements. Many larvae have control of their vertical position and can effectively exploit the vertical differences in current velocities and thereby retain or return the offspring to the parent habitat. Unusual circulation patterns have the potential to seriously affect recruitment success, since larvae have only simple stereotyped behaviors, such as phototaxis or geotaxis. Because success or failure in larval drift is a frequent determinant of year class size and, consequently, commercial catch, an understanding of larval drift and the susceptibility of larvae to environmental variability is important to understanding fluctuations in commercial fisheries (Wooster, 1983). Because larval behaviors may vary among species and life stages, numerous recruitment mechanisms have been proposed for estuarine and coastal larvae, although most mechanisms may be conceptually modeled by changes in vertical distribution which exploit vertical differences in estuarine circulation.

A complete field analysis of larval drift for a given species requires a sampling scheme with a temporal and spatial resolution beyond the resources of a single research vessel. The problem is generally approached by partitioning a field study into separate studies of temporal and spatial variability of larvae. A small number of stations is sampled intensively over a relatively long time period, or a large array of stations is sampled less frequently over a short time period. In practice the results of the two types of studies are often difficult to reconcile. We describe here a modeling-monitoring approach as a new technique which may aid our understanding of larval dynamics and fluctuations in recruitment to commercial stocks.

The circulation model (MECCA) produces rapidly updated synoptic and event-oriented information with fine detail on scales appropriate to tracking planktonic larvae. MECCA is coupled to field processes by using field data for boundary conditions and forcing functions (Hess, 1985). By comparing the results of the drift model with observed larval distributions, we may evaluate various concepts of recruitment. If a verified drift model disagrees with observed larval distribution, the results will suggest appropriate hypotheses for additional research. Conversely, if the verified drift model simulates observed larval distributions, then the model may be used to optimize fisheries management and to evaluate environmental impacts.

Table 7-1. Seasonal distribution of the larvae of selected Chesapeake Bay species.

Species	Month J F M A M J J A S O N D
FISH*	
Ammodytes americanus (sand eel)	L-------L
Anchoa spp. (bay anchovy)	EL-------E--L
Brevoortia tyrannus (menhaden)	L---------L L----L
Cynoscion regalis (weakfish)	L----------L
Fundulus heteroclitus	L
Gobiesox strumosus	L----------L
Gobiosoma ginsburgi	L----------L
Gobiosoma bosci	L-------L
Hippocampus erectus (sea horse)	L L----L
Hypsoblennius hentzi	L----------L
Lieostomus xanthurus (spot)	J-A--J
Membras martinica	L----------L
Menida beryllina	L----L
Menticirrhus spp.	L-------L
Micropogonias undulatus (croaker)	J---L----L
Microgobius thalassinus	L-------L
Ophidion marginatum	L-L
Paralichthys dentatus (s. flounder)	L
Peprilus spp.	L----L
Prionotus spp.	EL
Pseudopleuronectes americanus (w. flounder)	L-------L
Rachycentron canadum (cobia)	E--A---E
Syngnathus fuscus	L-------L
Scophthalmus aquosus	L
Symphurus sp.	E--L---EL
Tautoga onitis	E
Trinectes maculatus	EL--------EL
CRUSTACEANS**	
Balanus sp. (barnacle)	L----A------L
Callinectes sapidus (blue crab)	L-------A-----L
Cancer irroratus (rock crab)	L--A-------L L--A--L
Crangon septemspinosa (sand shrimp)	L----------A----L
Euceramus praelongus	L-----A-----L
Hexapanopeus angustifrons	L-----A-----L
Neopanope sayi	L-----A-----L
Ogyrides limicola	L----------L
Pagurus longicarpus (hermit crab)	L--AAA----------L
Palaemonetes spp.	L----A---------L
Pinnixa chaetopterana	L---A-----A---L
Pinnotheres ostreum (pea crab)	L---A------L
Polyonyx gibbesi	L-----A----L
Rhithropanopeus harrisii	L---A----L
Sesarma reticulatum	L-A------L
Uca sp. (fiddler crab)	L-----A---L
Upogebia affinis	L---A--------L
MOLLUSCS***	
Barnea truncata (boring bivalve)	L----------L
Crassostrea virginica (oyster)	L----------L
Donax variabilis (coquina clam)	L----------L
Mercenaria mercenaria (hard shell clam)	L----------L
Modiolus demissus (ribbed mussel)	L----------L
Mya arenaria (soft shell clam)	L-----L
Petricola pholadiformis	L----------L
Rangia cuneata (brackish water clam)	L-----L
Spisula solidissima (surf clam)	L----L
Teredo navalis (ship worm)	L----------L

E=eggs, L=larvae, J=juvenile, A=period of peak abundance

*=Birdsong et al. 1984., Cowan and Birdsong 1985, Olney 1983
**=Birdsong et al. 1985, Johnson 1982, Sandifer 1972
***=Chaney and Andrews 1971

Based solely on the availability of cloud-free satellite images, the period of 10-24 April 1982 was chosen for the initial study. We have selected 54 species, including most commercial species, to illustrate the seasonal distribution of the eggs and larvae typical of Chesapeake Bay species (Table 7-1)[1]. The majority of the Bay's fauna spawn in the late spring and summer months; consequently few larval forms are present in the plankton during April. Those local species with high larval abundance in April are: Crangon septemspinosa (sand shrimp), Balanus spp. (barnacle) and Membras martinica (silverside). None of these three taxa are harvested commercially, although barnacles place an economic cost on boating interests. Because larvae of commercial species are not abundant during April, the version of the drift model used in these simulations represents passive surface drift.

7.2 Objectives

Our primary objective in this phase of drift modeling was to develop a general transport model that can be used to assess recruitment for commercial species that have planktonic larvae.

A second objective was to test the accuracy of the drift model calculations.

Our third objective was to model surface drift for the study period of 10-24 April 1982.

7.3 Model Formulation

We have developed a Lagrangian drift model to be used in conjunction with the three-dimensional numerical model for estuarine and coastal circulation (MECCA). The larval-trajectory model (LARTREK) is implemented as a collection of subroutines called by MECCA.

In LARTREK, the initial positions of the drifters may be anywhere within the MECCA grid and within any of nine vertical layers. At the end of each iteration of MECCA (10 minutes of simulated time in the tests described below), LARTREK calculates new positions for each drifter by numerically integrating the velocities provided by MECCA. LARTREK interpolates the u and v components of velocity within and between grid cells and computes the drift displacement for the 10 minute time step. The velocity regime at the end point of the trajectory is compared to the velocity regime at the starting point and if a difference exists, an iterative procedure recalculates the displacement at regular intervals along the path. This feature is particularly useful when drift trajectories are curved. Also, model drifters are prevented from approaching any closer than 10 m of a land-water boundary.

---

[1] Although April overlaps the spawning period of several species of anadromous fish, they are not considered here. These fish spawn in the upper reaches of the Bay's tributaries beyond the resolution of the available satellite data as well as outside the bounds of the numerical model.

7.4 Model Testing

The first test of LARTREK assigned various constant (positive and negative) values to the u and v velocity components. This test was performed to ensure that drift trajectories followed the appropriate straight line, and that the model properly recorded the positions on the MECCA grid system. The results showed no deviations from the expected path, and the drifter positions were recorded accurately.

The second test of LARTREK was a comparison of model output with the analytical solution for the case of a solid-body rotation. In this test all velocities were constant over time, but they varied spatially. The tangential velocity (V) is calculated as

$$V = ar \tag{7.1}$$

where a is a constant and r is the distance to the center of rotation. The radial velocity is zero. The velocities increase with distance from the center of rotation, such that regardless of the distance from the center, all drifters should complete a circular path with the same elapsed time (Figure 7-1). For the range of velocities tested (which are much larger than are likely to be encountered in Chesapeake Bay), the results show uniformly small errors (Figure 7-2).

Another test compared the model output to the analytical solution for a velocity field that varied temporally, but not spatially. The u and v components (u = east, v = north) of velocity are calculated as

$$u = b \sin(2\pi t/T) \tag{7.2}$$

$$v = b \cos(2\pi t/T) \tag{7.3}$$

where b is a constant, and t is elapsed time. T represents the period of rotation, which was set as 24 hours. In this case, the model drifters also follow a circular path. Because the velocities at each grid are the same at any instant, the iterative procedure which accommodates curved trajectories is not invoked by the program. A small error thus accumulates as a result of the curved path being approximated by a series of straight lines. This error is proportional to the velocity, but the errors are small even for velocities much larger than are likely to be found in Chesapeake Bay (Figure 7-3). A random error is also introduced at the completion of an orbit, because the point of origin may not coincide with the point of the trajectory that lies closest to a perfect circle (Figure 7-3).

These tests check the ability of LARTREK to calculate precise drift tracks with a given velocity distribution. Verification requires that simulations of defined time periods be compared to corresponding field measurements. The following simulation represents our initial simulation of the drift conditions in and adjacent to Chesapeake Bay, during a defined time period.

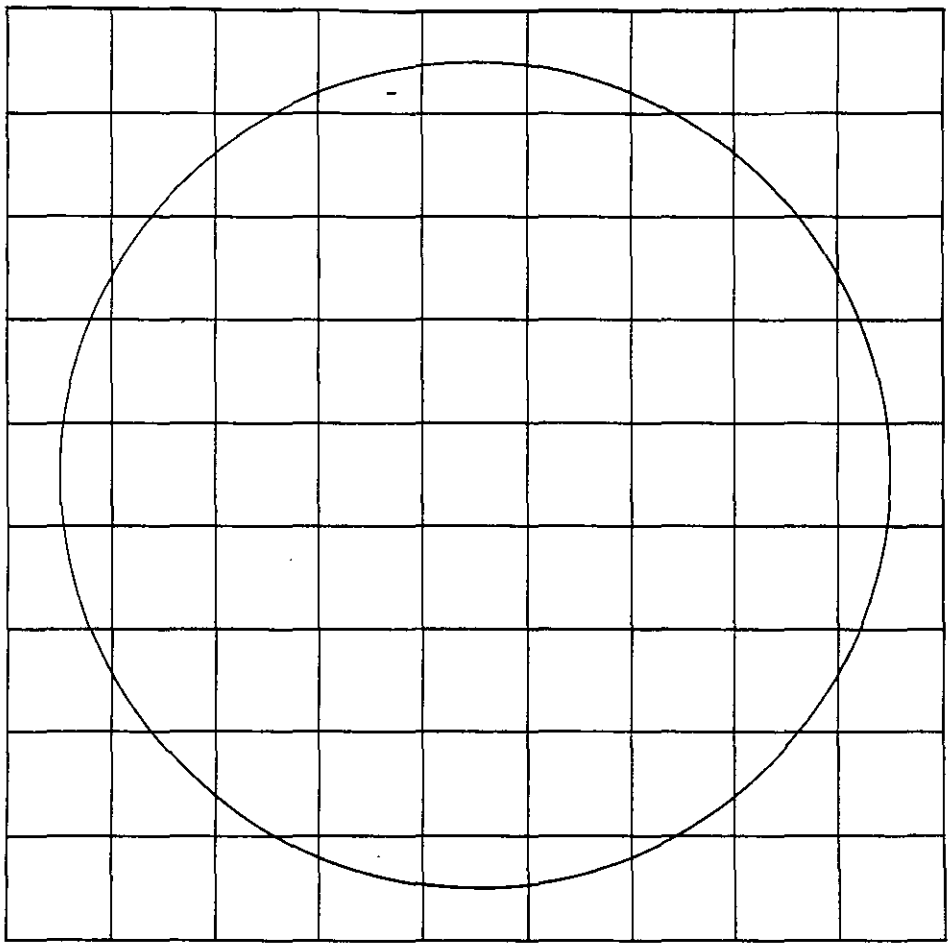

Figure 7-1. Plot of a sample drift orbit from the solid body rotation test of LARTREK. Grid size= 10 x 10 km, orbit radius= 40 km, V= 2 m/sec.

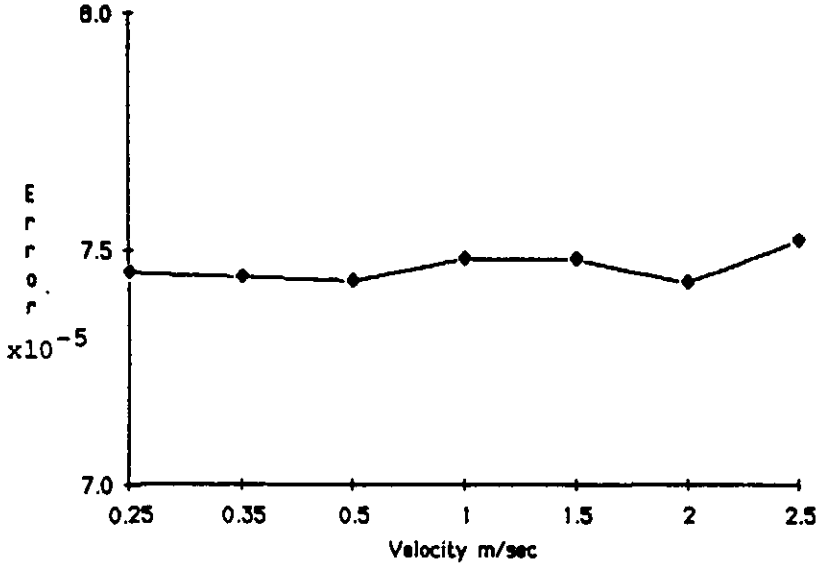

Figure 7-2. Error versus current velocity for the solid body rotation test. Error= (distance between predicted and analytical endpoints)/path length.

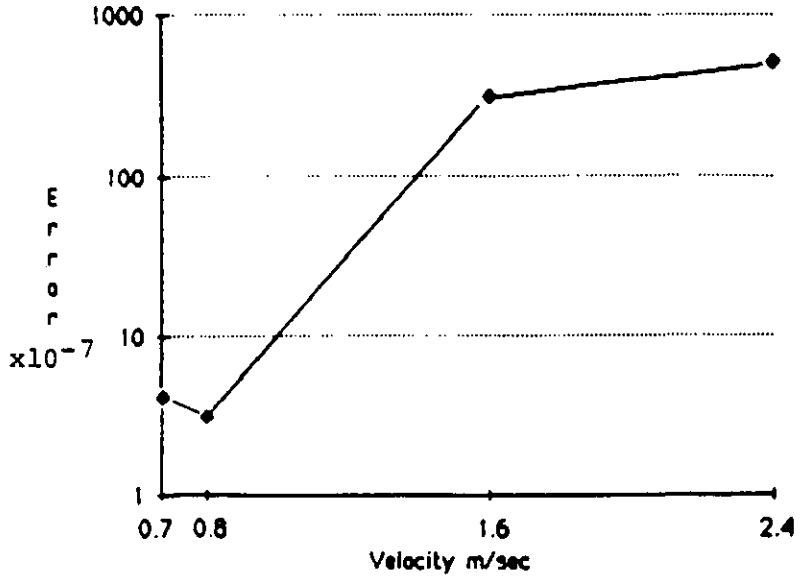

Figure 7-3. Error versus current velocity for a velocity field varying temporally, but not spatially. Error= (distance between predicted and analytical endpoints)/path length. Note logarithmic scale on vertical axis.

7.5 Simulation of Surface Drift: 10-24 April 1982

Five days were added to the beginning of the simulation of surface drift for the period of 10-24 April 1982 for model initialization and spin-up. Figure 7-4 shows the trajectories of four surface drifters plotted at 12-hour intervals; in effect this is the non-tidal drift. Figure 7-5 shows the same drifters with their positions plotted at one-hour intervals.

The simulation for the drifter initially in the Bay mouth shows a strong northward drift with an offshore component near the end of the two week period. We do not have comparable field data for the circulation conditions during this period. However, the simulated surface drift appears to be a reasonable facsimile of the local conditions, as known both from published results of circulation studies and by circulation inferred from satellite imagery (see Chapter 3). A progressive vector diagram of the corrected LFM winds during this two week period shows a net northward and offshore drift, but the path for the shelf drifter shows little resemblance to the wind diagram (Figure 7-6). Even accounting for the influence of coriolis the discrepancies between the path of the shelf drifter and the wind diagram warrant an analysis in the next phase of this study.

7.6 Future Applications

In the next phase of this project, we will simulate the fate of blue crab larvae over a season for several individual years. The seasons will be selected from several years for which we have access to field data on blue crab larval distributions, so the model data may be compared with actual field conditions and larval distributions. The first year's run will be used to calibrate the model. Succeeding years will serve as verification runs. We may repeat the simulation for other seasons, and thereby assess the probable level of recruitment provided by various regimes of winds and currents. We will also run several scenarios such as spawns during spring or neap tides, various river flow conditions, and the passage of atmospheric storms. With vertical swimming velocity added to the LARTREK model, we will also evaluate the impact of various strategies of larval behavior on fisheries recruitment. Ultimately, we may be able to assess blue crab recruitment one year prior to the commercial catch of that year class. Furthermore, the drift model can be modified for applications to sediment transport and plume behavior. As one modification, the swimming velocity would be replaced by a settling velocity. Simulations could then show erosional patterns, sediment transports, and deposition patterns.

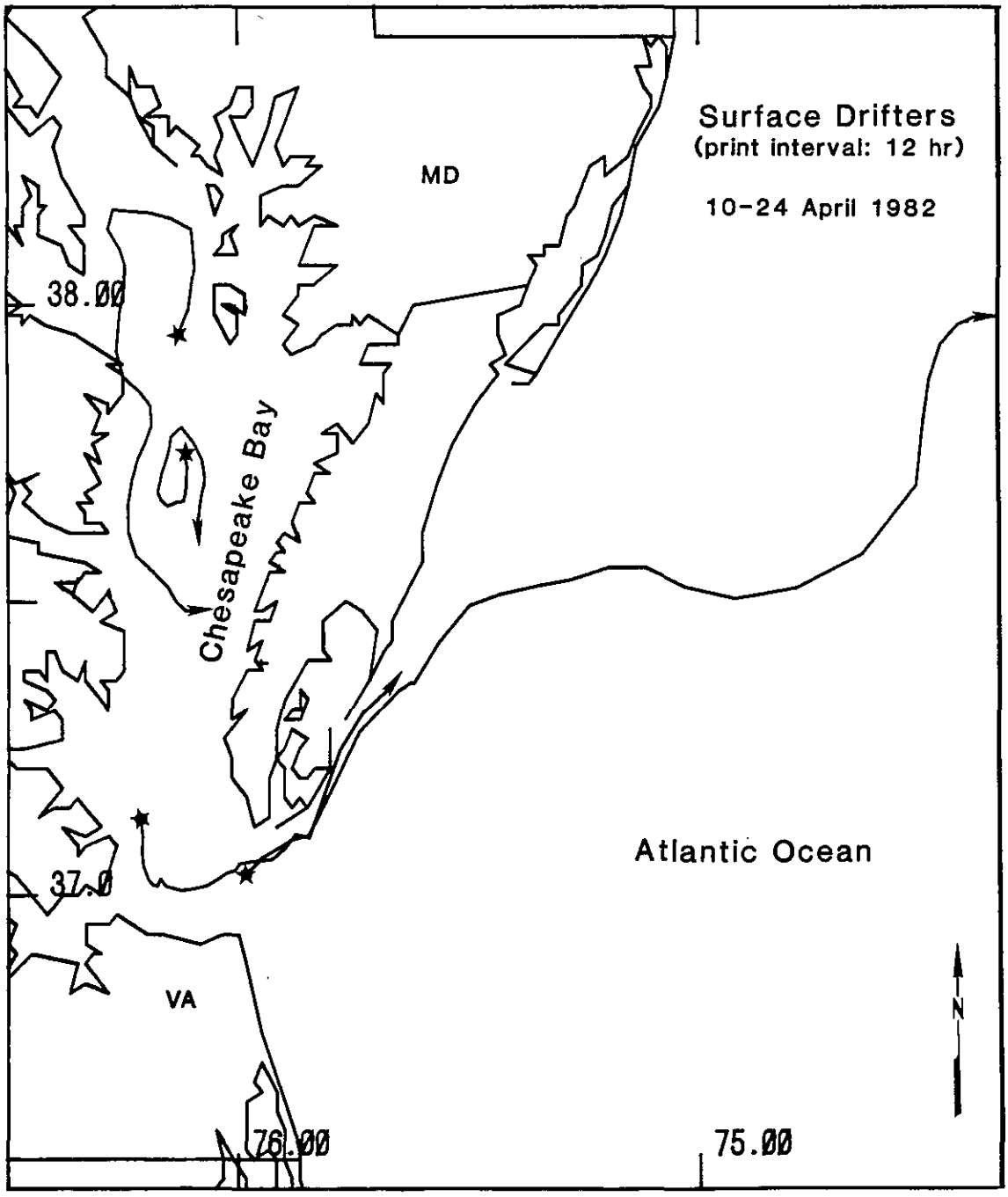

Figure 7-4. Simulation of surface drift conditions for 10-24 April 1982. Drifter positions were plotted each 12 hours. Star indicates initial position. Arrow indicates end point. The tick mark interval on the vertical axis represents 30 NM.

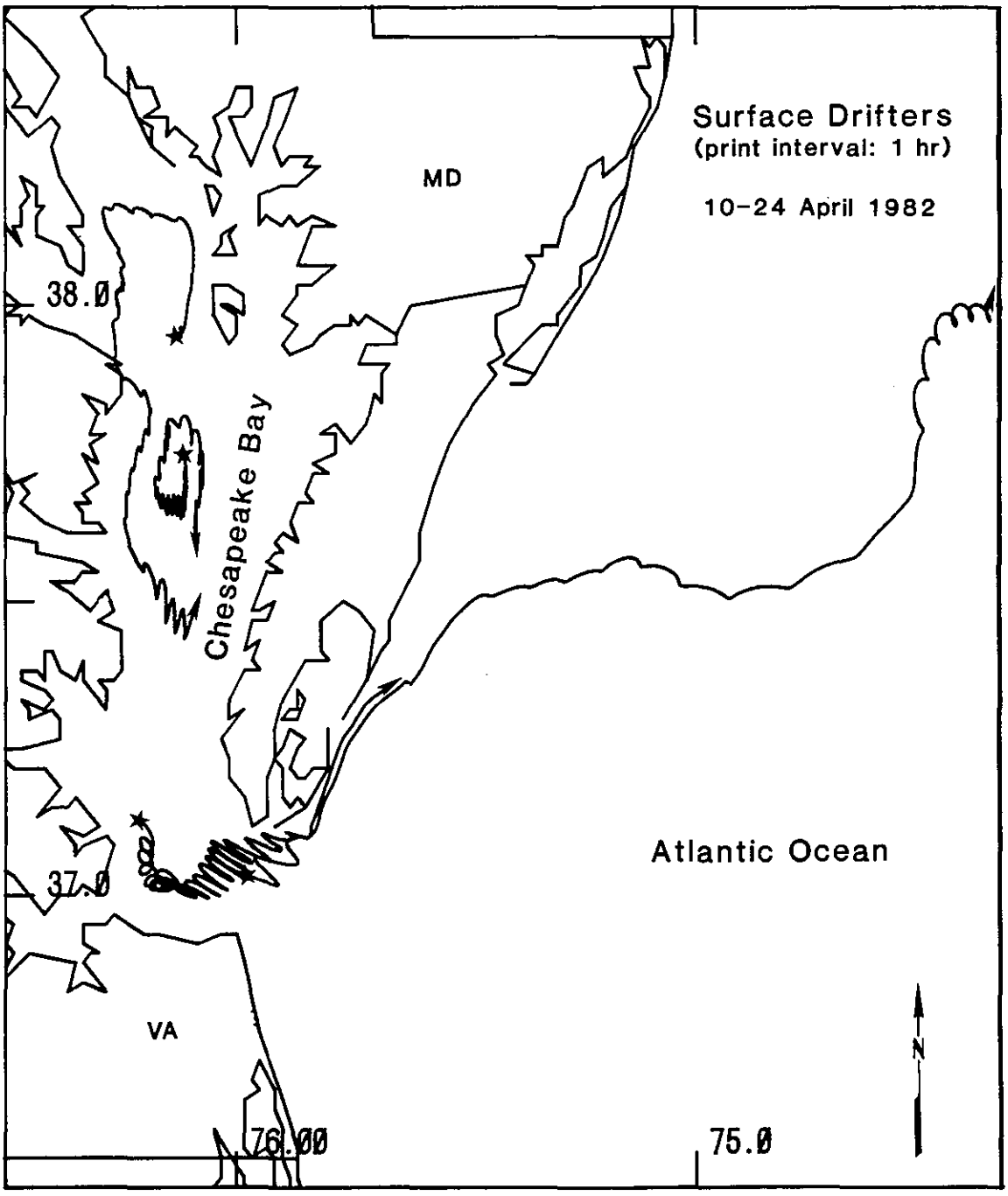

Figure 7-5. Simulation of surface drift conditions for 10-24 April 1982. Drifter positions were plotted each hour. Star indicates initial position. Arrow indicates end point. The tick mark interval on the vertical axis represents 30 NM.

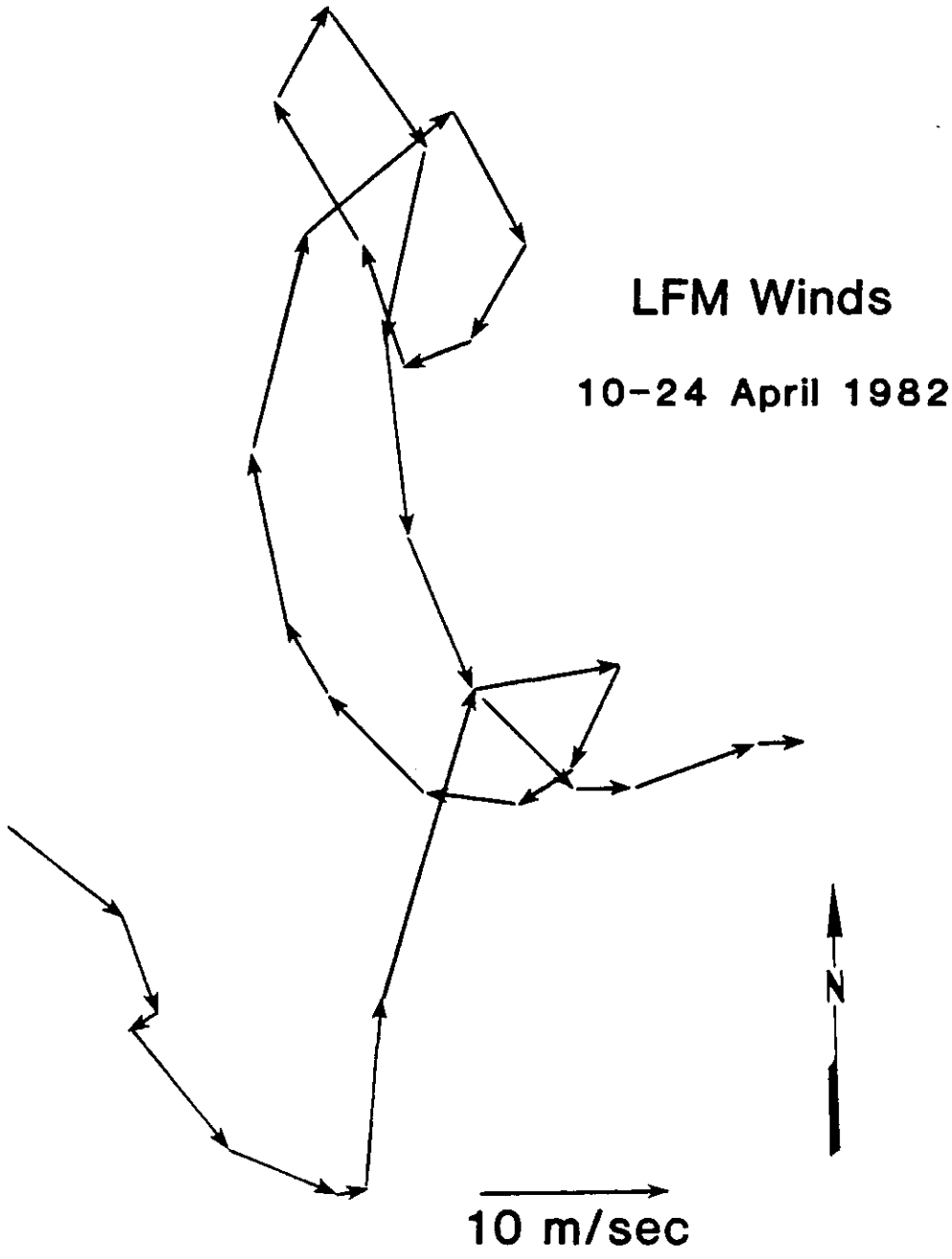

Figure 7-6. Progressive vector diagram of corrected LFM winds (Point 5, Figure 5-1). Winds are plotted for each 12 hour interval from 0600 GMT, 10 April 1982 to 1800 GMT, 24 April 1982.

7.7 References

Birdsong, R. S., R.L. Bedenbaugh and R.D. Owen. 1984. Fin fish seasonality and utilization of Hampton Roads and the entrance channel. (unpublished manuscript) Applied Marine Research Lab, Old Dominion University, Norfolk, VA 100 pp.

Birdsong, R.S., D. W. Byrd, J. F. Matta and B. W. Parolari, Jr. 1985. Meroplankton monitoring data from a fixed platform in the Chesapeake Bay mouth, 1982-1983. (unpublished manuscript) Applied Marine Research Lab, Old Dominion University, Norfolk, VA 55 pp.

Chaney, P. and J. D. Andrews. 1971. Aids for identification of bivalve larvae of Virginia. Malacologia 11:45-119.

Cowan, J. H., Jr. and R. S. Birdsong. 1985. Seasonal occurrence of larval and juvenile fishes in a Virginia Atlantic coast estuary with emphasis on drums (Family Sciaenidae). Estuaries 8:48-59.

Hess, K.W. 1985. Assessment model for estuarine circulation and salinity. NOAA Technical Memorandum NESDIS AISC 3, NOAA, U.S. Dept. Commerce, 39 pp.

Johnson, D. F. 1982. A comparison of recruitment strategies among brachyuran crustacean megalopae of the York river, lower Chesapeake Bay and adjacent shelf waters. Ph.D. Dissertation, Old Dominion University, 97 pp.

Olney, J. E. 1983. Eggs and early larvae of the bay anchovy, Anchoa mitchilli, and the weakfish, Cynoscion regalis, in lower Chesapeake Bay with notes on associated ichthyoplankton. Estuaries 6:20-35.

Sandifer, P. A. 1972. Morphology and ecology of Chesapeake Bay decapod crustacean larvae. Ph.D. Dissertation, University of Virginia, Charlottesville, VA, 532 pp.

Wooster, W. S. 1983. On the determinants of stock abundance. In: Year to Year (Ed: Warren S. Wooster) Washington Sea Grant, University of Washington, Seattle, 1-10.

8. CONCLUSIONS AND RECOMMENDATIONS

This interdisciplinary study describes new and developing technology that when used as an integrated approach will aid our understanding of fisheries resources and aid in assessments of environmental impacts. The following conclusions were drawn from this initial study.

1. Satellite imagery was essential in the production of maps of sea surface temperature, turbidity and plant pigments. Selected temperature data were useful as environmental input for the circulation model. Turbidity and plant pigment indices require *in situ* data for further refinement of the indices. One of the major limitations of satellite data is the availability of near-nadir, cloud-free data.

2. The Limited-area, Fine-mesh Model (LFM) wind predictions are a useful aid both for the identification of large-scale wind influences on the thermal and circulation features of estuarine and shelf waters, and as forcing functions for the circulation model. These wind predictions are especially relevant here because one of the recently cited causes of variability in recruitment success for species with planktonic larvae is inter-annual variation of wind stress on coastal waters. We calibrated the LFM wind predictions for the Chesapeake Bay area and demonstrated that the adjusted predictions are accurate estimates of local winds. Further studies are needed to calibrate LFM forecasts (up to 48 hours in advance) to estuarine and coastal circulation models.

3. A numerical circulation model, MECCA, was used successfully to simulate water currents, salinities, and temperatures. The mean tide ranges at several stations throughout the Bay-shelf region were calibrated to an accuracy of 10 cm and the mean time lags to a half an hour. Mean tidal currents were calibrated to within 0.3 m/sec for all cases, and to within 0.1 m/sec for most cases. Further adjustment of the bathymetry, bottom friction coefficient, and the horizontal eddy viscosity may increase the model's accuracy.

The surface water temperature computed by the model for a point in the shelf region had a root mean square error of 1.3 °C, while for a point within the Bay the error was 2.6 °C as compared to satellite imagery. The deviations may be reduced if the spatial variations in water turbidity are considered.

Another method of increasing accuracy of the circulation model is by reducing the grid cell size. A uniform halving of cell size would increase computation time a factor of eight. With a horizontally varying grid spacing, however, cells in shallow water could be made smaller, thus increasing the resolution in the Bay with less increase in computation time.

4. We developed an accurate generalized drift model that may be used to assess recruitment for commercial species that have planktonic larvae. Given an initial distribution of drifters in or adjacent to the model space for Chesapeake Bay, the drift model, LARTREK, can estimate the future distribution of the drifters using the circulation model's current vectors. We tested the computational accuracy of the model formulation and found errors less than 0.0075 percent of the distance traveled.

Conclusions

Recommendations

For the next phase of this project, we recommend simulation of the drift of blue crab larvae. We would select from several seasons for which we have field data on blue crab larval distributions, so our model results may be verified. Ultimately we may be able to assess whether the winds and currents would provide a high, medium or low probability of recruitment. That capability could assist fisheries managers in predicting fishery-related economic impacts of changes in seasonal weather patterns.